Futile substrate cycles in brown adipose tissue

Josef Robert Oeckl

Table of contents

List of abbreviations

2DG	2-Deoxyglucose
3-GPA	3-Guanidinopropionic acid
AA	Antimycin A
ACAC	Acetyl-CoA carboxylase
ACSL	Long chain fatty acyl-CoA ligase
ADP	Adenosine diphosphate
AGPAT	1-Acyl-sn-glycerol-3-phosphate acyltransferases
AMP	Adenosine monophosphate
AMPK	AMP-activated protein kinase
ATF3	Activating transcription factor 3
ATGL	adipose tissue triglyceride lipase
ATP	Adenosine triphosphate
BAT	Brown adipose tissue
BIP	Binding immunoglobulin protein
BSA	Bovine serum albumin
Ca^{2+}	Calcium
cAMP	Cyclic AMP
CHOP	C/EBP homologous protein
CK	Creatine kinase
CKB	Creatine kinase B
CM	Cytoplasmic mitochondria
CoA	Coenzyme A
COX	Cytochrome c oxidase
CPT1	Carnitine palmitoyltransferase 1
DG	Diglyceride
DGAT	Diacylglycerol O-acyltransferase
DsiRNA	Dicer-Substrate Short Interfering RNA
e^{-}	Electrons
ER	Endoplasmic reticulum
ETC	Electron transport chain
FA	Fatty acid
FABP	Fatty acid-binding protein
FAc	Formic acid
FASN	Fatty acid synthase
FCCP	Carbonyl cyanide-4-(trifluoromethoxy)phenylhydrazone
FFA	Free fatty acid
G3P	Glycerol-3-phosphate
GPAT	Glycerol-3-phosphate acyltransferases
GPD	Glycerol-3-phosphate dehydrogenase
H^{+}	Protons
HFD	High-fat diet
HSL	Hormone-sensitive lipase
iBAT	Interscapular brown adipose tissue
IRE1	Inositol-requiring protein 1

Iso	Isoproterenol
ITPR	Inositol 1,4,5-trisphosphate receptor type
iWAT	Inguinal white adipose tissue
kDa	Kilodalton
LPA	Lysophosphatidic acid
LPL	Lipoprotein lipase
MG	Monoglyceride
MGL	Monoglyceride lipase
MS	Mass spectrometry
NE	Norepinephrine
NMR	Nuclear magnetic resonance
NST	Non-shivering thermogenesis
O_2	Oxygen
OCR	Oxygen consumption rate
Oligo	Oligomycin
OXPHOS	Oxidative phosphorylation
PA	Phosphatidic acid
PDM	Peridroplet mitochondria
PERK	Protein kinase RNA-like ER kinase
PKA	Protein kinase A
PLIN	Perilipin
PTP	Permeability transition pore
RYR	Ryanodine receptor
SERCA	Sarco/endoplasmic reticulum Ca^{2+}-ATPase
SVF	Stromal vascular fraction
TCA	Tricarboxylic acid
TG	Triglyceride
TNAP	Tissue nonspecific alkaline phosphatase
UCP1	Uncoupling protein 1
UCP1KO	Uncoupling protein 1-knockout
UPR	Unfolded protein response
WAT	White adipose tissue
WT	Wild type
XBP1	X box-binding protein 1
XBP1S	Spliced X box-binding protein 1

List of figures

List of tables

Abstract

Brown adipose tissue (BAT) is the main site of non-shivering thermogenesis in mammals. Uncoupling protein 1 (UCP1), a protein abundantly expressed in the inner membrane of BAT mitochondria, converts chemical energy into heat by uncoupling substrate oxidation from ATP synthesis. This enables rodents and small hibernators to survive in a cold inhospitable environment. UCP1-knockout (UCP1KO) mice, however, are not cold sensitive when slowly and gradually acclimated to lower ambient temperatures. This finding necessarily implies that UCP1KO mice can recruit and rely on thermogenic mechanisms that operate completely independent of UCP1 to maintain their body temperature. It has been suspected for decades that futile substrate cycles may compensate for the genetic ablation of UCP1 in mouse models. Futile substrate cycles and their thermogenic properties, which are primarily based on the futile turnover of ATP, could thus explain why UCP1KO mice do not develop hypothermia when exposed to a cold environment. In this work, several potentially thermogenic substrate cycles were investigated in brown adipocytes of UCP1KO mice. Among the three mechanisms studied, a calcium cycle, a creatine cycle, and a lipid cycle, the lipid cycle that includes triglyceride lipolysis and esterification of fatty acids was found to be the major source of cellular non-shivering thermogenesis. This ATP-consuming mechanism has been extensively studied at the molecular level by using pharmacological inhibitors and RNA interference. Futile lipid cycling in brown UCP1KO adipocytes strictly depends on a constant supply of free fatty acids. The lipase ATGL contributes to this process, as it mediates the major part of fatty acid release by hydrolyzing triglycerides stored in lipid droplets. Once the released fatty acids have been activated in an ATP-dependent reaction, they can be transferred onto a glycerol backbone by a variety of acyltransferases. The acyltransferase DGAT1 plays a key role, because it has been shown that its catalytic activity accounts for a large part of fatty acid re-esterification during active lipolysis. Using different experimental readouts, it was proven beyond doubt that lipid cycling activity is significantly higher in UCP1KO adipocytes compared to wild type cells, which is also particularly supported by the recruitment of directly or indirectly involved enzymes. Moreover, by targeting specific metabolic pathways, the role of glucose – serving as an energy substrate and providing glycerol backbones – in futile lipid cycling was further elucidated. In addition, preliminary insights regarding the possible protective functions of this substrate cycle were gained and putative regulatory mechanisms were identified. Taken together, these results suggest that futile lipid cycling partly mediates adaptive non-shivering thermogenesis in BAT of UCP1KO mice.

Zusammenfassung

Braunes Fettgewebe (englisch: Brown Adipose Tissue, BAT) ist der Hauptort der zitterfreien Thermogenese bei Säugetieren. Das Entkopplungsprotein 1 (englisch: Uncoupling Protein 1, UCP1), ein Protein, das in großen Mengen in der inneren Membran der Mitochondrien des BAT exprimiert wird, wandelt chemische Energie in Wärme um, indem es die Substratoxidation von der ATP-Synthese entkoppelt. Dadurch erst wird das Überleben von Nagetieren und kleinen Winterschläfern in einer kalten unwirtlichen Umgebung ermöglicht. UCP1-Knockout (UCP1KO) Mäuse sind jedoch nicht kälteempfindlich, wenn sie langsam und schrittweise an niedrigere Umgebungstemperaturen akklimatisiert werden. Dieser Befund impliziert, dass UCP1KO Mäuse wärmegenerierende Mechanismen, die unabhängig von UCP1 ablaufen, zur Aufrechterhaltung ihrer Körpertemperatur rekrutieren können. Schon seit geraumer Zeit wird vermutet, dass bestimmte Substratzyklen, die vermehrt Wärme freisetzen, die genetische Ablation von UCP1 in Mausmodellen kompensieren. Diese Art der Wärmerzeugung, welche auf dem Umsatz von ATP beruht, könnte somit erklären, wie es UCP1KO Mäusen gelingt auch bei niedrigen Temperaturen ein Absinken ihrer Körpertemperatur zu verhindern. In dieser Arbeit wurden verschiedene potenziell wärmerzeugende Substratzyklen in braunen Fettzellen von UCP1KO Mäusen untersucht. Unter den drei untersuchten Mechanismen, ein Calciumzyklus, ein Creatinzyklus und ein Lipidzyklus, hat sich der Lipidzyklus, der sich aus Lipolyse von Triglyceriden und der Veresterung von Fettsäuren zusammensetzt, als Hauptquelle der zellulären zitterfreien Thermogenese erwiesen. Dieser ATP-verbrauchende Mechanismus wurde auf molekularer Ebene durch den Einsatz von pharmakologischen Inhibitoren und RNA-Interferenz ausführlich beleuchtet. Der Lipidzyklus in braunen UCP1KO Adipozyten beruht auf einem konstanten Zustrom von freien Fettsäuren. Die Lipase ATGL katalysiert diesen Schritt und vermittelt den Hauptteil an Freisetzung von Fettsäuren, indem sie die in Lipidtröpfchen gespeicherten Triglyceride hydrolysiert. Nachdem die freigesetzten Fettsäuren unter Verbrauch von ATP aktiviert worden sind, können sie durch Acyltransferasen wiederum auf ein Glycerolgerüst übertragen werden. Die Acyltransferase DGAT1 hat hier eine Schlüsselrolle, da durch deren katalytische Aktivität der überwiegende Teil an aktivierten Fettsäuren re-verestert wird solange die Lipolyse aktiv ist. Mit Hilfe verschiedener Messverfahren wurde zweifelsfrei bewiesen, dass die Aktivität dieses Lipidzyklus in UCP1KO Adipozyten im Vergleich zu Wildtyp Zellen signifikant höher ist, was explizit durch die Rekrutierung von direkt oder indirekt beteiligten Enzymen unterstützt wird. Außerdem konnte der Beitrag von Glucose – Energiegewinnung als auch Bereitstellung von Glycerolgerüsten – zum reibungslosen Ablauf des Lipidzyklus bestimmt werden. Darüber hinaus wurden erste Erkenntnisse bezüglich der möglichen protektiven Funktionen dieses Substratzyklus gesammelt und weitere potenziell regulatorische Mechanismen identifiziert. Diese Ergebnisse deuten auf eine wichtige Rolle des Lipidzyklus bei der adaptiven zitterfreien Thermogenese im BAT von UCP1KO Mäusen hin.

1 Introduction

1.1 Brown adipose tissue and endothermy

Endothermy is defined as the ability to maintain a core body temperature above the ambient temperature through endogenous metabolic heat production[1]. Processes contributing to heat generation include: All reactions required to sustain vital body functions (basal metabolic rate), diet-induced thermogenesis, physical activity, shivering thermogenesis, and non-shivering thermogenesis (NST)[2]. To date, birds and mammals are considered as the only extant universally endothermic groups of animals[3].

In small-bodied mammals, and especially in rodents, NST is by far the most important factor in maintaining stable body temperature in a cold environment. In these animals, brown adipose tissue (BAT) is the main source of NST[4]. Although BAT was first mentioned in 1551[5], it was not until 1961 that its thermogenic function was recognized[6]. Several years later, uncoupling protein 1 (UCP1), the protein that mediates NST, was finally discovered in 1978[7]. In contrast to white adipose tissue (WAT), which is mainly responsible for storing excess energy in the form of triglycerides (TGs) and releasing it when needed, BAT is characterized by a brownish, reddish appearance and it can be morphologically very clearly distinguished by its multilocular (multiple smaller lipid droplets per cell) adipocytes[8]. In addition, BAT has a high degree of innervation[9] and vascularization[10], a mitochondrial density comparable to that in skeletal muscle, and an immense oxidative capacity[11]. Ultimately, the combination of exactly these features gives rise to the thermogenic phenotype.

The larger BAT depots in mice are anatomically localized in a way that they almost form a "heating jacket" worn around the upper body[12]. These subcutaneous depots include axillary, cervical, interscapular, subscapular, and suprasternal BAT. Inside the thorax, additional BAT depots are found in the immediate vicinity of the larger mediastinal blood vessels, the heart, and the descending aorta, while within the peritoneum, brown fat partially surrounds the kidneys and adrenal glands[8]. The fact that the larger BAT depots, such as the interscapular BAT (iBAT), are highly capillarized and also have larger blood vessels (in the case of iBAT, it is the Sulzer's vein) directly draining blood from them – or are located very close to larger blood vessels – is extremely favorable. This, consequently, ensures the provision of sufficient substrates and oxygen (O_2), while at the same time allowing the heat generated to be distributed quickly and efficiently throughout the body.

1.2 Uncoupling protein 1 mediates non-shivering thermogenesis

But what is known so far about the mechanism of heat generation in BAT, or UCP1-mediated thermogenesis? UCP1 is 32-kilodalton (kDa) protein located in the inner membrane of brown fat mitochondria that belongs to the mitochondrial carrier family SLC25[13,14]. In cold-acclimated rodents, UCP1 can account for a significant proportion of up to five percent or even more of mitochondrial protein[15]. Once UCP1 is active, it facilitates the entry of protons (H^+) across the inner mitochondrial membrane into the matrix, thereby dissipating protonmotive force. As a direct consequence, O_2 consumption is uncoupled from adenosine triphosphate (ATP) synthesis and chemical energy derived from nutrients is converted into heat. UCP1 is believed to be inherently inactive[16], while it is activated by fatty acids (FAs)[17] and inhibited by purine nucleotides[18]. Nevertheless, at the molecular level, the exact mechanism of H^+ transport remains elusive and the association between FA and H^+ translocation is still controversial[19]. Several mechanistic models have been discussed: UCP1 is an ion channel and allosteric binding of FAs to UCP1 induces conformational changes causing translocation of H^+ or hydroxide (OH^-)[20,21]; UCP1 is a H^+ transporter and FAs bind in the pore of the UCP1 H^+ channel where the FA carboxyl group is directly involved in H^+ translocation[22]; UCP1 is a FA transporter and catalyzes the translocation of H^+ only indirectly by transporting protonated long chain FAs across the inner mitochondrial membrane, which are then deprotonated on the matrix side releasing H^+ again[23]; and similarly, a model that combines certain aspects of previous theories, which is also based on the "symport" of H^+ and FAs catalyzed by UCP1, but in this case FAs remain bound to the carrier molecule[24]. However different these explanations may be, they all agree that an increase in intracellular FA levels precedes the activation of UCP1.

1.3 Adrenergic signaling activates cold-induced thermogenesis

In contrast, the processes occurring in a mouse from the perception of a cold stimulus to the lipolytic release of FAs from lipid droplets in brown adipocytes are well described. Almost immediately after a mouse is placed in a cold environment, sympathetic outflow to BAT increases and norepinephrine (NE) is released from postganglionic neurons[25]. NE then binds to adrenergic receptors of brown adipocytes triggering an intracellular signaling cascade. Among the five subtypes of adrenergic receptors (α_1, α_2, β_1, β_2, and β_3), which belong to the group of G protein-coupled receptors, the β_3-receptor is the most important subtype in promoting lipolysis in murine adipocytes. Activation of β_3-adrenergic receptors induces canonical G_s-signaling, which involves elevated cyclic adenosine monophosphate (cAMP) levels and increased protein kinase A (PKA) activity[26]. In adipose tissues, lipolysis is predominantly mediated by adipose tissue triglyceride lipase (ATGL) and hormone sensitive lipase (HSL). ATGL catalyzes the first and quantitatively most important step in the breakdown of TGs, but the exact mechanism of how adrenergic stimulation increases ATGL activity has not been fully elucidated[27]. In

stark contrast to ATGL, HSL has broad substrate specificity, but the main function is diglyceride (DG) hydrolysis[28]. Phosphorylation of HSL and perilipin (PLIN), a lipid droplet coating protein regulating lipid metabolism, by PKA directly leads to enhanced lipolytic activity and thereby causes an increased release of FAs[29]. These newly released FAs then serve a dual purpose, as they can activate UCP1, on the one hand, and can be oxidized in mitochondria and contribute to maintaining the proton gradient across the inner mitochondrial membrane on the other. This immediate response is complemented by a temporary increase in shivering-based thermogenesis and a simultaneous reduction in heat loss by decreasing thermal conductance[30,31]. Long-term adaptation comprises expressing more UCP1 and expanding oxidative capacity through increased mitochondrial biogenesis in BAT[32,33]. In parallel with the adaptations in existing brown fat cells, BAT expands by recruiting additional new brown adipocytes[34]. Nevertheless, it should be mentioned that WAT also undergoes significant cold-induced remodeling. This whole process is called "browning" and mainly refers to the appearance of UCP1-positive cells within white adipose tissue, which mainly occurs in subcutaneous inguinal white adipose tissue (iWAT)[35]. The resulting cell type is referred to as a brite ("brown in white") or beige (due to color) fat cell, because it represents an intermediate phenotype between brown and white fat cells with respect to UCP1 expression, mitochondrial density, and transcript signature[36,37]. Even though the contribution of NST in brite adipose tissue to total thermogenesis increases with decreasing ambient temperature, BAT still represents by far the largest source of UCP1-mediated NST.

1.4   Life without UCP1: Futile substrate cycles

Considering the important role of BAT and particularly UCP1 in adaptive thermogenesis, it was even more surprising that although UCP1-knockout (UCP1KO) mice are acutely cold sensitive[38], they are in fact able to survive and defend their body temperature when stepwise acclimated to cold[39]. This clearly indicates that alternative UCP1-independent means of heat generation are recruited for adaptive thermogenesis in the absence of UCP1. A very simple and obvious explanation would be that UCP1KO mice dramatically expand their capacity for muscle-based shivering thermogenesis. Nevertheless, the literature on this topic is highly conflicting and contradictory, and ultimately does not support the conclusion that enhanced shivering thermogenesis is sufficient to compensate for the loss of UCP1.

A more elegant but still controversial explanation would be that UCP1KO mice specifically recruit futile substrate cycles for NST in adipose tissues[40]. Futile cycles consist of two or more separate, simultaneously active metabolic pathways or reactions, in which the net effect of the forward reaction catalyzed by one enzyme or a series of enzymes is directly neutralized by the action of the reverse reaction catalyzed by a different enzyme or group of enzymes. As soon as the involved reactions are non-equilibrium reactions, futile substrate cycling activity is by definition coupled to the dissipation of chemical energy as heat, i.e. commonly to the hydrolysis of ATP. Since the forward reaction cancels

out the effect of the reverse reaction, substrate levels do not change and consequently the net effect of "one turn" of the cycle is solely the consumption of ATP[41]. Theoretically, this means that the flux can be enhanced, which increases ATP consumption and at the same time the thermogenic output, while levels of the reactants and products involved still remain constant. And precisely because no net substrate to product conversion is achieved, although chemical energy is being dissipated, the term "futile substrate cycle" was coined. However, the utility of substrate cycles, instead of their futility, is now well appreciated, as more and more aspects that are beneficial were discovered. While the potential advantages may not be immediately obvious, futile cycles, in addition to their contribution to NST, facilitate precise and sensitive metabolic control, and allow greater metabolic flexibility in an energetically challenging setting[42-45]. Futile substrate cycles are a classic, long-standing concept. The underlying theoretical framework was proposed already 60 years ago[46]. In the meantime, numerous examples have been described in various different invertebrate and vertebrate species: An inter-organ lipid cycle involving liver and adipose tissue as well as an intracellular FA/TG cycle in human and rodent adipocytes[47-49], substrate cycling between glycolysis and gluconeogenesis in insects[50], and a futile calcium (Ca^{2+}) cycle in the heater organ of a large pelagic predatory fish, the blue marlin[51]. Since futile substrate cycles were first mentioned in the context of NST, the topic has been picked up from time to time but has meanwhile fallen into oblivion with a few rare exceptions. In particular in the last few years, scientific interest in futile substrate cycles has increased again especially due to the fact that ATP driven cyclic Ca^{2+} pumping[52] and interconversion of creatine/creatine-phosphate[53] were identified as contributors to NST in murine adipose tissues and the control of whole body energy homeostasis. However, these studies have predominantly focused on beige adipose tissue or wild type mice (WT), while we still have only a rudimentary understanding of the thermogenic processes occurring in BAT of UCP1KO mice. Since the metabolic activity of human BAT accounts for only a fraction of total energy expenditure, long-neglected futile substrate cycles may be of much greater importance for energy balance than originally thought[54,55], and therefore deserve considerably more attention.

1.5 Research objective

The primary goal of this work was to investigate alternative thermogenic pathways and their contribution to cellular heat production using brown adipocytes of UCP1KO mice as a paradigm for UCP1-independent heat generation.

1. Therefore, an unbiased pre-selection was conducted in brown UCP1KO adipocytes and the most promising futile substrate cycles, i.e. Ca^{2+}, creatine, and lipid cycling, were examined in more detail.

2. Once a specific mechanism, namely futile lipid cycling, had been objectively determined, efforts were made to identify key enzymes and, ideally, to uncover regulatory mechanisms on a cellular level.

3. In the last step, initial evidence was examined as to whether this futile cycle of lipolysis and re-esterification could also occur *in vivo* and whether the enzymes presumably involved are upregulated in BAT of UCP1KO mice in response to cold exposure.

2 Material & Methods

2.1 Animals

All animals were bred at a specific pathogen-free facility of the Technical University of Munich as approved by the Government of Upper Bavaria and in accordance with the German Animal Welfare Act. Animals were kept under controlled housing conditions (55 % relative humidity, 23 °C ambient temperature, and 12 h/12 h light dark cycle) and had *ad libitum* access to food and water. All mice were killed by CO_2 asphyxiation.

WT and homozygous UCP1KO mice on a 129S1/SvImJ[38] genetic background were used for the isolation of primary pre-adipocytes and subsequent *in vitro* analyses.

WT and homozygous UCP1KO mice on a C57BL/6N[56] genetic background were used to analyze changes in the proteome of iBAT and iWAT upon cold-acclimation (Regierung von Oberbayern, reference number ROB-55.2-2532.Vet_02-16-166). Animals were acclimated to cold as followed: At the age of 8 weeks, male UCP1KO and WT mice were single caged and transferred to climate cabinets set to 23 °C and 55 % relative humidity. From then on, mice were fed a control diet (Snifff Cat. No S5745-E702) and assigned to experimental groups based on body weight. After 1 week at 23 °C, an experimental group (5 °C) was gradually acclimated to cold by decreasing the temperature to 20 °C, 15 °C, 10 °C, and finally 5 °C for 1 week, whereas a control group was kept at 23 °C (23 °C) for 4 weeks. At the end of the experiment, iBAT and iWAT were dissected, weighed, and immediately snap frozen in liquid nitrogen. Tissues were stored at -80 °C until further processing.

2.2 Isolation of primary pre-adipocytes and differentiation into adipocytes

Stromal vascular fraction (SVF) was isolated from iBAT and iWAT of 5 – 7 week old WT and UCP1KO mice as previously described[57]. Adipose tissues were dissected, rinsed with PBS-A, and remaining connective tissue and muscle tissue was removed. Adipose tissue was minced into small pieces (< 1 – 2 mm^3) using scissors, transferred into 15 ml tubes, and 7 ml of collagenase solution were added to start the digestion reaction. Tubes were placed horizontally into an orbital shaker and incubated at 37 °C (120 – 180 rpm) for 45 min to 1 h 15 min. Tubes were vigorously shaken by hand for 10 s every 15 min to facilitate digestion. When almost no visible pieces of adipose tissue were left and the mixture became homogenous, the digestion process was completed. The mixture was filtered through a 250 µm nylon mesh and flow through was collected in a new 15 ml tube. The tube, in which the digestion was carried out, was rinsed with 7 ml of wash buffer. The liquid was then filtered through the same nylon mesh and the flow through combined. Combined flow through was centrifuged at 250 x g for 5 min at room temperature. The tube was carefully inverted several times to break up the fat layer floating on top and centrifuged again at 250 × g for 5 min at room temperature. Fat layer and supernatant were completely removed, 2 ml of an NH$_4$Cl-based red blood cell lysis buffer were added, and the cell pellet was broken up by carefully pipetting up and down. The mixture was incubated for 5 min at room temperature, then 13 ml of wash buffer were added, and the liquid was centrifuged at 500 × g for 5 min at room temperature. Supernatant was completely removed, growth medium was added, and cells were resuspended by carefully pipetting up and down. Prior to seeding, the suspension was filtered through a 40 µm cell strainer into a reagent reservoir or a 10 cm petri dish. When cells were seeded into Seahorse XF24 or XF96 cell culture microplates, plates were left to rest in the cell culture hood for 1 h after seeding. At least 6 h after seeding or on the next day, growth medium was removed and fresh growth medium was added. Growth medium was replaced every other day. When cells reached 80 – 100 % confluency, (day 0) growth medium was replaced with induction medium. After 48 h, (day 2) induction medium was removed and differentiation medium was added. Differentiation medium was replaced every other day for 6 days until cells were considered as fully differentiated adipocytes (day 8).

Table 1: PBS-A

Reagent	Supplier (order number)	Final Concentration
PBS	Fisher Scientific (18912014)	n/a
Penicillin-Streptomycin	Sigma-Aldrich (P4333)	40 units/ml, 40 µg/ml
Gentamicin	Sigma-Aldrich (G1272)	40 µg/ml
Amphotericin B	Sigma-Aldrich (A2942)	500 ng/ml

Table 2: Wash buffer

Reagent	Supplier (order number)	Final Concentration
HBSS	Fisher Scientific (11540476)	n/a
Albumin Fraction V	Carl Roth (8076)	3.5 % (w/v)
Penicillin-Streptomycin	Sigma-Aldrich (P4333)	40 units/ml, 40 µg/ml
Gentamicin	Sigma-Aldrich (G1272)	40 µg/ml
Amphotericin B	Sigma-Aldrich (A2942)	500 ng/ml

Table 3: Collagenase solution

Reagent	Supplier (order number)	Final Concentration
HBSS	Fisher Scientific (11540476)	n/a
Albumin Fraction V	Carl Roth (8076)	3.5 % (w/v)
Glucose	Sigma-Aldrich (G7021)	0.55 mM
Collagenase Type I	Sigma-Aldrich (C1-BIOC)	0.1 % (w/v)
Penicillin-Streptomycin	Sigma-Aldrich (P4333)	40 units/ml, 40 µg/ml
Gentamicin	Sigma-Aldrich (G1272)	40 µg/ml
Amphotericin B	Sigma-Aldrich (A2942)	500 ng/ml

Table 4: Red blood cell lysis buffer, pH 7.3

Reagent	Supplier (order number)	Final Concentration
ddH_2O	n/a	n/a
NH_4Cl	Carl Roth (P726)	154 mM
K_2HPO_4	Carl Roth (T875)	10 mM
EDTA	Carl Roth (8043)	0.1 mM

Table 5: Growth medium

Reagent	Supplier (order number)	Final Concentration
DMEM	Sigma-Aldrich (D5796)	n/a
FBS	Sigma-Aldrich (S0615)	20 % (v/v)
Penicillin-Streptomycin	Sigma-Aldrich (P4333)	40 units/ml, 40 µg/ml
Gentamicin	Sigma-Aldrich (G1272)	40 µg/ml
Amphotericin B	Sigma-Aldrich (A2942)	500 ng/ml

Table 6: Induction medium

Reagent	Supplier (order number)	Final Concentration
DMEM	Sigma-Aldrich (D5796)	n/a
FBS	Sigma-Aldrich (S0615)	10 % (v/v)
Penicillin-Streptomycin	Sigma-Aldrich (P4333)	40 units/ml, 40 µg/ml
Gentamicin	Sigma-Aldrich (G1272)	40 µg/ml
Insulin	Sigma-Aldrich (I9278)	850 nM
T3	Sigma-Aldrich (T2752)	1 nM

Rosiglitazone	Biomol (Cay71740)	1 µM
Dexamethasone	Sigma-Aldrich (D1159)	1 µM
IBMX	Sigma-Aldrich (I5879)	500 µM
Indomethacine	Sigma-Aldrich (I7378)	125 µM

Table 7: Differentiation medium

Reagent	Supplier (order number)	Final Concentration
DMEM	Sigma-Aldrich (D5796)	n/a
FBS	Sigma-Aldrich (S0615)	10 % (v/v)
Penicillin-Streptomycin	Sigma-Aldrich (P4333)	40 units/ml, 40 µg/ml
Gentamicin	Sigma-Aldrich (G1272)	40 µg/ml
Insulin	Sigma-Aldrich (I9278)	850 nM
T3	Sigma-Aldrich (T2752)	1 nM
Rosiglitazone	Biomol (Cay71740)	1 µM

2.3   siRNA-mediated gene silencing

Reverse transfection with Dicer-Substrate Short Interfering RNA (DsiRNA) or Negative Control DsiRNA was carried out on day 7 of the differentiation procedure as previously published[57]. 25 µl of transfection mix (Opti-MEM™ supplemented with 30 µl/ml Lipofectamine™ RNAiMAX and 300 nM DsiRNA) per well were added into a Seahorse XF96 cell culture plate and incubated for 20 min at room temperature. In the meantime, cells were washed twice with PBS. PBS was removed and Trypsin-EDTA-Collagenase solution was added. 6-well cell culture plate was returned to the cell culture incubator and left to incubate for 5 – 10 min. Once cells were detached and floating, differentiation medium without antibiotics was added to inactivate trypsin. Cell suspension was centrifuged at 250 × g for 5 min at room temperature. Supernatant was completely removed and cells were resuspended in differentiation medium without antibiotics. 125 µl of cell suspension were added to each well of a Seahorse XF96 cell culture plate. After 24 h medium was removed and fresh differentiation medium (containing antibiotics) was added. After another 48 h cells were subjected to oxygen consumption analysis (day 10). Following the respiration assay, RNA was isolated from the pooled content of 16 wells of a XF96 cell culture microplate and knockdown efficiency determined by qPCR.

Table 8: Trypsin-EDTA-Collagenase solution

Reagent	Supplier (order number)	Final Concentration
Trypsin-EDTA	Sigma-Aldrich (59417C)	n/a
Collagenase Type I	Sigma-Aldrich (C1-BIOC)	0.05 % (w/v)

Table 9: Transfection mix stock

Reagent	Supplier (order number)	Final Concentration
Opti-MEM™	Fisher Scientific (10149832)	n/a
Lipofectamine™ RNAiMAX	Fisher Scientific (10601435)	30 µl/ml
DsiRNA	Integrated DNA Technologies	300 nM

Table 10: Transfection mix in well

Reagent	Supplier (order number)	Final Concentration
Opti-MEM™	Fisher Scientific (10149832)	n/a
Lipofectamine™ RNAiMAX	Fisher Scientific (10601435)	5 µl/ml (in well)
DsiRNA	Integrated DNA Technologies	50 nM (in well)

2.4 Microplate-based respirometry

Cellular oxygen consumption was measured at 37 °C with an XF24 or XF96 Extracellular Flux Analyzer as previously published[57]. Adipocytes were assayed on day 8 (regular culture conditions) or day 10 (DsiRNA-mediated knockdown). On the day of the assay, all but 20 µl of the differentiation medium was removed and 200 µl of fresh respiration base medium were added. This step was repeated one more time, leaving 20 µl behind after each wash. After the second wash, if not otherwise stated, 160 µl of respiration assay medium were added to each well for a final volume of 180 µl per well (inhibitors were already added to the assay medium and were present in the medium during the measurement). Cells were incubated for 1 hour at 37°C in a laboratory non-CO_2 incubator prior to the measurement. One measurement cycle consisted of a 4 min "Mix", no "Wait", and a 2 min "Measure" period. If not otherwise stated, injections were added in the following order: Isoproterenol (Iso), oligomycin (Oligo), carbonyl cyanide-4-(trifluoromethoxy)phenylhydrazone (FCCP), and antimycin A (AA).

Table 11: Respiration base medium, pH 7.4

Reagent	Supplier (order number)	Final Concentration
ddH$_2$O	n/a	n/a
DMEM	Sigma-Aldrich (D5030)	n/a
Glucose	Sigma-Aldrich (G7021)	25 mM
NaCl	Sigma-Aldrich (S5886)	31 mM
Phenol Red	Sigma-Aldrich (P5530)	15 mg/l
GlutaMAX™	Fisher Scientific (13462629)	2 mM
HEPES	Sigma-Aldrich (H0887)	5 mM

Table 12: Respiration assay medium, pH 7.4

Reagent	Supplier (order number)	Final Concentration
Respiration base medium	n/a	n/a
BSA fatty acid-free	Sigma-Aldrich (A3803)	2 % (w/v)

Table 13: Seahorse injections

Port: Compound (volume per port)	Supplier (order number)	Final concentration in well (μM)
Port A: Oligomycin (20 μl)	Sigma-Aldrich (O4876)	5
Port B: Isoproterenol (22 μl)	Sigma-Aldrich (I6504)	0.1
Port C: FCCP (24 μl)	Sigma-Aldrich (C2920)	7.5
Port D: Antimycin A (27 μl)	Sigma-Aldrich (A8674)	5

Table 14: Seahorse assay command protocol

Steps	Time	Cycles
Calibration		
Equilibration		
Mix	4 minutes	4
Wait	0 minutes	
Measure	2 minutes	
Injection, Port A (Oligomycin)		
Mix	4 minutes	4
Wait	0 minutes	
Measure	2 minutes	
Injection, Port B (Isoproterenol)		
Mix	4 minutes	4
Wait	0 minutes	
Measure	2 minutes	
Injection, Port C (FCCP)		
Mix	4 minutes	3
Wait	0 minutes	
Measure	2 minutes	
Injection, Port D (Antimycin A)		
Mix	4 minutes	4
Wait	0 minutes	
Measure	2 minutes	

2.5   Chemicals and inhibitors

The role of futile substrate cycles in thermogenesis was studied using various chemicals and pharmacologically active substances. Lyophilized reagents were reconstituted in the appropriate solvent and stored according to the supplier's recommendations.

Table 15: Overview of chemicals and inhibitors used

Action/inhibitor target	Chemical/inhibitor name (supplier, order number)	Final concentration in well (µM)	Incubation time (h)
Adrenergic-α,β receptor agonist	Norepinephrine (Sigma-Aldrich, 74480)	0.1	Acute
Adrenergic-β$_3$ receptor agonist	CL-316,243 (Abcam ,ab144605)	0.1	Acute
Adipose triglyceride lipase (ATGL)	Atglistatin (Sigma-Aldrich, SML1075)	40	1
Hormone-sensitive lipase (HSL)	Hi-76-0079 (Schweiger et al.[58])	20	1
Carnitine palmitoyltransferase I (CPTI)	Etomoxir (Sigma-Aldrich, E1905)	50	1
Impairs opening of the mitochondrial permeability transition pore	Cyclosporin A (Sigma-Aldrich, 30024)	4.2	72
Diacylglycerol O-Acyltransferase 1 (DGAT1)	T863 (Sigma-Aldrich, SML0539)	40	16
Diacylglycerol O-Acyltransferase 2 (DGAT2)	PF-06424439 (Sigma-Aldrich, PZ0233)	40	16
Sarco/endoplasmic reticulum Ca^{2+}-ATPase (SERCA)	Thapsigargin (Sigma-Aldrich, T9033)	5	1
Selective Ca^{2+} chelator	BAPTA-AM (Sigma-Aldrich, 196419)	20	1
Shuts down glycolysis/competitive inhibition of glucose-6-phosphate isomerase	2-deoxy-D-glucose (Carl Roth, CN96.3)	50,000	1
Long chain fatty acyl-CoA ligase (or synthetase)	Triacsin C (SCBT, sc-200574)	5	1
Lowers intracellular creatine levels and may competitively inhibit creatine kinase	β-guanidinopropionic acid (Sigma-Aldrich, G6878)	5,000	2
Tissue-nonspecific alkaline phosphatase	MLS0038949 (Merck Millipore,613810)	1	1
AMPK activator	AICAR (Sigma-Aldrich, A9978)	500	1
AMPK inhibitor	Compound C (Merck Millipore, 171261)	50	1

2.6 Quantification of glycerol and free FAs in cell culture supernatant

Adipocytes were cultured in 96-well plates and the release of glycerol and free fatty acids into the medium was measured on day 8. Cells were washed twice with respiration base medium and respiration assay medium was added to a final volume of 180 µl per well (inhibitors were added to the assay medium at this point and were present in the medium during the measurement). The cell culture plate was incubated for 1 hour at 37 °C in a laboratory non-CO_2 incubator. After that, isoproterenol, oligomycin, or a combination of both was added to the medium. The cell culture plate was placed back into a laboratory non-CO_2 incubator and incubated at 37 °C. After an additional hour, conditioned media were harvested and stored for further analysis. Free glycerol was determined with the Free Glycerol Determination Kit (Sigma-Aldrich) and free FAs were quantified with the NEFA-HR(2) Assay (FUJIFILM Wako Chemicals). Free FA re-esterification rate was calculated as previously described[47,59].

$$Free\ FAs\ re\text{-}esterified\ = 3 \times glycerol - free\ FAs$$

2.7 RNA isolation from cultured cells, cDNA synthesis, primer design, and RT-qPCR

Total RNA was isolated by TRIsure™-chloroform extraction and subsequent column purification using columns from the SV Total RNA Isolation System (Promega) according to the manufacturer's recommendations. Cell culture medium was aspirated and cells were washed once with ice cold PBS. PBS was removed and 1 ml TRIsure was added per 10 cm^2 of growth area. Plates were briefly scraped with a cell scraper and the TRIsure/cell lysate was transferred into a new tube. Samples were incubated for 2 min at room temperature and 200 µl of chloroform per 1 ml of TRIsure were added. Tubes were shaken vigorously for 15 s, incubated for 3 min at room temperature, and centrifuged at 12,000 x g for 15 min at 4 °C. The upper, clear, and aqueous phase, which contains RNA, was carefully removed using a pipette and transferred into a new tube. 500 µl of ethanol (75 % in DEPC-treated water) per 1 ml of TRIsure were added to the aqueous phase and the solution was thoroughly mixed. Samples were transferred onto spin columns of the SV Total RNA Isolation and further processed according to Promega's recommendations. RNA concentration was determined spectrophotometrically with a NanoDrop™ 2000. Isolated RNA was stored at -80 °C.

First-strand cDNA synthesis was performed with the SensiFAST™ cDNA Synthesis Kit (Bioline) according to the manufacturer's recommendations. This kit uses a blend of random hexamers and anchored oligo (dT) primers. Maximal 500 ng of RNA were used per 10 µl reaction and cDNA was diluted to a final concentration of 5 ng/µl with nuclease-free water.

Primer pairs were designed and optimized with Primer-BLAST and ordered at Eurofins Genomics Germany. Primer-BLAST was run with default settings, exceptions for: amplicon length (100 – 200

base pairs), primer position on the transcript, which should span an exon-exon junction where possible, total GC content (between 40 % and 60 %) and GC content within the first five 3' bases (<3).

5 ng of cDNA were employed per 12.5 µl qPCR reaction. RT-qPCR was carried out on a LightCycler®480 Real-Time PCR System (Roche) using SensiMix™ SYBR® No-ROX Kit (Bioline). Relative transcript abundance was quantified with an arbitrary standard curve consisting of pooled cDNA from various samples. Relative transcript abundance was normalized to the expression of Gtf2b. After 45 amplification cycles, a melting curve analysis was performed to confirm that only a single amplicon was generated.

Table 16: RT-qPCR reaction mix

Reagent	Supplier (order number)	Final Concentration
Nuclease-free water	n/a	n/a
SensiMix™	Bioline (QT650-05)	1 x
Template cDNA	n/a	0.4 ng/µl
Primer forward	Eurofins Genomics Germany	0.25 µM
Primer reverse	Eurofins Genomics Germany	0.25 µM

Table 17: RT-qPCR cycler command protocol

Step	Temperature	Time	Cycles
Initial denaturation	95 °C	7 min	
Denaturation	95 °C	10 s	
Annealing	53 °C	15 s	45
Elongation	72 °C	20 s	
Melting curve	60 – 95 °C	20 min	

Table 18: RT-qPCR primers

Gene	Forward primer	Reverse primer
Atf3	GAGGATTTTGCTAACCTGACACC	TTGACGGTAACTGACTCCAGC
Atp2a2	ACCTTTGCCGCTCATTTTCCAG	AGGCTGCACACACTCTTTACC
Bip	ACTTGGGGACCACCTATTCCT	ATCGCCAATCAGACGCTCC
Chop	CTGGAAGCCTGGTATGAGGAT	CAGGGTCAAGAGTAGTGAAGGT
Dgat1	GGAATATCCCCGTGCACAA	CATTTGCTGCTGCCATGTC
Dgat2	CCGCAAAGGCTTTGTGAA	GGAATAAGTGGGAACCAGATCAG
Gpd1	CCTTGTGGACAAGTTCCCCTT	GACAGTCCTGATGACGGGTG
Gtf2b	TGGAGATTTGTCCACCATGA	GAATTGCCAAACTCATCAAAACT
Xbp1s	GGTCTGCTGAGTCCGCAGCAGG	AGGCTTGGTGTATACATGG

2.8 Protein isolation, BCA assay and immunoblotting

Total protein was isolated with RIPA buffer. Cells were scraped off the plate and samples were incubated with constant agitation for 15 min at 4 °C. Homogenates were then centrifuged at 16,000 x g for 15 min at 4 °C and supernatant was collected.

Protein concentrations were determined with the Pierce™ BCA Assay Kit (Thermo Fisher Scientific) according to the manufacturer's recommendations. Samples were prepared in Laemmli buffer and 20 µg of protein per lane were loaded onto 4 – 20 % Mini-PROTEAN® TGX Stain-Free™ precast gels (Biorad). Proteins were separated by electrophoresis using a Tris-glycine running buffer. Proteins were blotted onto a nitrocellulose membrane at 1 mA per cm² using the Trans-Blot semi-dry transfer cell (Biorad) and Bjerrum Schafer-Nielsen transfer buffer. Membranes were blocked in 3 % (w/v) BSA in PBS for 3h at room temperature. Membranes were incubated with primary antibody solution overnight at 4 °C. Total OXPHOS Rodent WB Antibody Cocktail (ab110413, Abcam) was diluted 1:1000 and HSP60 (#12165, Cell Signaling Technology) 1:5000 in PBS with 3 % (w/v) BSA. Membranes were washed with PBS-0.1 % Tween-20 for 5 min for a total of four times. Secondary antibodies goat anti-rabbit IRDye® 800CW and donkey anti-mouse IRDye® 680CW were diluted 1:20,000 in PBS with 3 % (w/v) BSA and membranes were incubated for 3 h at room temperature. Membranes were washed again with PBS-0.1 % Tween-20 for 5 min for a total of four times. Prior imaging, membranes were washed with Milli-Q® and dried for 5 min. Membranes were scanned on an Odyssey Infrared Imaging System (LI-COR) and band intensities were quantified using the Image Studio™ Lite Software (LI-COR) v.5.2.

Table 19: RIPA buffer

Reagent	Supplier (order number)	Final Concentration
ddH$_2$O	n/a	n/a
Tris-HCl	Carl Roth (9090)	50 mM
NP-40	Sigma-Aldrich (NP40S)	1 % (v/v)
Sodium deoxycholate	Sigma-Aldrich (D6750)	0.25 % (w/v)
NaCl	Sigma-Aldrich (S5886)	150 mM
EDTA	Sigma-Aldrich (03690)	1 mM
Protease inhibitor	Sigma-Aldrich (P8340)	0.1 % (v/v)

Table 20: Laemmli buffer

Reagent	Supplier (order number)	Final Concentration
ddH$_2$O	n/a	n/a
Tris-HCl, pH 6.8	Carl Roth (9090)	33 mM
SDS	Sigma-Aldrich (L3711)	5 % (w/v)
Glycerol	Sigma-Aldrich (G5516)	25 % (v/v)
Bromophenol blue	Sigma-Aldrich (114391)	0.1 % (w/v)
β-mercaptoethanol	Sigma-Aldrich (M3148)	5 % (v/v)

Table 21: Tris-glycine running buffer, pH 8.3

Reagent	Supplier (order number)	Final Concentration
ddH$_2$O	n/a	n/a
Tris	Carl Roth (4855)	25 mM
Glycine	Sigma-Aldrich (G7126)	250 mM
SDS	Sigma-Aldrich (L3711)	0.1 % (w/v)

2.9 Proteome analysis

Proteome analyses were performed at the Bavarian Center for Biomolecular Mass Spectrometry (Technical University of Munich) and at the Chair of Proteomics and Bioanalytics (TUM School of Life Sciences of the Technical University of Munich).

2.9.1 Cell lysis and protein digestion

Cells lysis was performed by adding 100 µl of lysis buffer consisting of 8 M urea in 50 mM Tris-HCl pH 8, in the presence of EDTA-free protease inhibitors cocktail (Roche) and phosphatase inhibitors mixture. Lysates were then sonicated in a Bioruptor Pico (Diagenode) using a 10 cycles program (30 s on, 30 s off), and cleared by centrifugation for 10 min at 20,000 g and 4 °C. iBAT samples were further lysed by mechanical disruption with single use pestles in protein Lobind tubes and on ice. Protein lysates (100 – 200 µg) were reduced with 10 mM DTT at 37 °C for 40 min, and alkylated with 55 mM chloroacetamide at room temperature for 30 min in the dark. For tryptic digestion, proteins were digested overnight at 37 °C with sequencing grade modified trypsin (Promega, 1:50 enzyme-to-substrate ratio) after 4-fold dilution with 50 mM Tris-HCl, pH 8. Digests were acidified by addition of formic acid (FAc) to 5 % (v/v) and desalted using Sep-Pak C18 cartridges, as previously described[60]. Eluted peptides were then frozen at -80 °C and dried *in vacuo*.

2.9.2 TMT labelling and peptide fractionation

TMT 10-plex or TMTpro 16-plex labeling was performed as previously described[60]. In brief, each digest was resuspended in 20 µl of 50 mM HEPES (pH 8.5). Five µl of 11.6 mM TMT reagents stock solution

(Thermo Fisher) in 100 % anhydrous ACN were then added to each sample. Labeling reaction was carried for 1 h at 25 °C, and quenched by adding 2 µl of 5 % hydroxylamine. Peptide solutions were pooled and acidified using 20 µl of 10 % FAc. The pooled sample was dried *in vacuo*, desalted and stored dried at -80 °C until further use.

For whole proteome analysis of WT and UCP1KO cells, dried peptides were re-suspended in 10 mM ammonium acetate, pH 4.7, and subjected to trimodal mixed mode chromatography on an Acclaim Trinity P1 2.1 × 150 mm, 3 µm column (Thermo Fisher) operated by a Dionex Ultra 3000 HPLC system (Thermo Fisher)[61]. A total of 32 fractions were collected.

For whole proteome analysis of iBAT, dried peptides were re-suspended in 2.5 mM ammonium bicarbonate, pH 8 and subjected to high pH RP fractionation instead, using a Waters XBridge BEH130 C18 2.1 x 150 mm, 3.5 µm column (Waters). Buffer A was 25 mM ammonium bicarbonate (pH = 8), buffer C was 100 % ultrapure water, buffer D was 100 % CAN. The proportion of buffer A was kept at 10 % at all times. Peptides were separated by a linear gradient from 7 % D to 45 % D in 44 min, and followed by a linear gradient from 45 % D to 85 % D in 6 min. A total of 96 fractions were collected every 30 seconds, and then concatenated to 48 fractions by adding fraction 49 to fraction 1, fraction 50 to fraction 2 and so forth.

All fractions were dried *in vacuo* and stored at -20 °C until nLC-MS/MS analysis.

2.9.3   LC-MS/MS

Nano flow LC-ESI-MS measurements were performed using a Dionex Ultimate 3000 UHPLC+ system coupled to a Fusion Lumos Tribrid mass spectrometer (Thermo Fisher). Peptides were delivered to a trap column (75 µm × 2 cm, packed in-house with 5 µm Reprosil C18 resin; Dr. Maisch) and washed using 0.1 % FAc at a flow rate of 5 µl/min for 10 min. Subsequently, peptides were transferred to an analytical column (75 µm × 45 cm, packed in-house with 3 µm Reprosil C18 resin, Dr. Maisch) applying a flow rate of 300 nl/min. Peptides were chromatographically separated using a 50 min linear gradient from 8 % to 34 % solvent B (0.1 % FAc, 5 % DMSO in ACN) in solvent A (0.1 % FAc in 5 % DMSO).

For the iBAT samples, the Fusion Lumos Tribrid mass spectrometer was coupled to a micro-flow LC-MS/MS system using a modified Vanquish pump (Thermo Fisher). Chromatographic separation was performed via direct injection on a 15 cm Acclaim PepMap 100 C18 column (2 µm, 1 mm ID, Thermo Fisher Scientific) at a flow rate of 50 µl/min, using a 25 min linear gradient (4 % to 28 %) of solvent B (0.1 % FAc, 3 % DMSO in ACN) and solvent A (0.1 % FAc in 3 % DMSO). The total measurement time for each sample was 27 min.

The Fusion Lumos was operated in a data-dependent acquisition (DDA) to automatically switch between MS and MS/MS. Briefly, survey full-scan MS spectra were recorded in the Orbitrap from m/z 360 to 1300 at a resolution of 60K, using an automatic gain control (AGC) target value of 4e5 charges and maximum injection time (maxIT) of 50 ms.

For the MS3-based TMT method, initial MS2 spectra for peptide identification were recorded in the ion trap in rapid scan mode with a top speed approach using a 2-s duration (isolation window m/z 0.7, AGC target value of 1e4, maxIT of 35 ms). Fragmentation was set to CID, with a NCE of 35 % and 0.25 activation Q. Then, for each peptide precursor, an additional MS3 spectrum for TMT quantification was obtained in the Orbitrap at 50K resolution (AGC of 5e4 charges, maxIT of 86 ms). The precursor was fragmented as for the MS2 analysis, followed by synchronous selection of the 10 most intense peptide fragments and further fragmentation via HCD using a NCE of 55 %. Dynamic exclusion was set to 90 s.

For the analysis of the TMTpro 16-plex samples, the following parameters were modified: top speed method duration of 1.2-s, isolation window m/z 0.6, AGC target value of 1.2e4, maxIT of 40 ms, fragmentation was set to HCD with a NCE of 32 %. MS3 ACG was set 1e5 charges, number of notches 8, and dynamic exclusion was set to 50 s.

2.9.4   Data processing

Peptide and protein identification and quantification was performed using MaxQuant (version 1.6.0.43) and its built in search engine Andromeda[62]. Spectra were searched against the UniProtKB database (Mus musculus, UP000000589, 55431 entries downloaded on 12.2019). Enzyme specificity was set to trypsin, allowing for 2 missed cleavages, and the search included cysteine carbamidomethylation as a fixed modification and Ntem-acetylation of protein, oxidation of methionine as variable modifications. TMT10 was set as label within a reporter ion MS3 experiment type. Precursor tolerance was set to 5 ppm, and fragment ion tolerance to 20 ppm. Results were adjusted to 1 % false discovery rate at protein, peptide, and site levels.

TMTpro 16-plex raw data file recorded by the mass spectrometer were processed and quantified with Proteome Discoverer (version 2.4, Thermo Scientific). Peak lists were generated with Proteome Discoverer with a signal-to-noise threshold of 1.5 and searched against the UP000000589 UniProtKB database using SequestHT as search engine. The database search was performed with the following parameters: a mass tolerance of ± 10 ppm for precursor masses, ± 0.6 Da for HCD-Ion trap fragment ions; two missed cleavages allowed; and cysteine carbamidomethylation as a fixed modification. Methionine oxidation and protein N-term acetylation were set as variable modifications. The enzyme was specified as trypsin, with a minimum peptide length of 6 amino acids. . All PSMs were validated with Percolator[63], and results were adjusted to 1 % false discovery rate at protein, peptide and PSM

level within Proteome Discoverer. TMTpro was set as label (static modification) and used by the Reporter Ions Quantifier node for the peptide and protein quantification. Default settings were used.

The mass spectrometry proteomics data have been deposited in the ProteomeXchange Consortium via the PRIDE partner repository[64] with the dataset identifier PXD025854.

2.9.5 Bioinformatic analysis

Data analysis was performed in Perseus (v. 1.6.1.1 and v. 1.6.15.0)[65] and R[66]. Proteome datasets were filtered to remove contaminants and decoy identifications, before performing data normalization of the intensity values by median centering, as implemented in Perseus.

For statistical tests, only proteins that have been quantified in at least 3 biological replica were considered. To identify significantly regulated proteins Welch's t-test was used, corrected for multiple hypotheses using a Benjamini-Hochberg false discovery rate of 5 %.

iBAT proteome dataset was filtered to retain only proteins that have been quantified in all the 4 biological replica in at least one experimental condition, and missing values were imputed in Perseus using default settings. Here, to identify significantly modulated proteins ANOVA test was used, corrected for multiple hypotheses using a Benjamini-Hochberg false discovery rate of 5 %, and followed by Tukey HSD post-hoc test in R. Heatmaps were generated in R using the package "pheatmap". Normalized protein intensities were scaled in the row direction and rows were clustered by Euclidean distance.

Gene ontology (GO) annotations were downloaded from UniProt. Categorical annotation was supplied by Gene Ontology biological process, molecular function, and cellular component; and the KEGG pathway database. The GO terms enrichment was calculated on the basis of a fisher's exact test with 0.05 false discovery rate. Scores were plotted as a two-dimensional annotation enrichment score[67].

2.10 Electron microscopy

Electron microscopy was performed at the Institute of Molecular Toxicology and Pharmacology (Helmholtz Center Munich) and at the Institute of Toxicology and Environmental Hygiene (TUM School of Medicine of the Technical University of Munich).

For electron microscopy, cells were grown in flat BEEM capsules (Plano GmbH, Wetzlar, Germany). Samples were fixed with 2.5 % glutaraldehyde in 0.1 M sodium cacodylate buffer, pH 7.4 (Electron Microscopy Sciences, Hatfield, USA) for 24 h at minimum. Thereafter glutaraldehyde was removed and samples were washed three times with 0.1 M sodium cacodylate buffer, pH 7.4. Postfixation and prestaining was done for 30 min with 1 % osmium tetroxide (10 ml 4 % osmium tetroxide (Electron

Microscopy Sciences), 10 ml ddH2O, 10 ml 3.4 % sodium chloride and 10 ml 4.46 % potassium dichromate (pH adjusted to 7.2 with KOH (Sigma Aldrich)). Samples were washed three times with 0.1 M sodium cacodylate buffer, pH 7.4 and dehydrated with an ascending ethanol series (10 min with 30 %, 50 %, 70 %, 90 % and 96 %, respectively, two times 20 min with 100 %, and 20 min with dehydrated EtOH (molecular sieve 3A°)). For embedding, EtOH was stepwise replaced by Epon (3.61 M glycidether 100, (Serva Electrophoresis GmbH), 1.83 M methylnadicanhydride (Serva Electrophoresis GmbH), 0.92 M dodecenylsuccinic anhydride (Serva Electrophoresis GmbH), 5.53 mM 2,4,6-Tris(dimethylaminomethyl)phenol (Serva Electrophoresis GmbH)). First, 20 min with Epon:100 % EtOH at a ratio of 1:1, then 20 min with Epon:100 % EtOH at a ratio of 2:1, then Epon overnight, lastly replacement with fresh Epon. The embedded samples were hardened at 60 °C for 48 h. Ultrathin sections were sliced with an Ultramicrotome (Ultracut E; Reichert und Jung, Germany) and automatically stained with UranyLess EM Stain (Electron Microscopy Sciences) and 3 % of lead citrate (Leica, Wetzlar, Germany) using the contrasting system Leica EM AC20 (Leica, Wetzlar, Germany). The samples were examined with a JEOL-1200 EXII transmission electron microscope (JEOL GmbH, Freising, Germany). Images were taken using a digital camera (KeenViewII, Olympus, Germany) and processed with the iTEM software package (anlySISFive; Olympus, Germany). Images were analyzed with Fiji[68]. Cytoplasmic and peridroplet mitochondria were manually counted. Mitochondria were classified as cytoplasmic mitochondria, if no clear contact site between mitochondrial and lipid droplet membrane was identified. Mitochondria were classified as peridroplet mitochondria, if at least one contact site was detected (the mitochondrial membrane could not be distinguished from the lipid droplet membrane). Lipid droplet perimeter as well as the sections of the lipid droplet perimeter occupied by mitochondria was manually quantified.

2.11 Statistical analyses

If not stated otherwise, data are presented as mean ± SEM.

Comparison of two groups: Normal distribution of data was tested using the Shapiro-Wilk test. Normally distributed data were compared with an unpaired t-test. When data violated the assumptions for a t-test, a Welch-test was performed.

Comparison of three or more groups: Normal distribution of residuals was tested using the Shapiro-Wilk test, and homogeneity of variance was assessed by Levene's test. If ANOVA's assumptions were met, one-way or two-way ANOVA was performed followed by Tukey's HSD multiple comparisons. When data violated the assumptions for an ANOVA, a Kruskal-Wallis one-way or two-way ANOVA was performed followed by multiple comparisons with a Bonferroni-corrected Mann-Whitney U test.

Values of $p < 0.05$ were considered statistically significant.

3 Results

Part of the data has already been published in a similar version[69].

3.1 Proteins associated with futile calcium and lipid cycling are acutely upregulated during active lipolysis in brown UCP1-knockout adipocytes

Multiple potentially thermogenic processes based on futile substrate cycles in adipose tissue of WT and UCP1KO mice have been discovered[40,53,70,71]. So far, these processes have only been studied separately, sometimes even in different model systems. Based on the assumption that futile substrate cycles contributing to NST are preferentially found in adipocytes lacking UCP1, we hypothesized that isoproterenol treatment of brown adipocytes from UCP1KO mice would cause an immediate acceleration of futile substrate cycling, and entail a consecutive upregulation of the involved enzymes providing additional capacity. Therefore, the cellular response of brown UCP1KO adipocytes to acute adrenergic stimulation was probed at the protein level to identify differentially expressed candidates and upregulated pathways for further investigation in an unbiased manner (Figure 1A). Enriched pathways and terms presumed as potentially thermogenic (Figure 1B) were either related to Ca^{2+} metabolism ("cardiac muscle contraction", "muscle contraction"), lipid metabolism ("cellular lipid metabolic process", "glycerophospholipid metabolism"), or the electron transport chain ("oxidative phosphorylation", "hydrogen transport"). No significantly regulated term specifically related to creatine metabolism was found, but this may be explained by the annotation of proteins associated to futile creatine cycling, as they are only part of a very limited number of categories in general, and these categories have either very few entries (less than 15) or numerous entries (more than 1000).

A

-/+ Isoproterenol

UCP1KO

TMT labeling & sample processing

LC-MS/MS & Data analysis

Intensity

m/z

B

GO: Biological Process

KEGG: Pathway

-log10 (pvalue)

-log10 (pvalue)
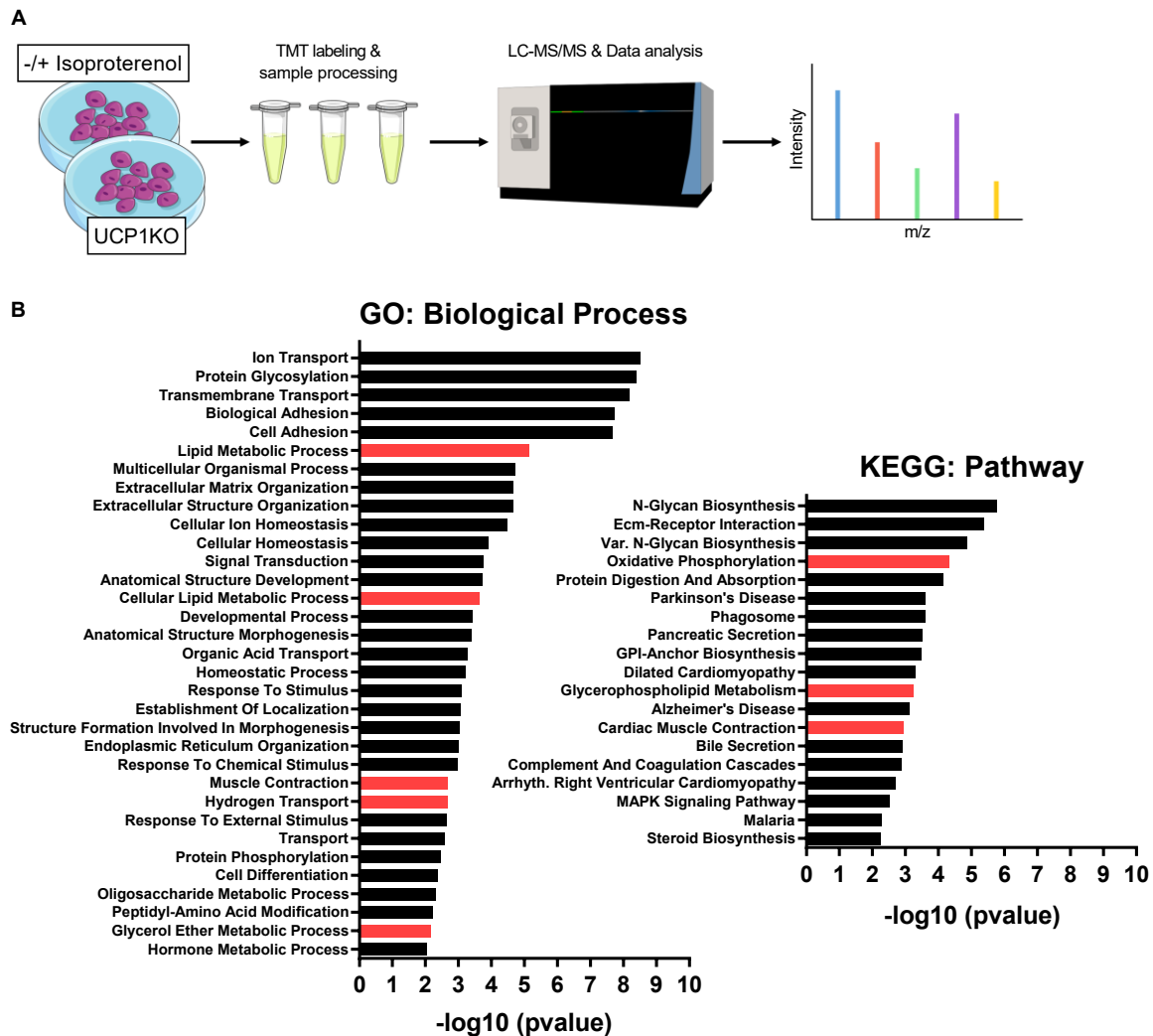
Figure 1: Pathways associated with futile calcium and lipid cycling are acutely upregulated during active lipolysis in brown UCP1-knockout adipocytes. A) Schematic depiction of sample generation, processing, and subsequent proteome analysis. Primary cultures of fully differentiated 129Sv/S1 brown UCP1-knockout (UCP1KO) adipocytes were stimulated with 500 nM isoproterenol (Iso) for 30 minutes. Pathway enrichment comparing Iso versus no treatment (Con) was performed. B) Pathway enrichment analysis showing biological processes and pathways, which are significantly upregulated upon adrenergic stimulation in brown UCP1KO adipocytes; GO: Biological process (left) and KEGG: Pathway (right). Terms related to futile substrate cycles are highlighted in red. The complete set of analyzed data can be found online as supplementary data to this article[69]. n = 5 independent biological experiments.

When looking at individual enzymes involved in the transport of Ca^{2+} into the endoplasmic reticulum (ER), i.e. sarco/endoplasmic reticulum Ca^{2+} ATPase (SERCA) isoforms, and the efflux of Ca^{2+} back into the cytosol, such as inositol triphosphate receptor and ryanodine receptor isoforms, we correspondingly observed a strong induction upon adrenergic stimulation (Figure 2A). Moreover, brown adipocytes lacking UCP1 also showed a pronounced upregulation of enzymes that directly or indirectly participate in TG (re-)synthesis (Figure 2B). Although not indicated by the pathway enrichment analysis, two out of three creatine kinase (CK) isoforms and the tissue nonspecific alkaline phosphatase (TNAP) were induced during active lipolysis (Figure 2A).

A **Futile Ca²⁺ & Creatine Cycling**
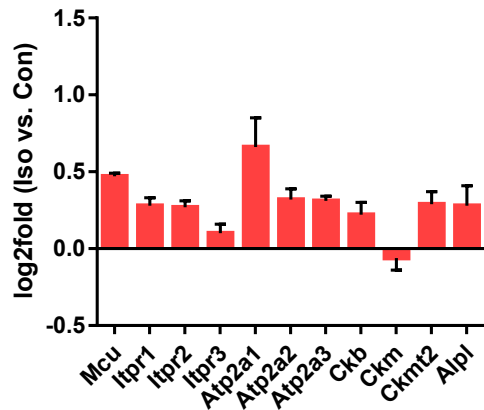
B **Futile FA/TG cycling**
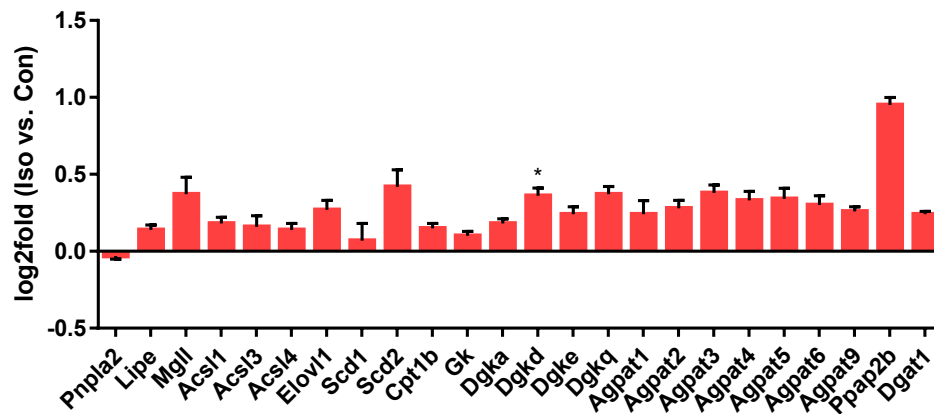
Figure 2: Adrenergic stimulation causes an upregulation of enzymes associated with futile calcium, creatine, and fatty acid/triglyceride cycling in brown UCP1-knockout adipocytes. Change of expression levels of selected proteins in primary cultures of 129Sv/S1 UCP1-knockout (UCP1KO) adipocytes in response to an adrenergic stimulus. n = 5 independent biological experiments. Asterisk (*) indicates a significantly regulated protein in response to the treatment. Proteins are designated by their gene name in parentheses: Mitochondrial calcium uniporter (Mcu), inositol 1,4,5-trisphosphate receptor type 1 (Itpr1), inositol 1,4,5-trisphosphate receptor type 2 (Itpr2), inositol 1,4,5-trisphosphate receptor type 3 (Itpr3), ATPase sarcoplasmic/endoplasmic reticulum Ca²⁺ transporting 1 (Atp2a1), ATPase sarcoplasmic/endoplasmic reticulum Ca²⁺ transporting 2 (Atp2a2), ATPase sarcoplasmic/endoplasmic reticulum Ca²⁺ transporting 3 (Atp2a3), creatine kinase B (Ckb), creatine kinase, M-type (Ckm), creatine kinase, mitochondrial 2 (Ckmt2), patatin like phospholipase domain containing 2 (Pnpla2), lipase E hormone sensitive type (Lipe), monoglyceride lipase (Mgll), acyl-CoA synthetase long chain family member 1 (Acsl1), acyl-CoA synthetase long chain family member 3 (Acsl3), acyl-CoA synthetase long chain family member 4 (Acsl4), ELOVL fatty acid elongase 1 (Elovl1), acyl-CoA desaturase 1 (Scd1), acyl-CoA desaturase 2 (Scd2), carnitine palmitoyltransferase 1B (Cpt1b), glycerol kinase (Gk), diacylglycerol kinase alpha (Dgka), diacylglycerol kinase delta (Dgkd), diacylglycerol kinase epsilon (Dgke), diacylglycerol kinase theta (Dgkq), 1-acylglycerol-3-phosphate O-acyltransferase 1 – 5 (Agpat1 – 5), glycerol-3-phosphate acyltransferase 4 (Agpat6), glycerol-3-phosphate acyltransferase 3 (Agpat9), phospholipid phosphatase 3 (Ppap2b), diacylglycerol O-acyltransferase 1 (Dgat1). A) Proteins associated with futile Ca²⁺ and creatine cycling. B) Proteins involved in futile FA/TG cycling.

Taken together, particular changes in the cellular proteome upon adrenergic stimulation detected in brown UCP1KO adipocytes suggested the presence of a futile Ca²⁺, a futile creatine, and a futile FA/TG substrate cycle acting separately or in a coordinated manner.

3.2 Acute stimulation of brown adipocyte respiration by adrenergic agonists

For a long time it has been known that adipocytes with very low UCP1 levels drastically increase their oxygen consumption in response to an adrenergic stimulus[46]. However, not too long ago the same phenomenon was described in brown and beige UCP1KO adipocytes[72].

To dissect the individual factors contributing to increased energy turnover and elevated respiration rates, brown WT and UCP1KO adipocyte bioenergetics were characterized in more detail. Basal oxygen consumption rates were not different between WT and UCP1KO cells, and the magnitude of the increase following the addition of isoproterenol was comparable (Figure 3A).
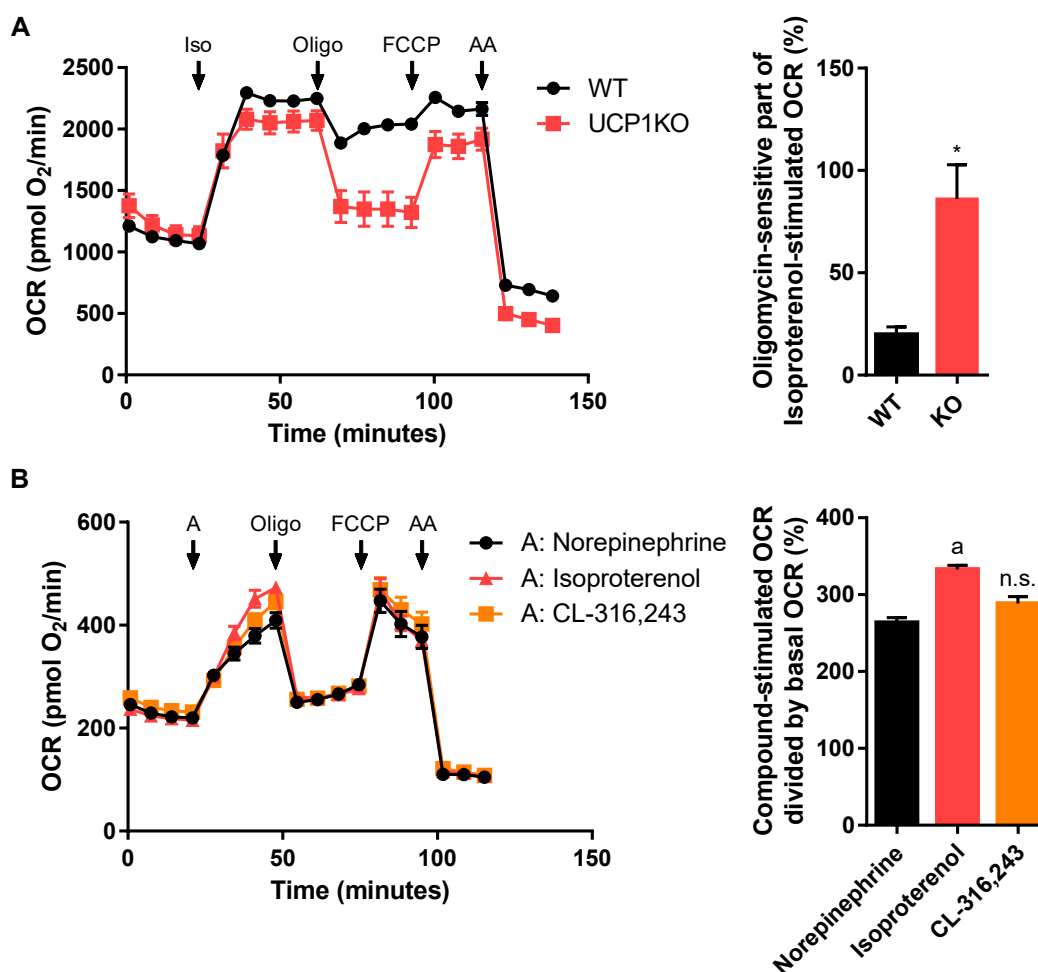
Figure 3: Adrenergic stimulation activates ATP consuming processes and increases oxygen consumption in murine brown UCP1-knockout adipocytes. A) Seahorse XF24 extracellular flux measurement of primary cultures of fully differentiated 129Sv/S1 brown wild type (WT) and UCP1-knockout (UCP1KO) adipocytes and quantification of the oligomycin-sensitive part of stimulated oxygen consumption rate (OCR). n = 10 – 12 wells from two independent biological experiments. A two-tailed Welch-test was applied. Asterisk (*) indicates a significant difference between the two groups. Isoproterenol (Iso), oligomycin (Oligo), carbonyl cyanide-4-(trifluoromethoxy)phenylhydrazone (FCCP), antimycin A (AA). B) Seahorse XF96 extracellular flux measurement of primary cultures of fully differentiated 129Sv/S1 brown UCP1-knockout (UCP1KO) adipocytes. Cells were acutely treated with norepinephrine (100 nM final), isoproterenol (100 nM final), or CL-316,243 (100 nM final) and the compound-dependent increase in OCR over basal OCR was quantified. (Continued on next page)

Nevertheless, oligomycin had a significant genotype-dependent effect on respiration, as it caused respiration rates of brown WT cells to drop only by around 20 %, whereas oxygen consumption of brown UCP1KO cells decreased by more than 85 %. Since oligomycin causes a transient hyperpolarization of the inner mitochondrial membrane, leak respiration after the addition of oligomycin is systematically overestimated due to the non-ohmic nature of mitochondrial proton leak[73]. Therefore, the isoproterenol-induced steep rise in oxygen consumption can be virtually completely reversed by blocking the mitochondrial ATP synthase with oligomycin. As mitochondrial ATP synthesis only increases when a higher cellular ATP demand has to be met, and cellular oxygen consumption grows proportionally with mitochondrial ATP synthesis, ATP turnover is supposedly proportional to the activity of futile substrate cycles. Consequently, oligomycin-sensitive respiration rates after the addition of isoproterenol were used as a surrogate marker to estimate the activity of futile substrate cycles in brown UCP1 adipocytes.

Moreover, brown UCP1KO adipocytes were treated with three different adrenergic agonists at identical molar concentrations to determine which adrenergic receptor isoform(s) mediate the effect on oxygen consumption rates. Norepinephrine, an α,β adrenergic receptor agonist, isoproterenol, a selective β receptor agonist, and CL 316243, a selective β_3 receptor agonist, all evoked a similarly powerful response (Figure 3B). There was no statistically significant difference between the norepinephrine and CL 316243, and between the CL 316243 and isoproterenol responses. This clearly indicates that the majority of the effect following adrenergic stimulation is mediated by the β_3 adrenergic receptor. Nevertheless, isoproterenol was numerically slightly more potent than CL 316243 and significantly more potent than norepinephrine in stimulating cellular oxygen consumption, and therefore isoproterenol was used for all following experiments.

Taken together, the decisive difference between brown WT and UCP1KO adipocytes is that stimulated respiration rates in WT cells are largely driven by UCP1, and consequently oligomycin-insensitive, while oxygen consumption in UCP1KO cells is almost fully sensitive to oligomycin treatment. This clearly proves that brown UCP1KO adipocytes markedly ramp up aerobic ATP production and futile substrate cycling activity following an adrenergic stimulus, which is predominantly mediated via β_3-adrenergic signaling *in vitro*.

3.3 Futile calcium cycling does not contribute to non-shivering thermogenesis in brown and brite UCP1-knockout adipocytes

To decipher the mechanism underlying elevated oxygen consumption and ATP turnover of brown UCP1KO adipocytes, we concentrated first on ATP-dependent Ca^{2+} cycling that was proposed to mediate NST in beige UCP1KO adipocytes[70]. Mechanistically, adrenergic signaling is thought to activate sarco/endoplasmic reticulum Ca^{2+} ATPase2b (SERCA2b) and the ryanodine receptor 2 (RyR2). This leads to ATP-dependent uptake of Ca^{2+} into the ER by SERCA2b and the transport of Ca^{2+} back into the cytosol via RyR2, thereby uncoupling mitochondrial oxygen consumption from oxidative phosphorylation.

Initially, Atp2a2, which is coding for SERCA2b, was knocked down to test the contribution of futile Ca^{2+} cycling to NST in our model of brown UCP1KO adipocytes. Cells treated with a DsiRNA targeting Atp2a2 did not differ significantly from the control group in any parameter, despite having a more than 80 % reduced endogenous expression of Atp2a2 (Figure 4A). Nevertheless, cells that received DsiRNA showed a trend towards slightly reduced respiration rates following the addition of isoproterenol, but the difference was rather small and did not reach statistical significance. Still, it should be mentioned that this concept of futile Ca^{2+} cycling was primarily studied in beige adipocytes. Consequently, it was tested whether this mechanism would then contribute to NST in beige UCP1-ablated adipocytes or whether this mechanism plays no role at all pertaining NST in the UCP1KO model system employed here. Therefore, the SERCA2b knockdown experiment was repeated in beige UCP1KO adipocytes with a very similar outcome. Although endogenous Atp2a2 expression was reduced by almost 75 %, the oxygen consumption traces of the control and the DsiRNA group hardly differed and the response to isoproterenol was not attenuated (Figure 4B).
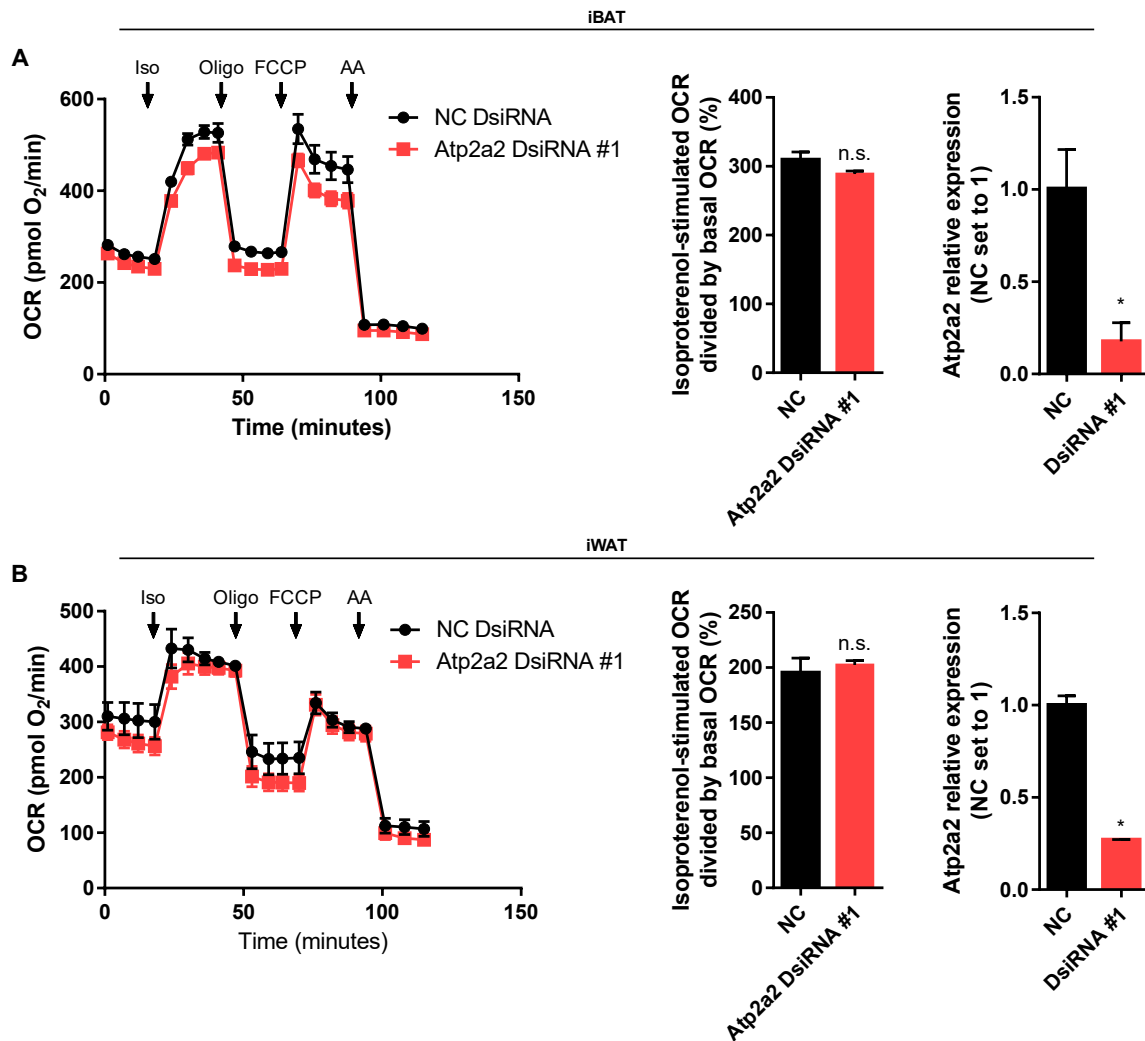
Figure 4: SERCA2b does not contribute to cellular thermogenesis in brown UCP1KO adipocytes. A) & B) XF96 extracellular flux measurements of primary cultures of fully differentiated 129Sv/S1 brown and brite UCP1-knockout (UCP1KO) adipocytes. Atp2a2 was knocked down in brown (A) and brite (B) UCP1KO adipocytes with DsiRNA as described in "Material & Methods" and the isoproterenol-induced increase in OCR (middle) was calculated. n = 17 − 25 wells (A) and 15 − 22 wells (B) from three independent biological experiments, respectively. A two-tailed t-test was applied. Not statistically significant (n.s.). Knockdown-efficiency (right) was determined by measuring the relative expression of Atp2a2. Content of all wells from one group was pooled within each biological experiment. n = 3 from three independent biological experiments, respectively. A two-tailed t-test was applied. Asterisk (*) indicates a significant difference between the two groups.

However, as another SERCA isoform might have compensated for the knockdown of Atp2a2, or a different isoform besides SERCA2b may mediate Ca^{2+} cycling in our experimental system, UCP1KO adipocytes were acutely treated with thapsigargin, a potent non-competitive inhibitor of all SERCA isoforms[74]. Since it was known that thapsigargin could modulate oxygen consumption[75], it was added to the medium just during the measurement, which enabled monitoring the isolated effect of thapsigargin on respiration rates in real-time. As already assumed and in line with previous publications, thapsigargin caused a very fast and pronounced increase in oxygen consumption rates. Nevertheless, in good agreement with the outcome of the knockdown experiments, pharmacological inhibition of SERCA did not decrease maximal oxygen consumption rates in response to adrenergic

stimulation. Similarly to the knockdown approach, thapsigargin had no effect in either brown or beige UCP1KO adipocytes (Figure 5A and B).
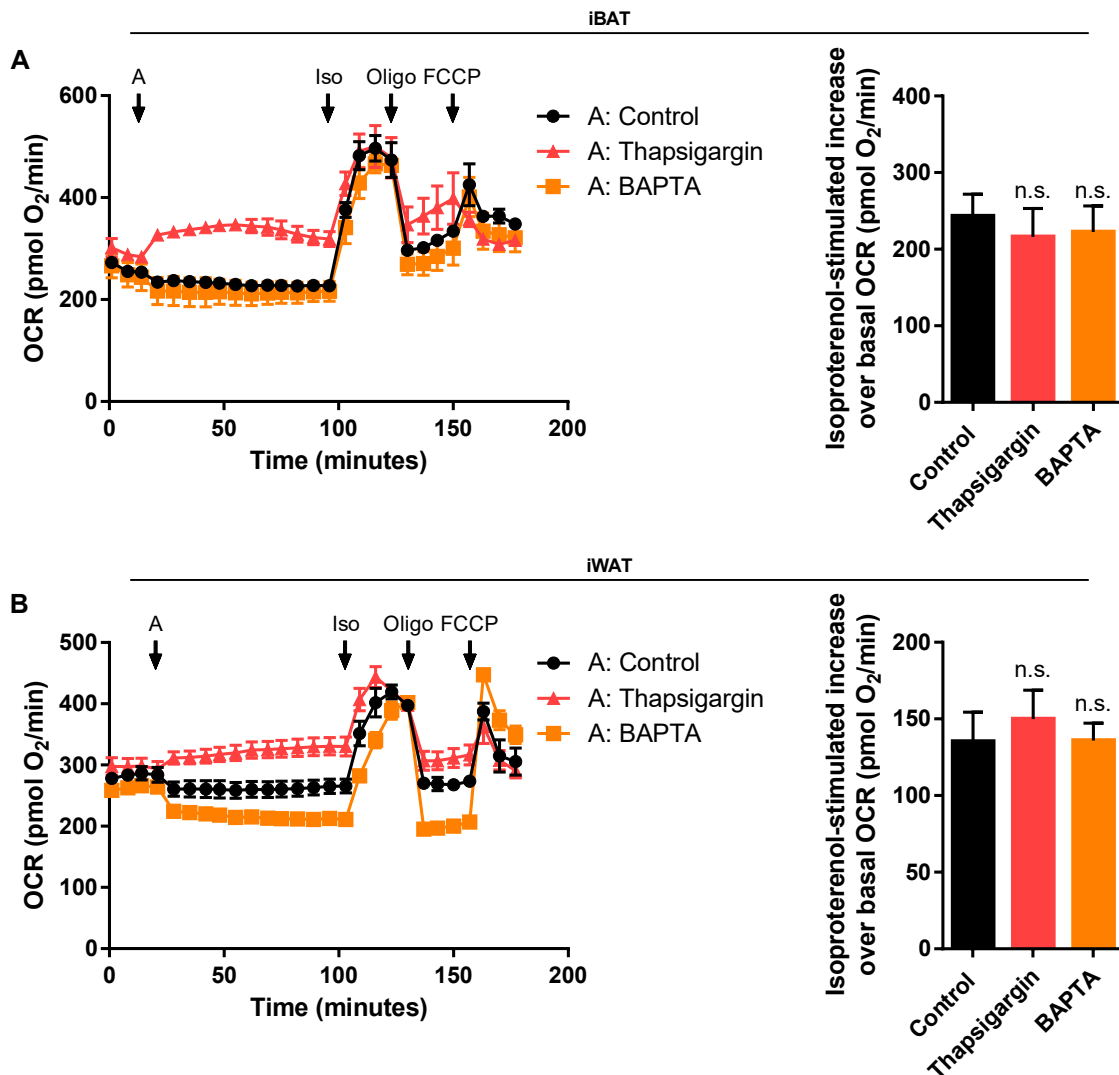
Figure 5: Futile calcium cycling does not contribute to non-shivering thermogenesis in murine brown and brite UCP1-knockout adipocytes. A) & B) *XF96 extracellular flux measurements of primary cultures of fully differentiated 129Sv/S1 brown and brite UCP1-knockout (UCP1KO) adipocytes. Brown **(A)** and brite **(B)** UCP1KO adipocytes were acutely treated with thapsigargin (5 µM final) or BAPTA (20 µM final) for 1 h and the response to isoproterenol was monitored. Compounds were added as an injection via port "A". The isoproterenol-induced increase in OCR over basal OCR (right) was calculated. n = 18 – 23 wells (A) and 16 – 20 wells (B) from three independent biological experiments, respectively. One-way ANOVA followed by Tukey's HSD was applied. Not statistically significant (n.s.).*

Even though the absolute increase induced by isoproterenol was smaller in cells treated with thapsigargin, this is only an artefact, because the acute injection of thapsigargin already led to higher respiration rates. To finally rule out any major contribution of futile Ca^{2+} cycling to cellular thermogenesis, intracellular Ca^{2+} flux was interrupted in a broad and untargeted manner by depleting endogenous Ca^{2+} levels using BAPTA[76], a highly selective Ca^{2+} chelator. BAPTA caused cellular

respiration to decrease slightly, but no effect on ATP turnover driving respiration rates stimulated by isoproterenol was detected (Figure 5A and B). Although the proteome analysis has revealed an upregulation of enzymes mediating a putative Ca^{2+} substrate cycle in brown UCP1KO adipocytes, the respirometry data clearly demonstrated that Ca^{2+} cycling is not the prime cause of increased energy turnover during adrenergic stimulation.

3.4 Futile creatine cycling does not mediate thermogenesis in brown UCP1-knockout adipocytes

The second candidate identified by the preceding analysis was a futile creatine substrate cycle. Just recently, the two proteins regulating futile creatine cycling in BAT were defined. Creatine kinase B (CKB) catalyzes the phosphorylation of creatine[77], which in turn consumes ATP, and generates phosphocreatine and adenosine diphosphate (ADP). TNAP simultaneously hydrolyzes phosphocreatine and regenerates creatine[78], thereby completing the futile cycle.
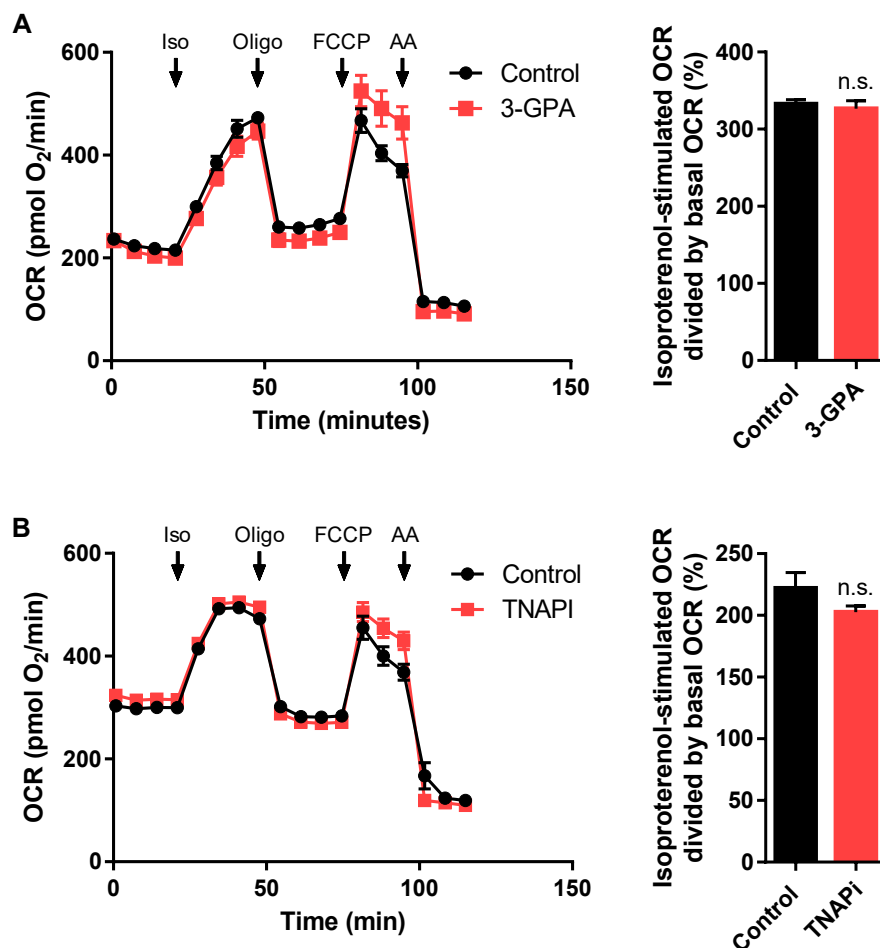
Figure 6: Futile creatine cycling does not mediate UCP1-independent thermogenesis in brown UCP1-ablated adipocytes. A) & B) XF96 extracellular flux measurements of primary cultures of fully differentiated 129Sv/S1 brown UCP1-knockout (UCP1KO) adipocytes. (Continued on next page)

Accordingly, the contribution of futile creatine cycling was determined by treating brown UCP1KO adipocytes with 3-guanidinopropioinic acid (3-GPA)[79], which effectively limits the amount of available intracellular creatine. 3-GPA is a creatine analogue that impairs creatine uptake and supposedly inhibits CK in a competitive manner. Yet again, there was no difference between the control and treatment group (Figure 6A). However, after it was not possible to verify whether 3-GPA in fact lowered creatine levels or attenuated CK activity, TNAP was the next logical target. Adipocytes were acutely treated with a highly selective and well-established TNAP inhibitor[80], but no effect on oxygen consumption per se and in particular following the addition of isoproterenol was detected (Figure 6B).

In summary, no evidence for a contribution of futile creatine cycling to NST in brown UCP1KO adipocytes was found.

3.5   Brown UCP1-knockout adipocytes recruit a futile cycle of lipolysis and fatty acid re-esterification for adaptive thermogenesis

The third and last candidate that emerged from the pre-selection was a futile substrate cycle related to TG metabolism, which at the same time is the oldest concept of the three mechanisms under consideration. Two mechanistically different futile cycles associated with defined subcomponents of lipid metabolism were proposed in the past: The first option is a cycle comprising lipolysis and re-esterification of FAs[47-49,54,81-87]. FAs released from TGs, DGs and monoglycerides (MGs) are believed to be immediately re-esterified onto glycerol-3-phosphate (G3P), MGs, and DGs (for ease of use, this cycle will be referred to as "FA/TG cycle"). The second option is a cycle consisting in degradation of FAs through β-oxidation, and *de novo* FA synthesis (this cycle will be referred to as "FAO/DNL cycle")[88]. In both cases, the activation of FAs, i.e. the ATP-dependent conversion of a FA into fatty acyl-coenzyme A (fatty acyl-CoA), would be the step that consumes energy. While the re-esterification of FAs onto a glycerol backbone necessarily requires prior activation, equally only fatty acyl-CoAs can be imported into mitochondria, where they then undergo β-oxidation. In addition, the formation of malonyl-CoA by acetyl-CoA carboxylase, which plays a key role in chain elongation during FA biosynthesis, also consumes ATP.

3.5.1 Futile lipid cycling depends on lipolysis

Since there were no particular key enzymes explicitly linked to futile lipid cycling defined at that time, a top-bottom approach was chosen by starting from very basic and general pathways, and then proceeding to refine subcomponents in yet greater detail.

Lipolysis is a key pathway in lipid metabolism directly connected to and downstream of canonical adrenergic receptor-cAMP-PKA-signaling[26]. ATGL and HSL are the main lipases, which predominantly mediate the enzymatic hydrolysis of TGs and DGs, and account for the majority of newly released FAs. Blocking HSL and ATGL activity with inhibitors[58,89] would clearly indicate whether the release of FAs from intracellular lipid stores acutely contributes to futile lipid cycling and the increased energy turnover it potentially entails. Both inhibitors and a combination of the two substances had only a minimal or no effect on basal oxygen consumption, which in turn shows that the lipolytic capacity is far from being fully exhausted under normal conditions. HSL inhibition clearly reduced the isoproterenol-induced rise in oxygen consumption of brown UCP1KO adipocytes by around 25 %, albeit without reaching statistical significance (Figure 7). Inhibiting ATGL, however, had a very pronounced effect, as the response to adrenergic stimulation was blunted by up to 60 %. Cells treated with a combination of the ATGL and the HSL inhibitor did hardly respond at all to the addition of isoproterenol translating into around 85 % reduced oxygen consumption rates. However, the futile ATP-consuming substrate cycle(s) activated by adrenergic stimulation may simply require FAs as a substrate for oxidation. Therefore, drastically limiting the release of FAs by lipolysis could impair cellular oxygen consumption and ATP synthesis, if FAs were an indispensable source of reducing equivalents following an adrenergic stimulus in brown UCP1KO adipocytes. Nevertheless, after the addition of a chemical uncoupler, FCCP, oxygen consumption of all groups largely exceeded prior isoproterenol-stimulated respiration rates. As maximal FCCP-uncoupled respiration is a function of substrate availability and oxidation, this clearly proves that inhibiting lipolysis does not impair the provision of reducing equivalents and the theoretically maximum achievable flow of electrons (e^-) through the mitochondrial electron transport chain. Consequently, FAs released in response to an adrenergic stimulus are not inevitably required for mitochondrial ATP synthesis, but instead directly or indirectly participate in ATP-consuming reactions related to thermogenesis in the absence of UCP1.
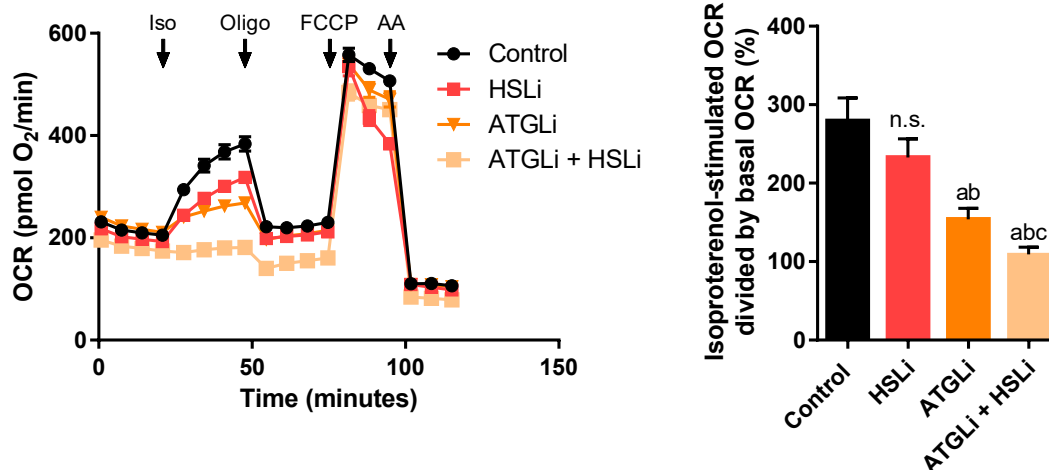
Figure 7: Futile ATP turnover in the absence of UCP1 depends on active lipolysis. *XF96 extracellular flux measurements of primary cultures of fully differentiated 129Sv/S1 brown UCP1-knockout (UCP1KO) adipocytes. Cells were pre-treated with an HSL inhibitor (HSLi, 20 µM final), an ATGL inhibitor (ATGLi, 40 µM final), or both inhibitors (ATGLi + HSLi) for 1 h prior to the measurement and inhibitors were present in the assay medium throughout the measurement. Isoproterenol-induced increase in oxygen consumption rate (OCR) was calculated. n = 18 – 24 wells from three independent biological experiments. One-way ANOVA followed by Tukey's HSD was applied. "a" indicates a significant difference from the control group, "b" from the HSLi group, and "c" from the ATGLi group. Not statistically significant (n.s.).*

3.5.2 UCP1-independent thermogenesis is initiated and sustained by lipolysis

Next, it still needed to be clarified whether a rapid surge in FA levels induced by isoproterenol only provides the initial impulse required to start the process or whether FAs need to be permanently released to keep the cycle going. Therefore, ATGL and HSL inhibitors were added during active lipolysis to acutely stop the release of FAs, and the immediate effect on oxygen consumption rates was compared to the action of oligomycin. Acute inhibition of ATGL and HSL activity during adrenergic stimulation immediately diminished ATP-dependent oxygen consumption equivalently to oligomycin regarding kinetics and efficacy (Figure 8A). The proportion of isoproterenol-stimulated respiration sensitive to the addition of oligomycin or a combination of the two lipase inhibitors was similar in both groups and was approximately 90 %. Consequently, the futile substrate cycle in brown UCP1KO adipocytes strictly depends on active lipolysis, because it is not only initiated, but also sustained by a continuous supply of FAs provided by ATGL and HSL lipase activity.
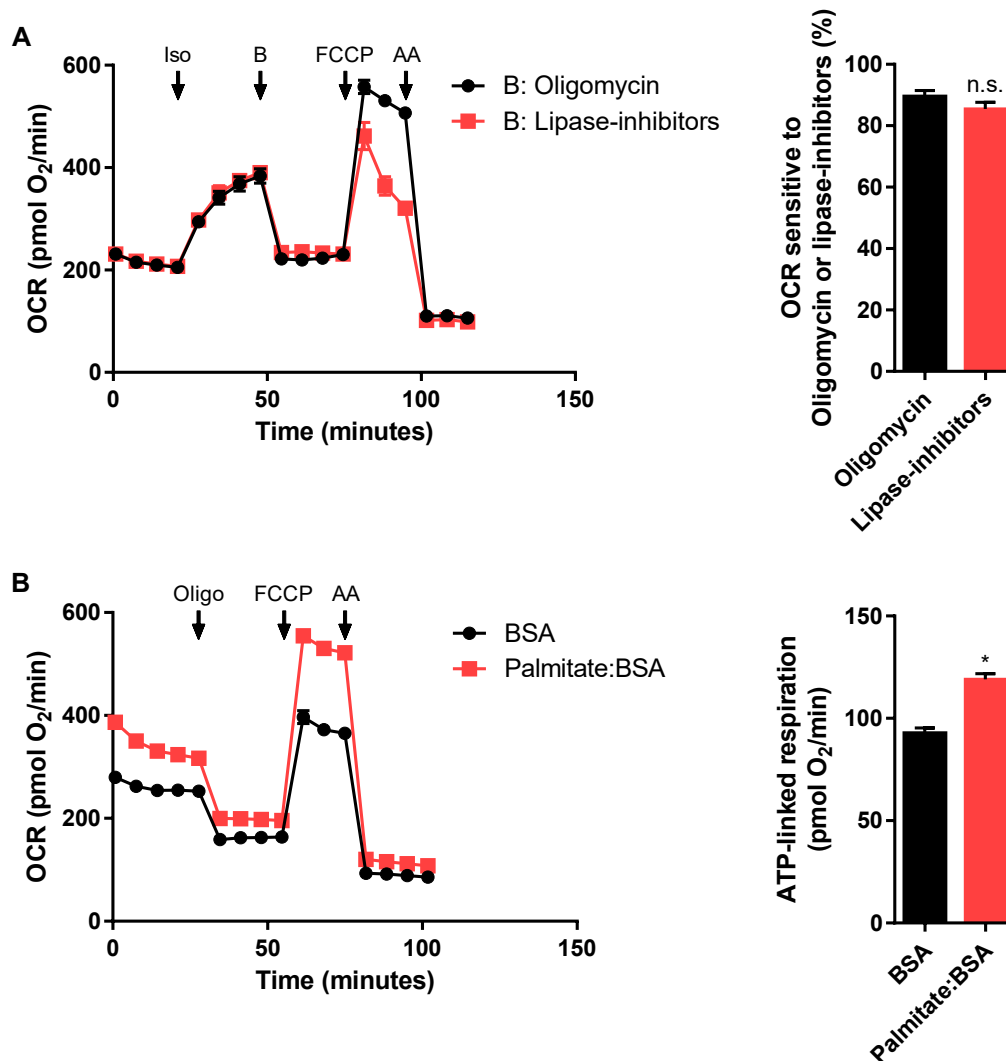
Figure 8: Futile substrate cycling is sustained by a constant supply of FAs derived from the lipolytic breakdown of lipid droplets but can but can also be triggered by a bolus of exogenously added FAs. A) & B) XF96 extracellular flux measurements of primary cultures of fully differentiated 129Sv/S1 brown and brite UCP1-knockout (UCP1KO) adipocytes. A) Oligomycin delivered via the second injection (port "B") was replaced with a combination of the ATGL and the HSL inhibitor. Portion of stimulated OCR sensitive to oligomycin or lipase-inhibitors was calculated. n =21 wells from three independent biological experiments. A two-tailed t-test was applied. Not statistically significant (n.s.). B) Palmitate conjugated to bovine serum albumin (Palmitate:BSA, 160 μM Palmitate:28 μM BSA final) or just BSA (28 μM final) was added to the BSA-free assay medium immediately prior to starting the measurement and ATP-linked OCR was quantified. n = 37 – 43 wells from three independent biological experiments. A two-tailed t-test was applied. Asterisk (*) indicates a significant difference between the two groups.

3.5.3 Intracellular lipolysis is dispensable for thermogenesis in the presence of an extracellular source of fatty acids

Nevertheless, whether adrenergic signaling is required in combination with the lipolytic release of FAs or whether the mere presence of FAs, regardless of their origin, is sufficient to trigger futile substrate cycling had not yet been investigated. To this end, a single bolus of palmitate coupled to albumin was added to brown UCP1KO adipocytes immediately before the start of the experiment, but in this case without additional adrenergic stimulation. Cells that received FAs had a substantially higher basal

oxygen consumption compared to the control group (Figure 8B). While the majority of this was due to significantly higher ATP-dependent respiration, a small portion was attributable to slightly increased proton-leak-linked respiration.

This clearly demonstrates that a bolus of exogenously supplied FAs without adrenergic stimulation is in fact sufficient to activate ATP-consuming processes in UCP1KO cells, which elevate cellular ATP demand and, therefore, eventually increase oxygen consumption. Interestingly, basal respiration of cells treated with palmitate constantly declined during the first five measurement periods, whereas initial rates of the control group were rather stable and only showed a minimal decline. Again, this strongly suggests that FAs are metabolized in an ATP-dependent manner and represent the driving force of increased oxygen consumption. As an increasing amount of FAs is cleared, there is less substrate available for futile lipid cycling translating into a declining ATP demand and gradually shrinking respiration rates. Besides the immediate effects, supplying exogenous FAs seemed to enhance oxidative capacity, in this case by augmenting substrate availability, when lipolysis was not pharmacologically activated, because FCCP-induced maximal respiration was largely increased in the palmitate group.

From a different perspective, these findings are of particular importance, as they provide a completely new perspective on futile lipid cycling, which may not be an exclusively intracellular process, but could represent an inter-organ cycle involving different adipose tissue depots or even non-adipose tissue organs, such as liver or skeletal muscle[83].

3.5.4 Fatty acid-induced uncoupling and permeability transition do not contribute to stimulated respiration rates

Nevertheless, before further pursuing the exact molecular source of NST in UCP1KO adipocytes, any last doubts that the observed phenomenon might simply be a non-specific side effect of high intracellular FA concentrations or caused by the detrimental accumulation of FAs should be resolved[90,91]. Two points arguing against a non-specific uncoupling effect are the fact that bovine serum albumin (BSA)-buffered medium was used during all experiments as a preventive measure[72], and that stimulated respiration rates in brown UCP1KO adipocytes are highly sensitive to oligomycin. If FA-mediated non-specific uncoupling were the main cause, this would be considered proton leak-linked respiration, which by definition should not be sensitive to oligomycin. However, this was not the case here.

Secondly, a rapid surge in FA levels is known to promote opening of the mitochondrial permeability transition pore (PTP) by directly interacting with proteins of the inner mitochondrial membrane[92,93]. PTP opening is characterized by an increased permeability of the mitochondrial inner membrane,

which results in the uncontrolled distribution of solutes with a molecular mass of up to about 1.5 kDa across the otherwise impermeable membrane representing an additional route for the dissipation of protonmotive force[94]. Cyclosporin A is a widely used and potent PTP inhibitor that binds to cyclophilin D, thereby preventing its interaction with the ADP/ATP translocase and consequently PTP formation[95]. Nevertheless, treating brown UCP1KO adipocytes with cyclosporin A had no effect on respiration rates in the basal state and following the addition of isoproterenol (Figure 9). In summary, neither non-specific uncoupling by FAs nor opening of the PTP contribute to phenomenon described here. Instead, the response of UCP1-ablated adipocytes to adrenergic stimulation is undoubtedly due to an increased ATP demand.
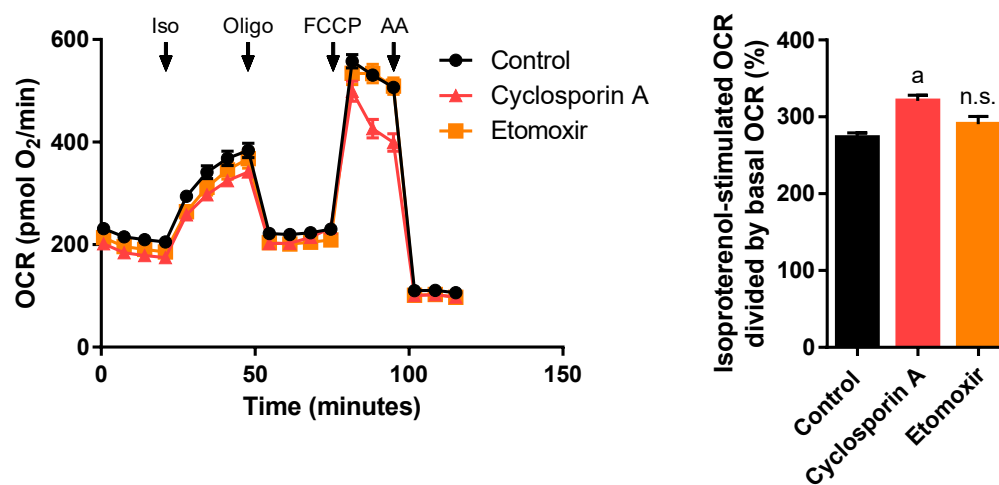
Figure 9: β-oxidation and permeability transition pore formation does not contribute to futile substrate cycling and UCP1-independent thermogenesis in brown adipocytes lacking UCP1. *XF96 extracellular flux measurements of 129Sv/S1 brown UCP1-knockout (UCP1KO) adipocytes. Cells were pre-treated with etomoxir (100 µM final) for 1 h or with cyclosporin A (4.2 µM final) for 72 h. Isoproterenol-induced increase in oxygen consumption rate (OCR) was calculated. n = 14 – 23 wells from three independent biological experiments.*

3.5.5 Newly released fatty acids are not degraded through β-oxidation

As briefly mentioned before, theoretically two different futile lipid cycles, i.e. a FA/TG cycle and a FAO/DNL cycle, could exist in adipocytes. To determine how much each of these individual mechanisms contributes to UCP1-independent heat generation, the first step was to shut down mitochondrial β-oxidation. Etomoxir is an inhibitor of carnitine palmitoyltransferase 1 (CPT1)[96] that is the rate limiting enzyme of the carnitine shuttle on the outer side of the mitochondrial membrane. Etomoxir irreversibly binds to the catalytic site of CPT1 preventing the formation of acyl-carnitine, which is an intermediate reaction product required for the import of FAs into the intermembrane space. This effectively prevents the import of FAs into the mitochondrial matrix and inhibits β-oxidation. However, blocking degradation of FAs in brown UCP1KO adipocytes did not affect oxygen consumption in the basal state, following adrenergic stimulation, or after the addition of FCCP (Figure

9). This again emphasizes that acetyl-CoA derived from mitochondrial β-oxidation is not required to sustain high respirations rates during active lipolysis. Moreover, the outcome of this experiment factually rules out the second variant of futile lipid cycling, "breakdown of FAs followed by FA re-synthesis". At the same time, as etomoxir did not affect oxygen consumption, it is evident that the mechanism or reactions requiring FAs and contributing to futile ATP turnover do not occur in the mitochondrial matrix.

3.5.6 DGAT1 mediates re-esterification of activated fatty acids

Based on these findings and the very characteristic proteome signature, the idea that murine brown UCP1KO adipocytes would immediately re-esterify a significant portion of FAs, which are released following adrenergic stimulation, onto G3P, MGs, and DAGs was favored. Since an adrenergic stimulus, such as isoproterenol, triggers lipolysis and TG synthesis at the same time[97,98], which are theoretically neutralizing each other's actions, one important criterion defining a futile substrate cycle is already met. The second prerequisite, dissipation of chemical energy as heat, would be fulfilled by the mandatory ATP-dependent activation of FAs preceding re-esterification onto a glycerol backbone. Consequently, blocking the activation of FAs should result in less of an increase in oxygen consumption during active lipolysis, as the ATP demand is lower, and less ADP, which stimulates cellular respiration, is generated. Therefore, brown UCP1KO adipocytes were treated with triacsin c. Triacsin c is a fungal metabolite that potently inhibits long chain fatty acyl-CoA ligase (ACSL)[99], the enzyme catalyzing the formation of fatty acyl-CoA, putatively by competing with long chain FAs for the active site of the enzyme[100]. Inhibition of ACSL, thereby reducing FA activation, attenuated stimulated oxygen consumption rate by 50 %. Treatment with triacsin c did not have an effect on basal oxygen consumption, whereas it marginally lowered proton leak-linked respiration (Figure 10A). On the contrary, maximal FCCP-uncoupled respiration was drastically reduced in the triacsin c group, although rates still substantially exceeded previous values after the injection of isoproterenol.
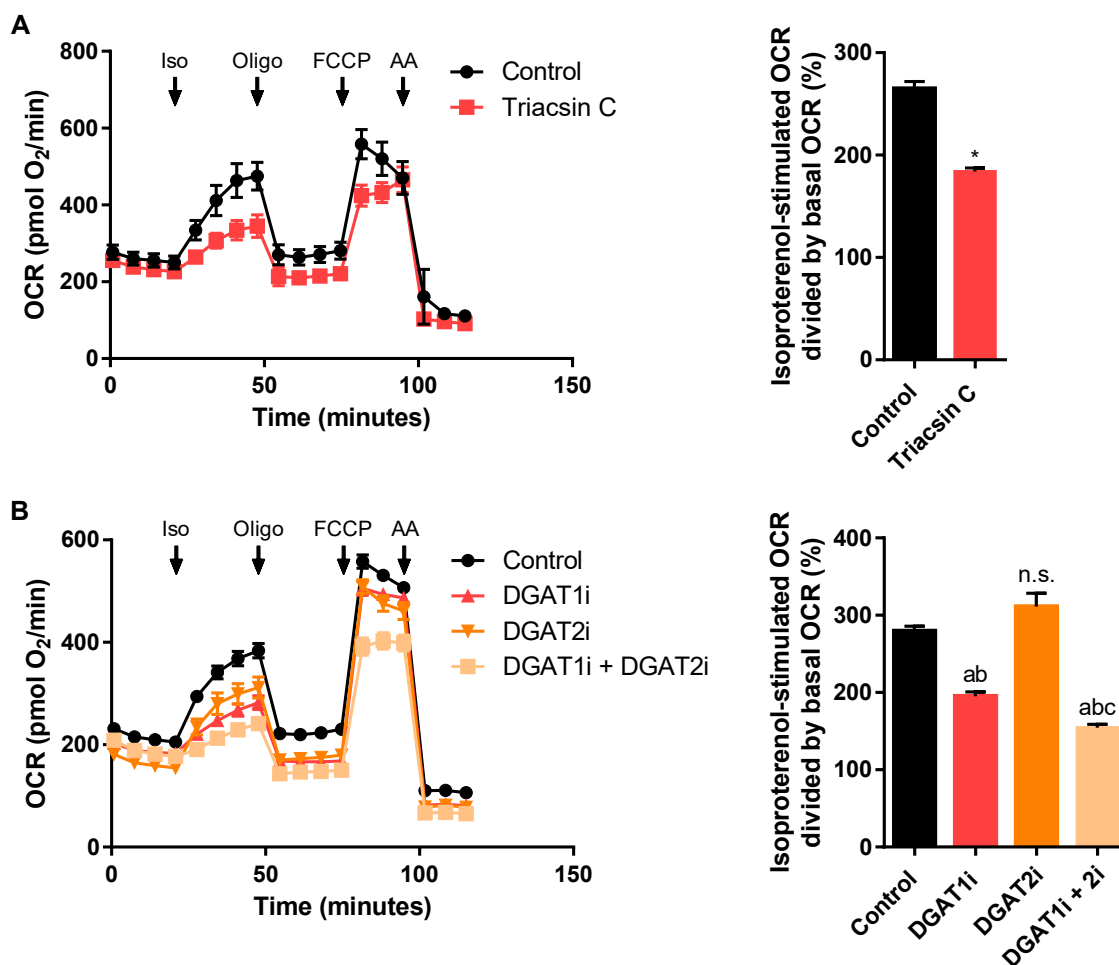
***Figure 10: A futile cycle of lipolysis and re-esterification of fatty acids mediates non-shivering thermogenesis in brown UCP1-knockout adipocytes. A) & B)** XF96 extracellular flux measurements of primary cultures of fully differentiated 129Sv/S1 brown UCP1-knockout (UCP1KO) adipocytes. **A)** Cells were pre-treated with a long-chain acyl-CoA synthetase inhibitor (Triacsin C, 5 µM final) for 1 h prior to the measurement and triacsin C was present in the assay medium throughout the measurement. Isoproterenol-induced increase in oxygen consumption rate (OCR) was calculated. n = 15 -22 wells from three independent biological experiments. A two-tailed t-test was applied. Asterisk (*) indicates a significant difference between the two groups. **B)** Cells were pre-treated with a DGAT1 inhibitor (DGAT1i, 40 µM final), a DGAT2 inhibitor (DGAT2i, 40 µM final), or both inhibitors (DGAT1i + DGAT2i) for 16 h prior to the measurement and inhibitors were present in the assay medium throughout the measurement. Isoproterenol-induced increase in oxygen consumption rate (OCR) was calculated. n = 20 -21 wells from three independent biological experiments. One-way ANOVA followed by Tukey's HSD was applied. "a" indicates a significant difference from the control group, "b" from the DGAT2i group, and "c" from the DGAT1i group. Not statistically significant (n.s.).*

This clearly indicates that interfering with activation of FAs, and especially of long chain fatty acids, in brown UCP1KO adipocytes slightly impairs oxidative capacity. However, as cells treated with triacsin still had spare capacity, substrate supply, provision, and oxidation was not limiting, but indeed less FAs were activated during active lipolysis translating into a reduced ATP demand due to lower futile substrate cycling activity.

The next logical step arising from these results was to test whether re-esterification of FAs is causally related to the increase in oxygen consumption of UCP1KO adipocytes upon adrenergic stimulation.

Several enzymes are involved in the TG synthesis pathway and specifically in the (re-)esterification of FAs. First, a fatty acyl-CoA is attached to G3P via an ester bond catalyzed by G3P acyltransferases (GPATs) forming lysophosphatidic acid (LPA). 1-acyl-sn-glycerol-3-phosphate acyltransferases (AGPATs) mediate the acylation of LPA, which generates phosphatidic acid (PA). DG is then generated from PA by removing the phosphate group, which is an important intermediate not only in TG synthesis but also in different branches of lipid metabolism. The final step in the synthesis of TGs and the quantitatively most important reaction in terms of (re-)esterification of FAs is catalyzed by diacylglycerol O-acyltransferase 1 (DGAT1) and DGAT2[101]. Although both enzymes mediate virtually the same reaction, DGAT1 and DGAT2 are nevertheless quite distinct in terms of structure and function. DGAT1 is located exclusively in the ER membrane and has a broad substrate specificity, as it can process various fatty acyl-CoA acceptor substrates besides DGs. DGAT2 is localized in the ER membrane but also on lipid droplets, and it can only utilize DGs as substrate. DGAT2 has a lower K_m, and therefore it supposedly operates at lower FA concentrations mediating TG storage, while DGAT1 presumably remains active at high substrate concentrations. DGAT1 and DGAT2 are believed to partially compensate for the loss of each other pertaining TG storage in the basal state. However, re-esterification of FAs during active lipolysis is most likely exclusively mediated by DGAT1 due to DGAT2 becoming inactive during this condition.

Unfortunately, only a very limited number of acyltransferase inhibitors has been developed so far and some are still poorly characterized. However, a few established DGAT inhibitors are available that have been tested in mouse studies or even human clinical trials[102,103]. Blocking the action of DGAT1 diminished the isoproterenol-induced increase in oxygen consumption rates by 50 %, whereas DGAT2 inhibition did not significantly affect stimulated respiration (Figure 10B). When administered individually, none of the two substances impaired maximal FCCP-induced respiration. Nevertheless, pharmacological inhibition of DGAT2 slightly lowered basal oxygen consumption. These findings support the notion that DGAT1 closely interacts with ATGL during lipolysis and FA re-esterification[104], while DGAT2 catalyzes *de novo* synthesis of TGs under normal conditions[105]. Moreover, the combined inhibition of DGAT1 and DGAT2 lowered oxygen consumption after the addition of isoproterenol even further by up to 70 %. This probably reflects the fact that DGAT2 can compensate the loss of DGAT1 activity but only to some very limited extent. It is also important to note that although the combined application of both inhibitors limited maximum oxidative capacity compared to the control group, the addition of FCCP still caused oxygen consumption rates to exceed previous rates after the injection of isoproterenol significantly. Thus, it can be concluded that inhibition of DGAT1-mediated re-esterification of FAs disrupts the futile FA/TG cycle and consequently oxygen consumption fails to increase.

Even though the DGAT1 and DGAT2 inhibitors were reported to be highly specific, off-target effects can never be completely ruled out. In addition, inhibitors are usually only tested in membrane fractions or cell lysates, which is why pharmacokinetics and concentrations to be used in intact cultured cells sometimes differ greatly from published values. Therefore, DsiRNA technology, which obviously has its own limitations, was used in a parallel approach to deplete DGAT1 and confirm its important function in re-esterification of FAs during lipolysis and FA/TG cycling. Cells that have received a DsiRNA targeting Dgat1 had 40 % reduced oxygen consumption rates following adrenergic stimulation clearly indicating less futile ATP-dependent re-esterification of FAs in brown UCP1KO adipocytes (Figure 11A).
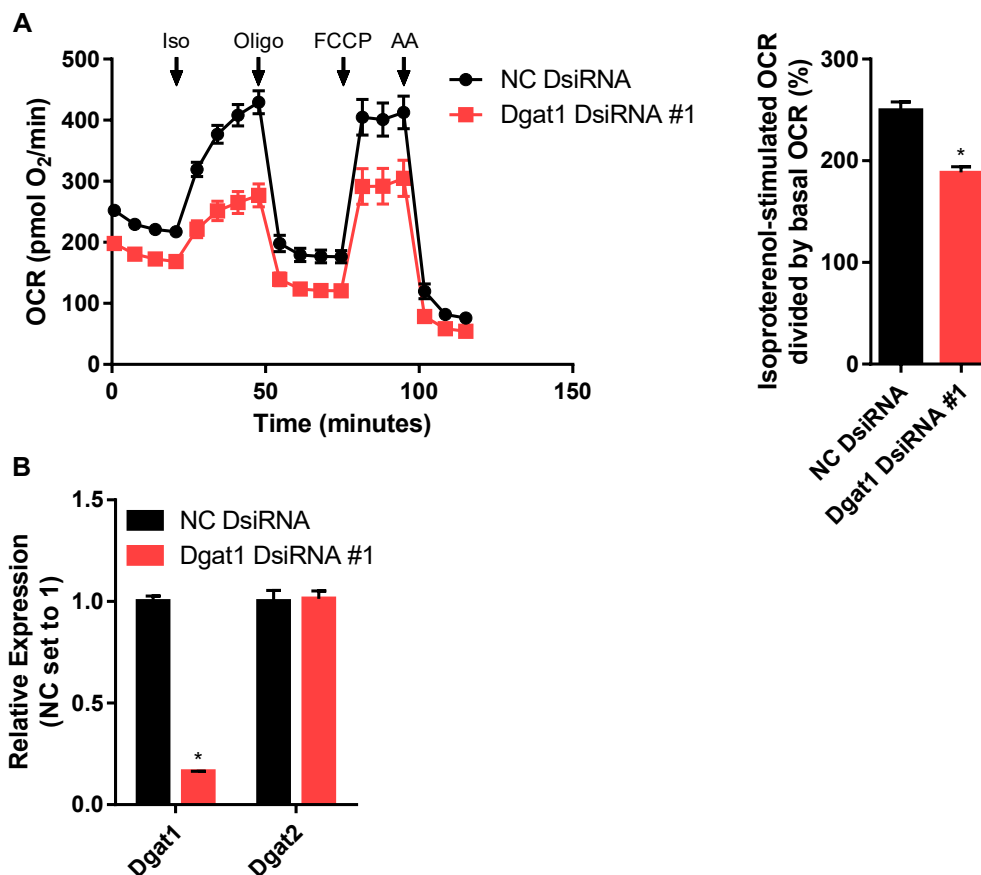
Figure 11: Lowering DGAT1 levels impairs UCP1-independent thermogenesis. A) *XF96 extracellular flux measurements of primary cultures of fully differentiated 129Sv/S1 brown UCP1-knockout (UCP1KO) adipocytes.Dgat1 was knocked down with DsiRNA as described in "Material & Methods" and the isoproterenol-induced increase in OCR was calculated. n = 27 – 30 from three independent biological experiments. A two-tailed t-test was applied. Asterisk (*) indicates a significant difference between the two groups.* **B)** *Knockdown-efficiency was determined by measuring the relative expression of Dgat1 and Dgat2. Content of all wells from one group was pooled within each biological experiment. n = 2 from three independent biological experiments, respectively. A two-tailed t-test was applied, respectively. Asterisk (*) indicates a significant difference between the two groups.*

Treatment with DsiRNA significantly reduced endogenous Dgat1 expression by almost 85 %, while Dgat2 levels were not altered (Figure 11B). In the control group, however, FCCP-induced levels were slightly below those induced by isoproterenol (Figure 11A). The opposite was observed in the

treatment group, albeit the difference between oxygen consumption following the addition of isoproterenol and FCCP was rather small. Taken together, DGAT1 is unequivocally a key player in the re-esterification part of FA/TG cycling, which was corroborated by pharmacological and genetic interference.

3.5.7 Glycolysis fuels UCP1-independent thermogenesis

However, inhibition or knockdown of DGAT1 did not completely prevent futile lipid cycling, and thus it seemed plausible that, on the one hand, other molecules besides DGs serve as FA acceptor molecules or, on the other hand, glycerol backbones must first be synthesized *de novo*. In this context, the fact that glucose uptake into BAT and cultured brown adipocytes functions per se independent of UCP1[59,106,107] is particularly worth mentioning. The exact intracellular metabolic fate of glucose in brown UCP1KO adipocytes remains unclear, as glucose can be metabolized to pyruvate and feed into the tricarboxylic acid cycle (TCA) cycle, it can be converted to lactate via anaerobic glycolysis supporting ATP synthesis, and it can act as a building block for various metabolic intermediates, such as G3P. Based on the previous findings, it was enticing to hypothesize that either G3P derived from glycolysis may represent a significant source of glycerol backbones onto which activated FAs can be attached or that aerobic degradation of glucose provides reducing equivalents required to fuel mitochondrial ATP synthesis during active FA/TG cycling in brown UCP1KO adipocytes. When brown UCP1KO adipocytes were stimulated with isoproterenol in the absence of glucose, the increase in oxygen consumption was massively blunted compared to the previous measurements (Figure 12A), which always included glucose. However, as soon as glucose was re-introduced into the system, oxygen consumption immediately started to rise steeply. Furthermore, acute addition of glucose resulted in an instantaneous increase in oxidative capacity, as judged by FCCP-stimulated oxygen consumption. Because both adipocytes measured in the absence and adipocytes measured in the presence of glucose could theoretically provide sufficient reducing equivalents to raise their oxygen consumption to levels above that after the addition of isoproterenol, the role of glucose had not yet been conclusively determined. To finally shed light on the role of glucose in the futile FA/TG cycle, brown UCP1KO adipocytes were treated with a combination of 2-deoxyglucose (2DG)[108], which is blocking glycolysis, and pyruvate. 2DG produced the same effect as a glucose-free medium, since cells showed virtually no response to adrenergic stimulation (Figure 12B).
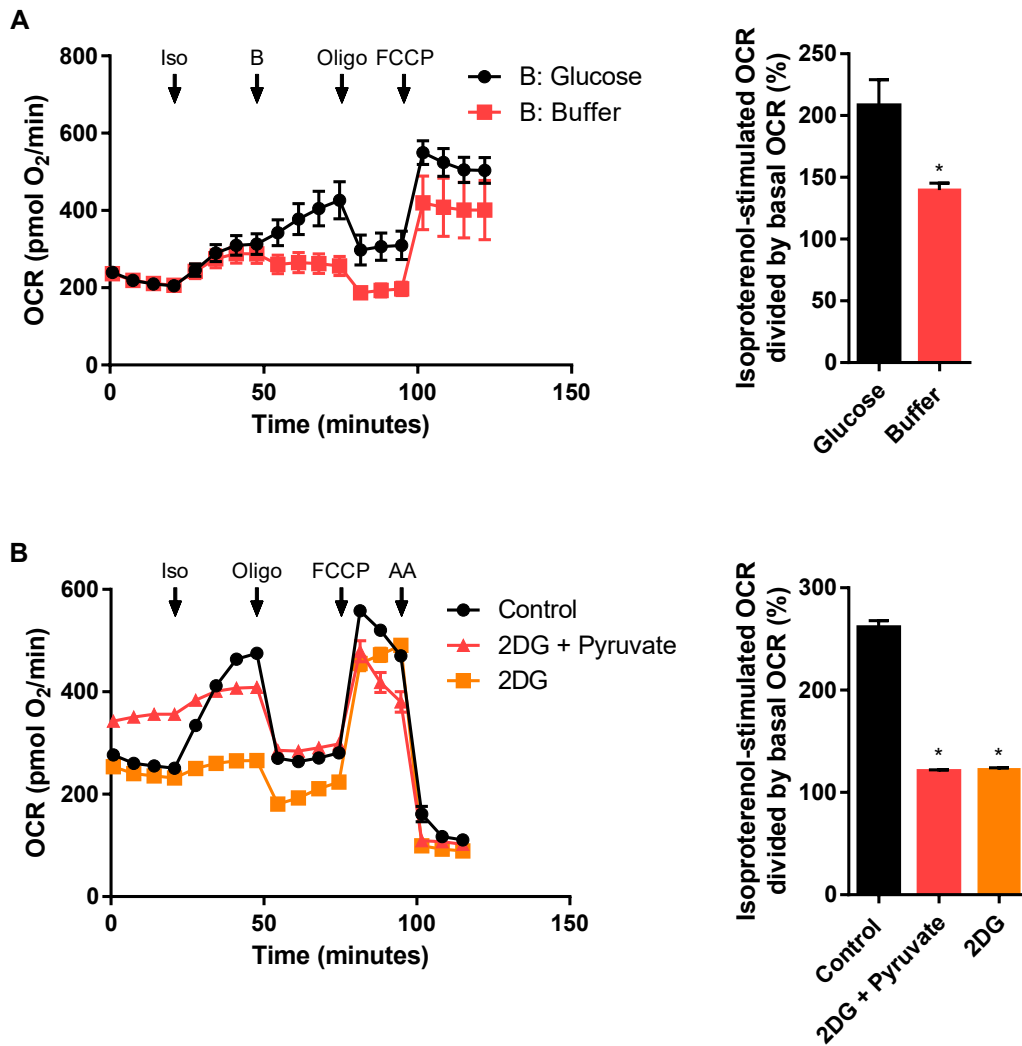
Figure 12: Glycolysis fuels UCP1-independent thermogenesis in brown adipocytes lacking UCP1. A) & B) *XF96 extracellular flux measurements of primary cultures of fully differentiated 129Sv/S1 brown UCP1-knockout (UCP1KO) adipocytes.* **A)** *Cells were assayed in glucose-free medium. Glucose (25 mM final) or buffer was delivered via the second injection (port "B") and the isoproterenol-induced increase in OCR was calculated. n = 10 – 16 wells from two independent biological experiments. A two-tailed t-test was applied. Asterisk (*) indicates a significant difference between the two groups.* **B)** *Cells were pre-treated with 2-deoxyglucose (2DG, 50 mM final) or a combination of 2DG and pyruvate (2DG + Pyruvate; 2DG 50 mM final, pyruvate 5 mM final). Isoproterenol-induced increase in OCR was calculated. n = 16 – 28 wells from three independent biological experiments. One-way ANOVA followed by Tukey's HSD was applied. Asterisk (*) indicates a significant difference from the control group.*

Moreover, blocking glycolysis with 2DG did not affect basal respiration and it only had a minor effect on maximal FCCP-uncoupled respiration. If glucose was converted only to pyruvate, which is then fed into the TCA cycle, the severe effect of 2DG during active lipolysis should be abolished by the parallel addition of pyruvate. Nevertheless, bypassing glycolysis with the addition of exogenous pyruvate was not able to restore respiration rates adequately. Pyruvate significantly increased basal respiration, which is a known phenomenon in certain cell types, where the glycolytic provision of pyruvate is a bottleneck. Therefore, the addition of pyruvate causes metabolism to completely shift to oxidative phosphorylation, which entails an inevitable increase in cellular oxygen consumption.

49

Lastly, WT adipocytes were also assayed in a glucose-free medium (Figure 13A) or treated with 2DG (Figure 13B) to exclude a general impairment of glucose and lipid metabolism that would undermine respiration rates, but both treatments had hardly any effect on WT cells.

In summary, these results indicate that brown UCP1KO adipocytes do not primarily require glucose to produce pyruvate but possibly to generate G3P backbones for FA re-esterification.
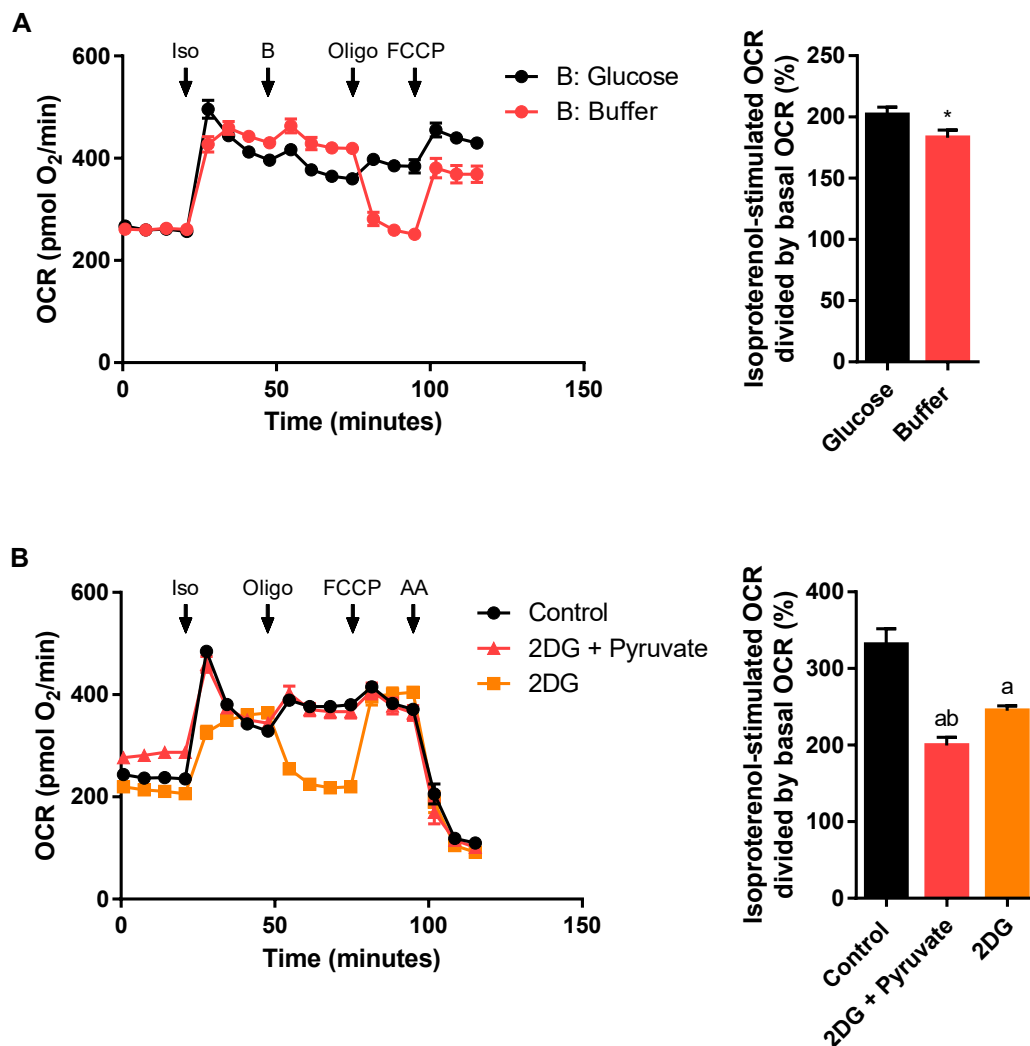
Figure 13: Glycolysis is dispensable for UCP1-mediated thermogenesis in brown adipocytes. A) & B) XF96 extracellular flux measurements of primary cultures of fully differentiated 129Sv/S1 brown wild type (WT) adipocytes. A) Cells were assayed in glucose-free medium. Glucose (25 mM final) or buffer was delivered via the second injection (port "B") and the isoproterenol-induced increase in OCR was calculated. n = 14 – 16 wells from two independent biological experiments. A two-tailed t-test was applied. Asterisk (*) indicates a significant difference between the two groups. B) Cells were pre-treated with 2-deoxyglucose (2DG, 50 mM final) or a combination of 2DG and pyruvate (2DG + Pyruvate; 2DG 50 mM final, pyruvate 5 mM final). Isoproterenol-induced increase in OCR was calculated. n = 24 – 37 wells from three independent biological experiments. One-way ANOVA followed by Tukey's HSD was applied. "a" indicates a significant difference from the control group, and "b" from the 2DG group.

Cellular G3P levels are tightly controlled by the G3P shuttle, which consists of the two enzymes glycerol-3-phosphate dehydrogenase 1 (GPD1) and GPD2[109]. The cytosolic isoform GPD1 catalyzes the

50

conversion of dihydroxyacetonephosphate to G3P, which regenerates NAD^+ by oxidizing NADH. The mitochondrial isoform GPD2 mediates the reverse reaction that produces $FADH_2$, which in turn is feeding e^- into the mitochondrial coenzyme Q pool. This allows reducing equivalents produced during glycolysis to be transported into mitochondria where they can be utilized to generate protonmotive force. Consequently, if a significant portion of glucose was converted to G3P and GPD1 activity contributed to the provision of G3P backbones, lowering the expression of GPD1 would negatively affect the capacity to re-esterify FAs without compromising oxidative capacity.
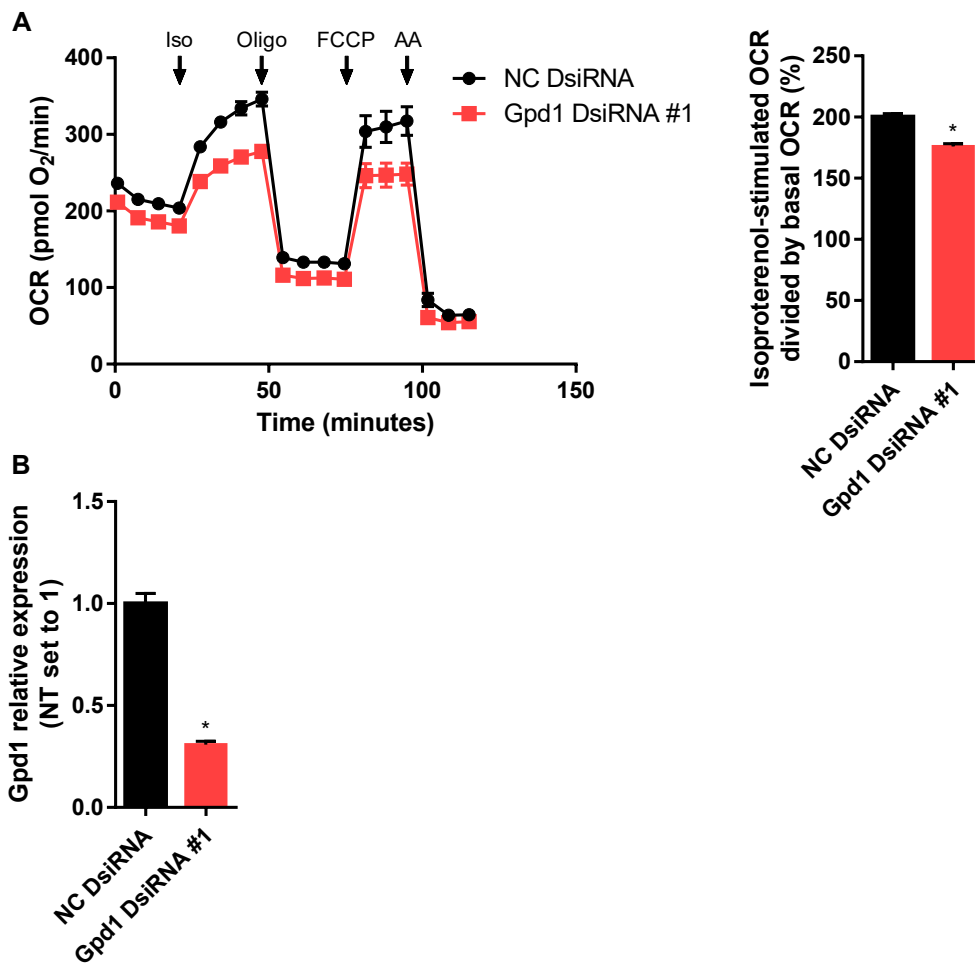
Figure 14: Futile FA/TG cycling partially depends on provision of glycerol backbones by GPD1. *A) XF96 extracellular flux measurements of primary cultures of fully differentiated 129Sv/S1 brown UCP1-knockout (UCP1KO) adipocytes. Gpd1 was knocked down with DsiRNA as described in "Material & Methods" and the isoproterenol-induced increase in OCR was calculated. n = 28 – 31 wells from three independent biological experiments. A two-tailed t-test was applied. Asterisk (*) indicates a significant difference between the two groups. B) Knockdown-efficiency was determined by measuring the relative expression of Gpd1. Content of all wells from one group was pooled within each biological experiment. n = 3 from three independent biological experiments. A two-tailed t-test was applied. Asterisk (*) indicates a significant difference between the two groups.*

In line with this hypothesis, DsiRNA-mediated reduction of Gpd1 expression resulted in a minimally lower basal oxygen consumption and approximately 30 % decreased oxygen consumption rates after brown UCP1KO adipocytes were stimulated with isoproterenol (Figure 14A). Gpd1 levels were decreased by 70 % (Figure 14B). In both the control and treatment groups, respiration rates after the addition of FCCP were slightly lower than the maximum following adrenergic stimulation (Figure 14A).

These findings highlight the interdependence of glucose and lipid metabolism, and clearly suggest that brown UCP1KO adipocytes do not exclusively convert glucose to pyruvate, but rather metabolize glucose to G3P via dihydroxyacetonephosphate. Thus, besides transporting reducing equivalents, G3P can serve as a backbone for re-esterification of FAs and TG synthesis sustaining futile lipid cycling upon adrenergic stimulation. This dual role could partially explain the impressive glucose uptake rates of activated BAT in UCP1KO mice.

3.5.8   Quantification of futile lipid cycling *in vitro*

Finally, to obtain an additional and more direct readout of lipid cycling activity, re-esterification rates were estimated based on the release of FAs and glycerol of cultured adipocytes under various conditions[47,59]. One TG molecule consists of three FA molecules and one glycerol molecule. When a triglyceride molecule is completely hydrolyzed, FAs and glycerol appear with a 3:1 ratio. Assuming that oxidation of FAs is negligible within this short period, all FAs that do not appear in the medium, in a 3:1 ratio as measured by the amount of glycerol released, are hypothetically re-esterified.

In the basal state brown WT and UCP1KO adipocytes re-esterified a comparable amount of FAs. UCP1KO adipocytes massively increased their re-esterification rate upon adrenergic stimulation, whereas WT adipocytes only showed a small non-significant response (Figure 15 A).
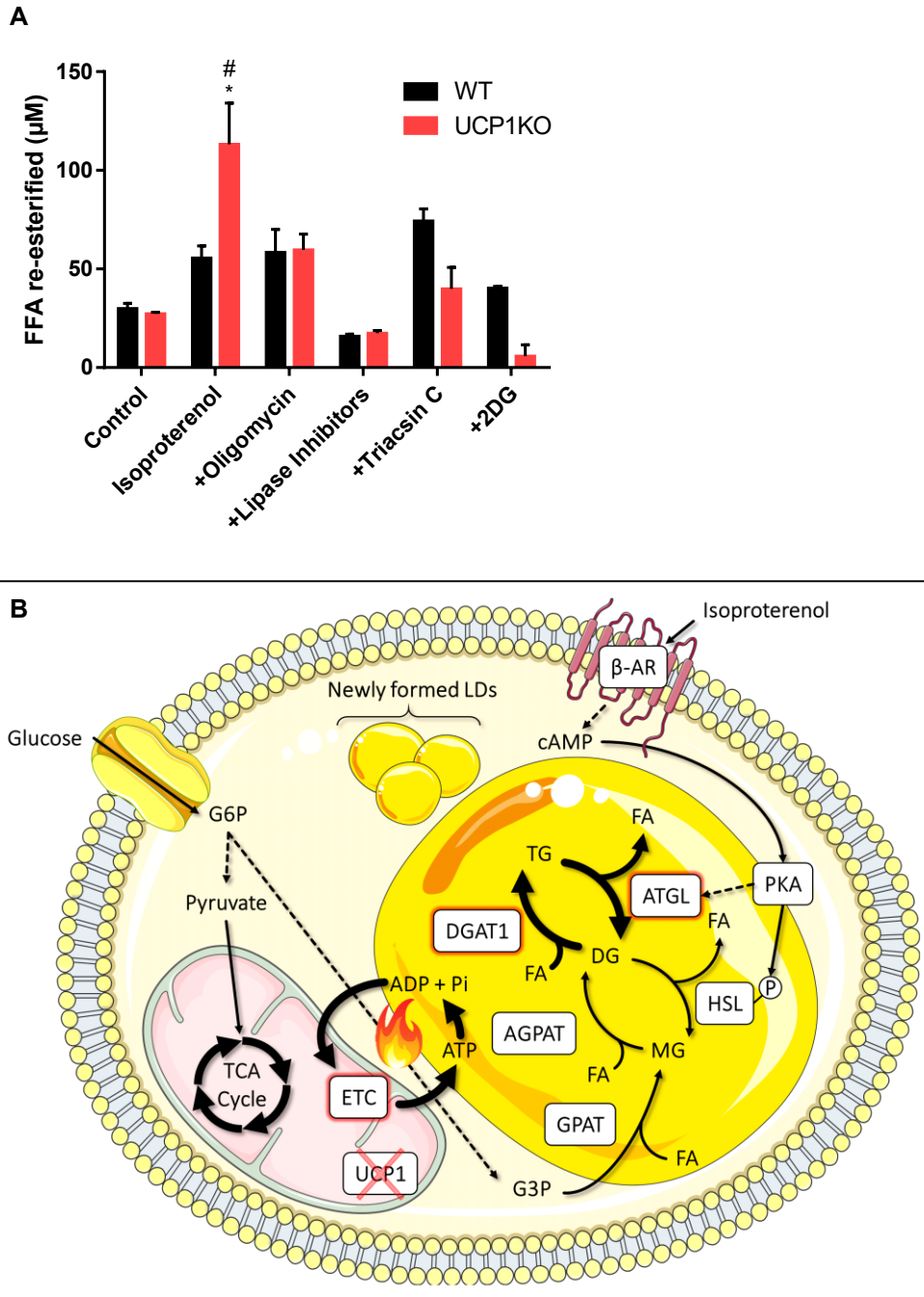
Figure 15: Futile lipid cycling is recruited for non-shivering thermogenesis in brown UCP1-knockoout adipocytes. A) 129Sv/S1 brown wild type (WT) and UCP1KO cells were pre-treated as described in "Material & Methods", glycerol and free fatty acids (FFAs) in the medium were quantified, and the amount of re-esterified FFA was calculated. 2-deoxyglucose (2DG, 50 mM final). n = two independent biological experiments (within each experiment, the content of 8 wells of each treatment level was pooled). Kruskal-Wallis two-way ANOVA followed by multiple comparisons with a Bonferroni-corrected Mann-Whitney U test was applied. Asterisk (*) indicates a significant difference from the control group of the respective genotype. Number sign (#) indicates a significant difference between the two genotypes within one treatment level. B) Graphical summary of futile fatty acid/triglyceride (FA/TG) cycling in adipocytes. This figure was created using Servier Medical Art templates, which are licensed under a Creative Commons Attribution 3.0 Unported License; https://smart.servier.com

In good agreement with the aforementioned findings based on respirometry, inhibiting mitochondrial ATP synthesis did hardly affect the stimulated FA cycling rate of WT adipocytes, while half of the cycling rate in brown UCP1KO adipocytes was sensitive to oligomycin treatment. Blocking lipolysis completely

prevented any increase in re-esterification rates independent of the genotype. Reducing ATP-dependent activation of FAs prior to DGAT1-mediated re-esterification attenuated re-esterification rates by 65 % in UCP1KO cells, whereas WT adipocytes, again, were not significantly affected. Lastly, the addition of 2DG, a glucose analogue that is blocking glycolysis at the level of hexokinase and glucose-6-phosphate isomerase, caused a massive reduction in the amount of re-esterified FAs, but only in UCP1KO cells.

Based on the *in vitro* data presented, the following model is proposed (Figure 15B): In response to a cold sensation, norepinephrine, here mimicked by isoproterenol, binds to adrenergic receptors and triggers the downstream cAMP-PKA-signaling cascade, which leads to the activation of lipolysis. ATGL and HSL-mediated hydrolysis of TGs and DGs causes an immediate increase in cellular FA levels. The majority of newly released FAs in brown UCP1KO adipocytes is re-esterified onto DGs and possibly to a lesser extent onto MGs as well as G3P. In this setting, more glucose is taken up to replenish the TCA cycle, maintain protonmotive force, and most importantly to provide G3P backbones serving as FA acceptor molecules. Primarily DGAT1 but potentially also other acyltransferases, such as GPATs and AGPATs, catalyze the esterification of FAs derived from intracellular TG stores or taken up from the circulation, which is preceded by the ATP-dependent activation. The breakdown of TGs is simultaneously counterbalanced by re-synthesis, and thus lipid flux in both directions accelerates causing ATP turnover to increase without altering metabolite levels. Thereby, ATP consumption, its anaerobic glycolytic provision, and generation of ATP via oxidative phosphorylation directly linked to the flux through the mitochondrial electron transport chain (ETC) can be adjusted by enhancing or reducing lipid flux, which represents the theoretical foundation of FA/TG cycling.

3.5.9 AMPK regulates futile lipid cycling activity by integrating cellular energy levels

Nevertheless, there was still the question of how this process is acutely regulated at the cellular level. It is apparent that a cyclic process based primarily on the release of FAs would also involve intracellular FA levels as an effector variable. Despite recent progress in identifying potential mechanisms, it remains largely unknown how FA levels are sensed and whether this is a direct or indirect process, and thus this area did not qualify for further experimental manipulation.

However, another key aspect of futile substrate cycles is the dissipation of energy, which is why it was hypothesized that the cellular energy status is directly linked to futile FA/TG cycling activity. AMP-activated protein kinase (AMPK) is a highly conserved metabolic switch that is regulating anabolic and catabolic reactions[110]. AMPK can directly sense AMP, ADP, and ATP concentrations, because binding of AMP or ADP to a regulatory site on its γ-subunit, i.e. displacement of ATP, represents a strong activating signal. When AMPK is activated, ATP-consuming processes are shut down and processes that

generate ATP are enhanced. The activity of AMPK in brown UCP1KO adipocytes was artificially modulated by using pharmacologically active substances and the resulting effects on FA/TG cycling were monitored. AICAR is an AMP analogue that allosterically activates AMPK[111], thereby mimicking low energy levels. Vice versa, compound C is a reversible AMPK inhibitor[112], which competes with ATP for the regulatory binding site and simulates a state of sufficient energy availability and production. Treatment with AICAR did not affect basal oxygen consumption, but massively impaired isoproterenol-stimulated respiration rates by up to 85 % (Figure 16). This may indicate that AMPK limits futile FA/TG cycling when only little ATP is available. On the contrary, blocking AMPK activity significantly increased cellular respiration in the basal state more than twofold, while it did not have affect oxygen consumption rates during adrenergic stimulation (Figure 16). However, proton leak-linked respiration was not different between the compound C and the control group, which clearly indicates that the initial difference was due to increased ATP turnover and synthesis most likely caused by enhanced futile substrate cycling. Acutely manipulating AMPK activity did neither impair nor expand oxidative capacity, as none of the substances used had any effect on maximal FCCP-induced respiration. Taken together, AMPK may represent a regulatory link between cellular energy homeostasis and futile FA/TG cycling in brown UCP1KO adipocytes. Nevertheless, it remains to be clarified whether AMPK can dynamically and mutually influence substrate cycling activity even in a physiological scenario without pharmacological interference or whether changes in the activation state of AMPK are only a downstream consequence of altered lipid turnover.
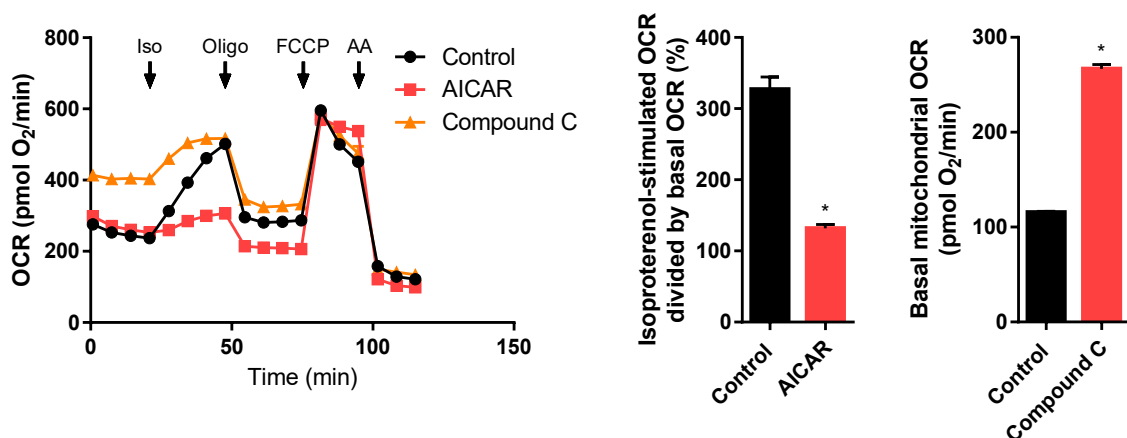
Figure 16: AMPK integrates cellular energy levels to control futile lipid cycling activity. XF96 extracellular flux measurements of primary cultures of fully differentiated 129Sv/S1 brown UCP1-knockout (UCP1KO) adipocytes. Cells were pre-treated with an AMPK activator (AICAR, 50 mM final) or an AMPK inhibitor (Compound C, 5 mM final) for 1 h prior to the measurement and chemicals were present in the assay medium throughout the measurement. Isoproterenol-induced increase in OCR (middle) and basal mitochondrial oxygen consumption (right) was calculated. n = 11 − 14 wells from two independent biological experiments. A two-tailed t-test was applied. Asterisk (*) indicates a significant difference between the two groups.

3.5.10 The association of lipid droplets and mitochondria in brown adipocytes supports thermogenesis

Directly related to energy metabolism and mitochondrial ATP provision, more extensive adaptations caused by the absence of UCP1 were discovered. Although WT and UCP1KO adipocytes respond similarly to adrenergic stimulation by increasing their oxygen consumption and ramping up glucose and FA uptake, the respective underlying mechanisms causing these events are vastly different. Based on a recent publication, which revealed distinct mitochondrial populations in BAT specialized on carrying out defined functions[113], the association between mitochondria and lipid droplets was explored (Figure 17A). Mitochondria bound to lipid droplets, peridroplet mitochondria (PDM), show considerable resemblance to cytoplasmic mitochondria (CM), but differ by having a higher ATP synthesis capacity to support TG synthesis and lipid droplet expansion. Even in the basal state, almost two third of all mitochondria in brown UCP1KO adipocytes are associated with lipid droplets compared to only slightly more than 40 % in WT cells (Figure 17B). Additionally, not only the frequency but also the quality of the association was stronger in UCP1KO cells, since on average around 30 % of total lipid droplet perimeter were occupied by mitochondria as opposed to less than 20 % in WT adipocytes.

In summary, the absence of UCP1 may have even more far-reaching consequences, since clear differences between WT and UCP1KO cells with respect to the interaction between mitochondria and lipid droplets were found. Therefore, this shift in mitochondrial subpopulations may at least partly support the observed phenotypic differences. Brown WT adipocytes rely on UCP1-mediated thermogenesis, and thus would require less PDM and more CM, as CM are specialized on β-oxidation fueling thermogenesis. On the contrary, UCP1KO adipocytes have an increased ATP demand due to higher rates of FA re-esterification favoring the occurrence of PDM, which may facilitate heat generation by futile lipid cycling.
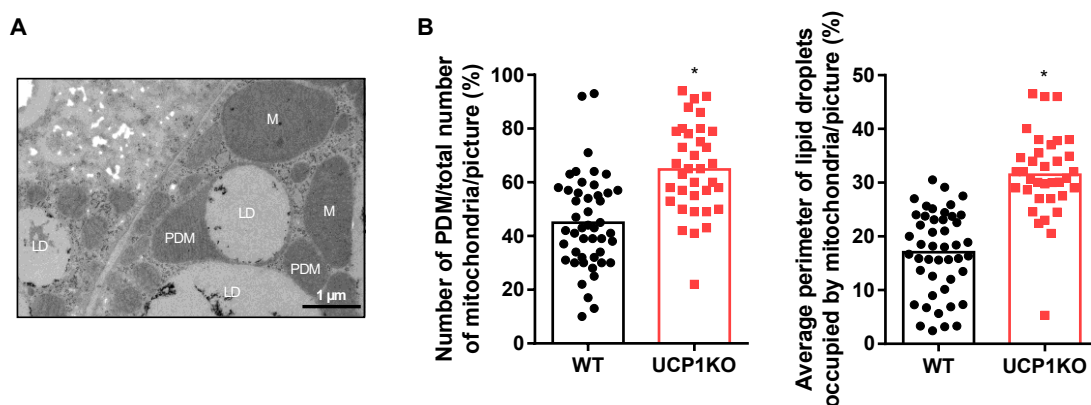
Figure 17: Brown UCP1-knockout adipocytes have a higher number of peridroplet mitochondria and mitochondria are tightly associated with lipid droplets. (Continued on next page)

A) Representative electron micrograph of a fully differentiated 129Sv/S1 brown UCP1-knockout (UCP1KO) cell including lipid droplets, mitochondria, and peridroplet mitochondria (PDM). Scale bar represents 1 µm. "LD" indicates a lipid droplet, "M" a mitochondrion, and "PDM" a peridroplet mitochondrion. B) (Left) Relative proportion of PDM in relation to the total number of mitochondria in 129Sv/S1 brown wild type (WT) and UCP1KO adipocytes. (Right) Relative proportion of lipid droplet perimeter occupied by mitochondria (Right). n = 35 – 46 pictures from two independent biological experiments. A two-tailed t-test was applied. Asterisk (*) indicates a significant difference between the two groups.

3.5.11 Re-esterification of fatty acids protects brown UCP1-knockout adipocytes from endoplasmic reticulum stress during active lipolysis

Another extremely interesting aspect is the fact that the close connection between mitochondria and lipid droplets may not only be related to UCP1-independent NST mediated by futile lipid cycling, but could also constitute a comprehensive protective mechanism against the detrimental accumulation of FAs. ER homeostasis is carefully monitored by a regulatory system known as unfolded protein response (UPR). Excessive misfolding of proteins, overloading the ER with secretory proteins, or changes in the lipid composition of the ER membrane can trigger the UPR, which primarily aims to restore normal ER function and to promote cell survival[114]. Recent publications demonstrated that DGAT1-mediated TG synthesis is key to avert FA-induced lipotoxicity and concomitant ER stress in WAT[101,105,115]. Since DGAT1 plays a very important role in the futile FA/TG cycle described here, one of the main functions of the futile cycle as a whole could also be to protect brown UCP1KO adipocytes from an uncontrolled buildup of lipids due to a rapid surge in intracellular FA levels. Accordingly, UCP1-ablated adipocytes were reported to be more susceptible to ER stress[116,117], and fine-tuning FA handling in particular appears to be a highly delicate operation.

Therefore, it was hypothesized that limiting FA/TG cycling by strongly attenuating ATP synthesis, or specifically inhibiting DGAT1-mediated re-esterification of FAs during active lipolysis would evoke a powerful UPR in brown UCP1KO adipocytes. To this end, brown WT and UCP1KO adipocytes were treated with either oligomycin or a DGAT1 inhibitor with or without acute adrenergic stimulation, respectively. Subsequently the expression of four ER stress-responsive genes, which represent different branches of the UPR, was quantified.

In general, all measured UPR markers were at least slightly elevated in UCP1KO cells compared to their WT counterparts in virtually all conditions (Figure 18).
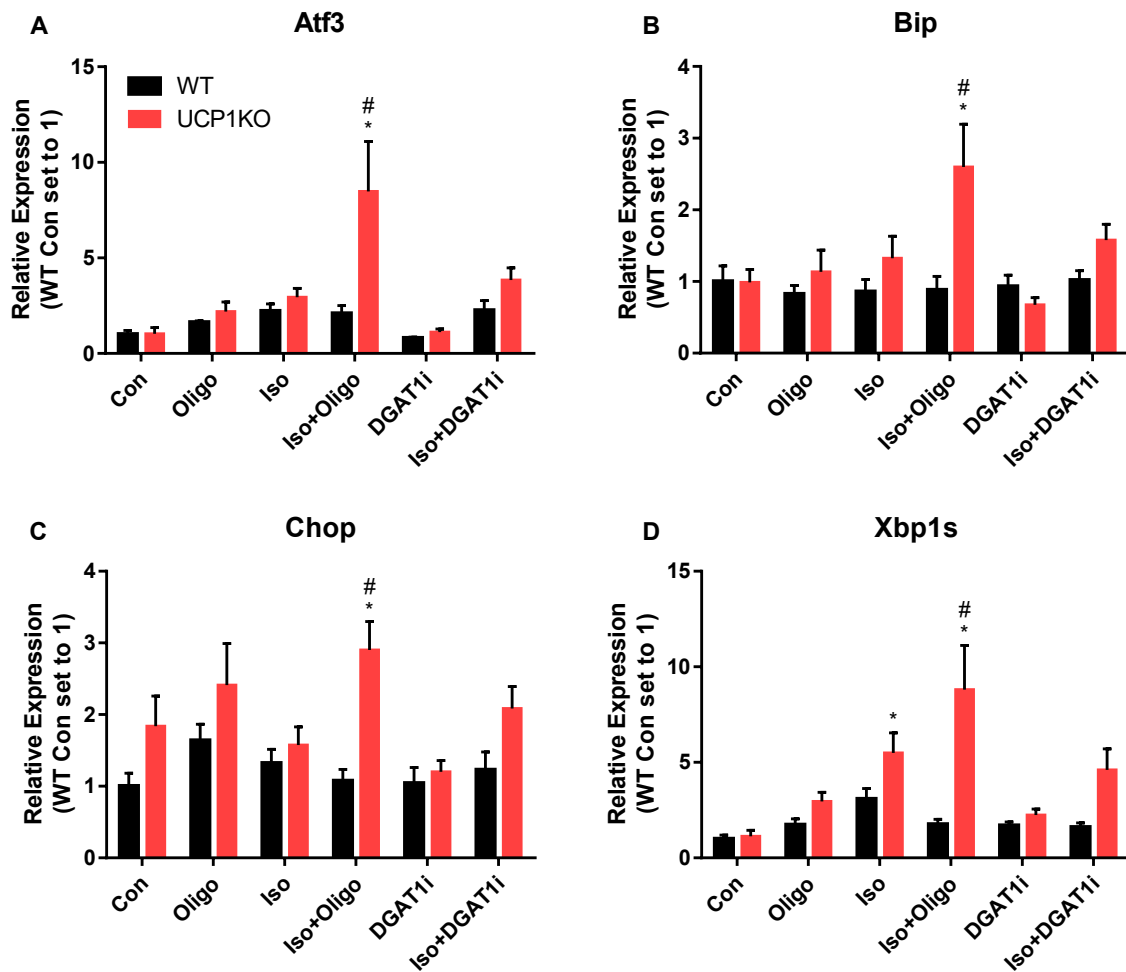
Figure 18: Futile lipid cycling protects brown UCP1-knockout adipocytes from endoplasmic reticulum stress during active lipolysis. 129Sv/S1 brown wild type (WT) and UCP1-knockout (UCP1KO) cells were pre-treated as described in "Material & Methods". Cells were washed twice with respiration base medium and assayed in respiration assay medium (inhibitors were added to the assay medium at this point and were present in the medium during the measurement). The cell culture plate was incubated for 1 hour at 37°C in a laboratory non-CO_2 incubator. After that, isoproterenol, oligomycin, or a combination of both was added to the medium. Cell culture plates were placed back into a laboratory non-CO_2 incubator and incubated at 37 °C. After an additional 3 hours, cells were harvested and the relative expression of endoplasmic reticulum stress-responsive genes was determined. n = five independent biological experiments. A two-way ANOVA followed by Tukey's HSD multiple comparisons was applied. Asterisk (*) indicates a significant difference from the control group of the respective genotype. Number sign (#) indicates a significant difference between the two genotypes within one treatment level.

Activating transcription factor 3 (ATF3) is an ER stress-induced transcription factor that acts as a hub by integrating multiple cellular signals[118]. ATF3 can modulate adipose tissue glucose and lipid metabolism by activating or repressing transcription of target genes. Stimulation with isoproterenol caused a mild two- to threefold upregulation of *Atf3* in WT and UCP1KO cells. However, combined treatment with oligomycin during adrenergic stimulation led to a significant more than eightfold increase in *Atf3* levels in UCP1-ablated cells, whereas it did not further elevate expression in WT cells (Figure 18A). Treatment with oligomycin alone resulted in only a minor increase and had approximately the same effect as the addition of isoproterenol. Blocking the action of DGAT1 during active lipolysis did not affect *Atf3* transcript levels in WT cells beyond that of isoproterenol alone. In contrast,

inhibition of DGAT1 during acute adrenergic stimulation caused an almost fourfold upregulation in UCP1KO cells compared to controls, while the DGAT1 inhibitor without isoproterenol had no effect on *Atf3* expression independent of the genotype.

Binding immunoglobulin protein (BIP), which is encoded by the *Hspa5* gene, is one of the most abundant ER proteins. BIP acts as a chaperone, and prevents the accumulation of misfolded proteins, as it ensures quality control and facilitates degradation of incorrectly folded proteins. Moreover, BIP is thought to be a direct ER stress sensor that modulates UPR activation by binding to and interacting with known UPR inducers, such as inositol-requiring protein 1 (IRE1) and protein kinase RNA-like ER kinase (PERK)[119]. Adrenergic stimulation resulted in a weak but non-significant induction of *Bip* in UCP1KO cells (Figure 18B). Combining isoproterenol and oligomycin treatment caused a strong almost threefold upregulation of *Bip*, but again, only in UCP1-ablated adipocytes. Moreover, a trend towards higher *Bip* expression in UCP1KO cells was observed, when DGAT1-mediated re-esterification was blocked during active lipolysis. Neither oligomycin nor the DGAT1 inhibitor administered alone had any effect on *Bip* transcript levels. Nevertheless, the observed genotype-dependent tendency towards higher expression of UPR genes in UCP1KO adipocytes continues in the case of *Bip*, although the magnitude of the effect is slightly lower.

C/EBP homologous protein (CHOP) is a transcription factor that regulates the expression of genes related to the cell cycle, cell differentiation, and cellular metabolism. CHOP plays a key role in ER-stress induced apoptosis and autophagy[120]. Under normal conditions, CHOP levels are rather low, but once a certain threshold of ER overload is exceeded, several upstream effectors representing different branches of the UPR response, i.e. IRE1 and PERK, cause a massive induction of CHOP expression[121]. *Chop* mRNA levels were overall slightly higher in UCP1KO than in WT cells (Figure 18C). Again, very similar to what was observed for BIP, a single administration of oligomycin or isoproterenol had no effect on *Chop* expression. However, when both substances were administered in combination, *Chop* transcript levels in UCP1KO cells were almost three times higher than in the corresponding WT group. Furthermore, the trend that impaired DGAT1 activity parallel to adrenergic stimulation leads to increased expression of *Chop* in brown adipocytes, but only when UCP1 is absent, was observed again.

The last parameter assessed in the context of UPR and ER stress was X box-binding protein 1 (XBP1) or in particular spliced X box-binding protein 1 (XBP1s). High ER stress activates the IRE1 signaling pathway consequently resulting in altered splicing of *Xbp1*[122]. This process generates the alternative transcript *Xbp1s*, which is translated into a transcription factor that controls the expression of genes involved in ER-associated degradation of aberrant proteins, protein folding, and phospholipid metabolism. XBP1s' actions aim to restore ER function and maintain ER membrane composition, and therefore represent a pro-survival signal[123]. Stimulation with isoproterenol caused a considerable

three- to fivefold upregulation of *Xbp1s* in WT and UCP1KO cells, respectively (Figure 18D). However, combined treatment with oligomycin during adrenergic stimulation led to a significant almost ninefold increase in *Xbp1s* levels in UCP1-ablated cells, whereas expression in WT cells even slightly dropped compared to the isoproterenol group. Treatment with oligomycin alone resulted in only a minor increase and had a smaller effect as the addition of isoproterenol. Blocking the action of DGAT1 during active lipolysis had no effect on *Xbp1s* transcript levels in WT cells. In contrast, inhibition of DGAT1 during acute adrenergic stimulation caused an almost fivefold upregulation in UCP1KO cells compared to controls, while the DGAT1 inhibitor without isoproterenol had only a very mild insignificant effect on *Xbp1s* expression in both cell types.

In summary, shutting down mitochondrial ATP generation, which limits the overall capacity to re-esterify FAs, or direct inhibition of DGAT1-mediated re-esterification while lipolysis is active triggers an acute UPR and markedly induces the expression of selected genes that modulate adaption to cellular stress and initiation of apoptosis. As originally assumed, these findings confirm that this phenomenon occurs exclusively or at least predominantly in brown adipocytes lacking UCP1. Moreover, these data suggest that either DGAT1 or DGAT2 activity is sufficient to prevent ER stress in the basal state. However, as soon as increasing amounts of FAs are released due to lipase activity, most likely only DGAT1 can avert lipotoxicity putatively caused by an unfavorable accumulation of certain lipid species in the ER. Unfortunately, it is still not known how defective or impaired FA/TG cycling is connected to ER stress in brown UCP1KO adipocytes, which lipid species cause this effect, and by which mechanism at the organelle level the detrimental buildup of lipids is sensed.

Looked at another way, these findings could also suggest that the primary function of this mechanism might not be heat generation, but heat may just be a byproduct that occurs when fat cells that do not express UCP1 or have only very low UCP1 levels need to protect themselves against lipotoxicity. Hypothetically, this concept may be applied to UCP1KO mice, since in a situation in which heat generation must be ramped up, sympathetic tone, lipolytic activity and, accordingly, FA levels are generally increased. Ultimately, however, the question would remain as to which of the two components – increased thermogenic demand or protection against lipotoxicity – is the driving force behind the futile FA/TG substrate cycle.

To better understand this process, oxygen consumption of UCP1KO cells was determined under similar conditions, resulting in a much longer measurement time than usual. Interestingly, treatment with a combination of isoproterenol and oligomycin at the beginning of the measurement led to an increase in respiration rates after approximately already one hour, which continued to gradually increase until the end of the measurement (Figure 19).
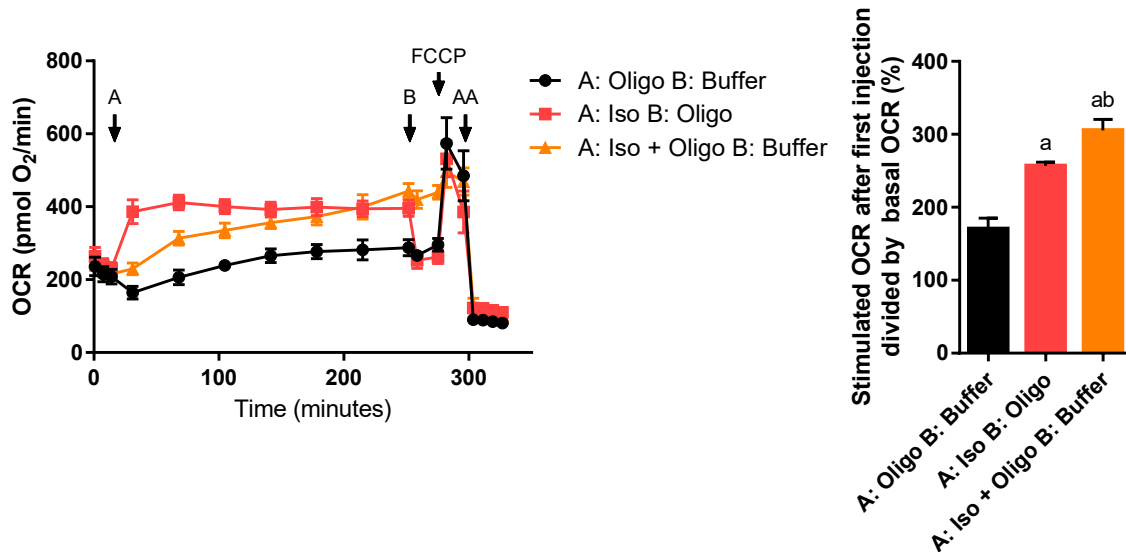
Figure 19: Acute non-specific uncoupling by fatty acids precedes induction of endoplasmic reticulum stress. *XF96 extracellular flux measurements of primary cultures of fully differentiated 129Sv/S1 brown UCP1-knockout (UCP1KO) adipocytes. Compound-induced increase in OCR after first injection was calculated. n = 12 – 15 wells from two independent biological experiments. Kruskal-Wallis two-way ANOVA followed by multiple comparisons with a Bonferroni-corrected Mann-Whitney U test was applied. Asterisk (*) indicates a significant difference from the control group of the respective genotype. "a" indicates a significant difference from the A: Oligo B: Buffer group, and "b" from the A: Iso B: Oligo group.*

After around four hours, oxygen consumption rates of brown UCP1KO adipocytes treated with isoproterenol and oligomycin even exceeded the consumption rates of cells stimulated with isoproterenol alone. In the control group that received only isoproterenol in the beginning, the addition of oligomycin after four hours, as expected, reduced respiration rates back to basal values suggesting that oxygen consumption following the addition of isoproterenol was in this case still entirely dependent on mitochondrial ATP synthesis. In contrast, oxygen consumption of the group that received isoproterenol and oligomycin simultaneously was most likely completely linked to proton leak or non-specific uncoupling, since oligomycin had hardly any effect. However, this was clearly caused by the combination of these two compounds, as cells, which were treated with only oligomycin at the start, transiently reduced their respiration rates, after which oxygen consumption returned to basal values after one hour and stayed stable for the remaining measurement. Neither treatment affected FCCP-uncoupled respiration, and thus maximal respiration was not significantly different between groups. The fact that UCP1KO adipocytes are most likely uncoupled by excess FAs – without apparent adverse effects on mitochondrial function – due to impaired re-esterification in a time frame that already induces ER stress under the same treatment rather supports the lipotoxicity hypothesis. However, this topic will be addressed in more detail later in the discussion.

3.6 Cold-induced changes in the brown adipose tissue proteome of wild type and UCP1-knockout mice

Regardless of the exact molecular function, the *in vitro* data presented here provide unequivocal evidence that an adrenergic stimulus directly leads to the activation of FA/TG cycling in brown UCP1KO adipocytes, manifesting in increased oxygen consumption and dissipation of chemical energy as heat. Nevertheless, by far the most pressing question is whether this mechanism could confer UCP1KO mice, at least in part, their so far unexplainable cold resistance. Since it is extremely complex and technically very challenging to directly and precisely determine FA/TG cycling rates in animals or even in cultured cells, one goal was to search for initial evidence that at least makes the existence of this process in a living organism seem very likely. To this end, WT and UCP1KO mice were kept at 23 °C, which is already mild cold stress for small rodents, or gradually acclimated to an ambient temperature of 5 °C, and the proteome of iBAT was analyzed subsequently (Figure 20A). The hypothesis was that UCP1KO mice would already exhibit a very characteristic protein signature when kept at 23 °C, indicative of UCP1-independent thermogenic mechanisms, particularly related to lipid metabolism. Furthermore, this trend was expected to become even more pronounced at a lower housing temperature, i.e. the proteome signature of UCP1KO mice should be even more distinct from that of WT mice. The main focus was undeniably on iBAT, but iWAT could be no less interesting for future studies in the context of UCP1-independent NST mediated by futile substrate cycles, as respirometry data clearly demonstrate that inter-organ cycling would be conceivable, white fat is abundant, has a high browning capacity, and has a high oxidative capacity after prolonged cold exposure.
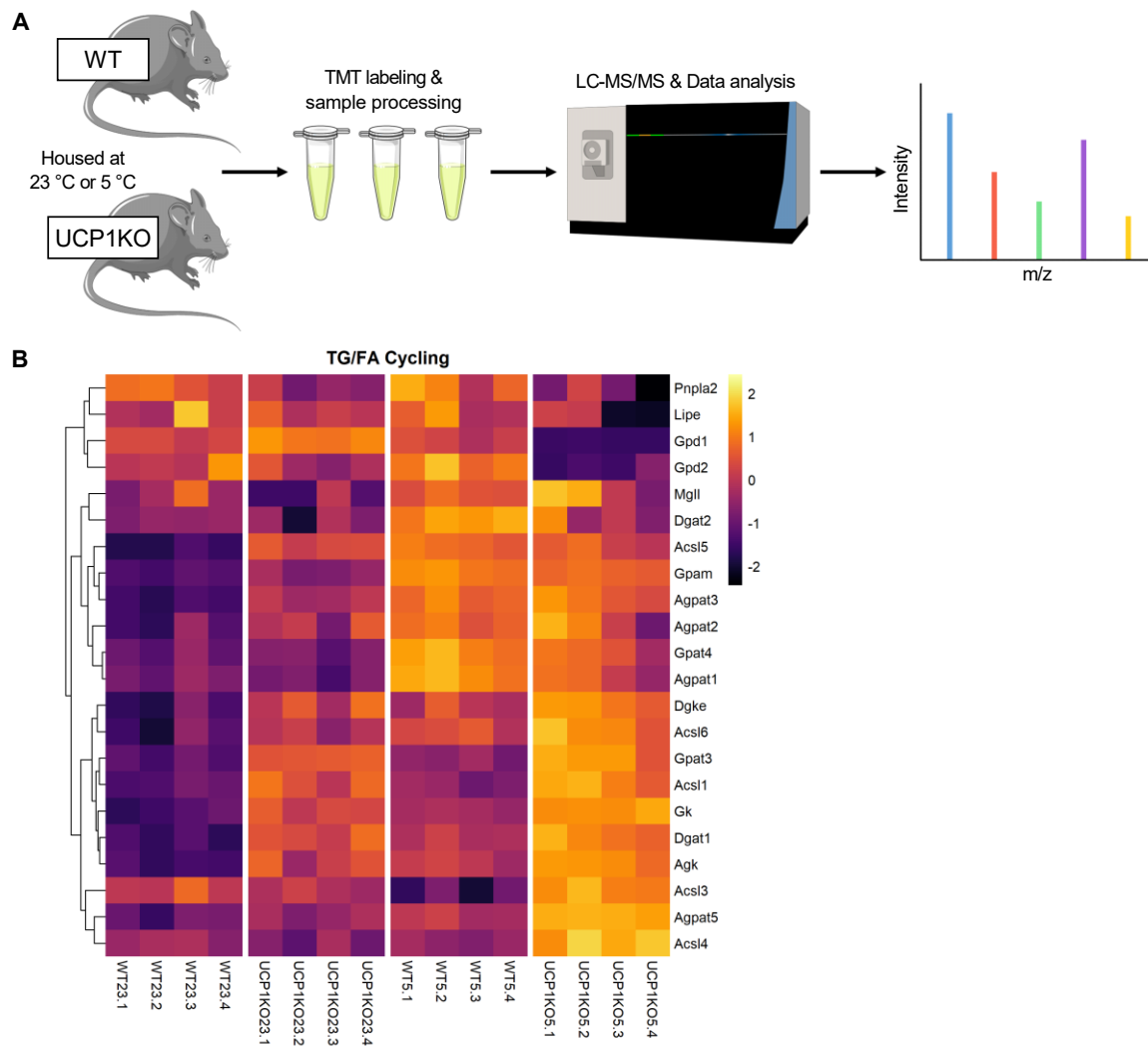
Figure 20: Regulation of proteins related to futile lipid cycling in iBAT of wild type and UCP1-knockout mice housed at room temperature and cold. A) *Schematic depiction of sample generation, processing, and subsequent proteome analysis. C57BL/6N wild type (WT) and UCP1-knockout (UCP1KO) mice were acclimated to 23 °C or 5 °C. WT and UCP1KO iBAT samples were processed and analyzed together.* ***B)*** *Regulation of proteins potentially involved in FA/TG cycling in iBAT of C57BL/6N WT and UCP1KO mice acclimated to 23 °C or 5 °C. The complete set of analyzed data can be found online as supplementary data to this article[69]. n = 4 animals. Column labels represent individual mice: WT (WT23) and UCP1KO (UCP1KO23) mice acclimated to 23 °C, WT (WT5) and UCP1KO (UCP1KO5) mice acclimated to 5°C. Row labels represent gene symbols of proteins. Normalized protein intensities were scaled by calculating z-scores for each protein. Cell color indicates z-score. Proteins are designated by their gene name in parentheses: Long-chain acyl-CoA synthetase (Acsl), acylglycerol kinase (Agk), 1-acylglycerol-3-phosphate O-acyltransferase (Agpat), diacylglycerol O-acyltransferase (Dgat), diacylglycerol kinase epsilon (Dgke), glycerol kinase (Gk), mitochondrial glycerol-3-phosphate acyltransferase (Gpam), glycerol-3-phosphate acyltransferase (Gpat), glycerol-3-phosphate dehydrogenase (Gpd), hormone-sensitive lipase (Lipe), monoglyceride lipase (Mgll), adipose tissue triglyceride lipase (Pnpla2).*

Nevertheless, in iBAT, neither genotype nor housing temperature had a significant effect on expression levels of ATGL (Pnpla2; for clarity, gene symbols are stated in brackets, when the gene name strongly deviates from the protein name), HSL (Lipe), and monoglyceride lipase (MGL, encoded for by the Mgll gene). A weak trend was observed that UCP1KO mice showed slightly increased MGL protein levels when housed at 5 °C, whereas ATGL and HSL tended to be decreased (Figure 20B). With respect to the enzymes involved in the provision of glycerol backbones, differences between WT and UCP1KO mice

were quite pronounced. UCP1-ablated animals kept at 23 °C had by far the highest GPD1 expression among all groups, but upon cold acclimation, GPD1 was significantly downregulated in iBAT of UCP1KO mice translating into the lowest expression among all groups. At 23 °C, WT mice had slightly lower GPD1 protein levels compared to their UCP1KO counterparts, but WT mice in turn exhibited increased expression once exposed to lower temperatures. GPD2 was not significantly regulated, but the direction of change between mice maintained at 23°C and animals maintained at 5°C as a function of genotype was the same as for GPD1. In contrast, a very clear genotype-dependent pattern emerged regarding protein expression of glycerol kinase (GK). Cold acclimation caused GK to be significantly upregulated in all animals. However, irrespective of ambient temperature, UCP1KO mice always had a significantly higher GK expression than WT mice. Moreover, four out of five detected ACSL isoforms, namely ACSL1, ACSL3, ACSL4, and ACSL6, catalyzing the ATP-dependent activation of FAs prior to re-esterification were significantly more abundant in UCP1KO animals exposed to mild cold stress in comparison to their WT controls. Expression of these enzymes increased even further in UCP1KO mice as a result of acclimation to 5 °C, while it was reduced in WT mice. ACSL5 protein levels were significantly lower in WT mice housed at 23 °C, but no difference was detected between WT animals acclimated to cold and UCP1-ablated acclimated to mild cold or cold. At 23 °C, no major differences between genotypes could be observed with respect to protein levels of GPAT and AGPAT isoforms. All detected acyltransferase isoforms were significantly upregulated upon cold acclimation in WT and UCP1KO mice. Nevertheless, in cold-acclimated mice, again, no significant differences between the two groups were detected, with the exception of AGPAT5, which was higher in UCP1KO animals. Interestingly, DGAT1 and DGAT2 protein expression was highly genotype-dependent, since UCP1KO mice had a significantly higher expression of DGAT1 compared to WT animals when housed at 23 °C. Additionally, DGAT1 levels of UCP1-ablated animals were even further upregulated in response to lowering the housing temperature to 5 °C. Although DGAT1 expression in the WT control group was minimally increased upon cold-acclimation, animals in the cold-acclimated UCP1KO group still had almost twofold higher protein levels. Conversely, there was no difference between the two 23 °C groups with respect to DGAT2. Nevertheless, DGAT2 was significantly upregulated in WT mice when acclimated to 5 °C, while expression in iBAT of UCP1KO mice was not altered. In summary, there appears to be no obvious recruitment on the part of the lipases involved in the release of FAs from lipid droplets. However, this is not very surprising, since the activity of these enzymes is known to be subject to posttranslational modifications, and it is under strict hormonal control. On the part of generating glycerol backbones, a pronounced shift from GPD1-mediated glyceroneogenesis to GK was observed in cold-acclimated UCP1KO mice compared to WT controls and animals maintained at 23 °C. Furthermore, enzymes that catalyze the activation of long chain FAs were preferentially recruited in UCP1-ablated mice with a change in ambient temperature from 23 °C to 5 °C. No genotype-dependent

differences were detected regarding acyltransferases using G3P or MAG as substrate, but a very distinct signature concerning DGAT1 and DGAT2 was found. This signature is in good agreement with the *in vitro* data, and suggests that DGAT1 may be recruited in the absence of UCP1 and thereby contribute to NST in iBAT of UCP1KO mice.

Apart from proteins associated with futile FA/TG cycling, various enzymes that are part of lipid metabolism were regulated in a genotype- and temperature-dependent manner. In general, expression of various perilipin isoforms, which protect lipid droplets from lipolytic degradation by ATGL and HSL, was lower in UCP1KO mice housed at 23 °C and 5°C (Figure 21).
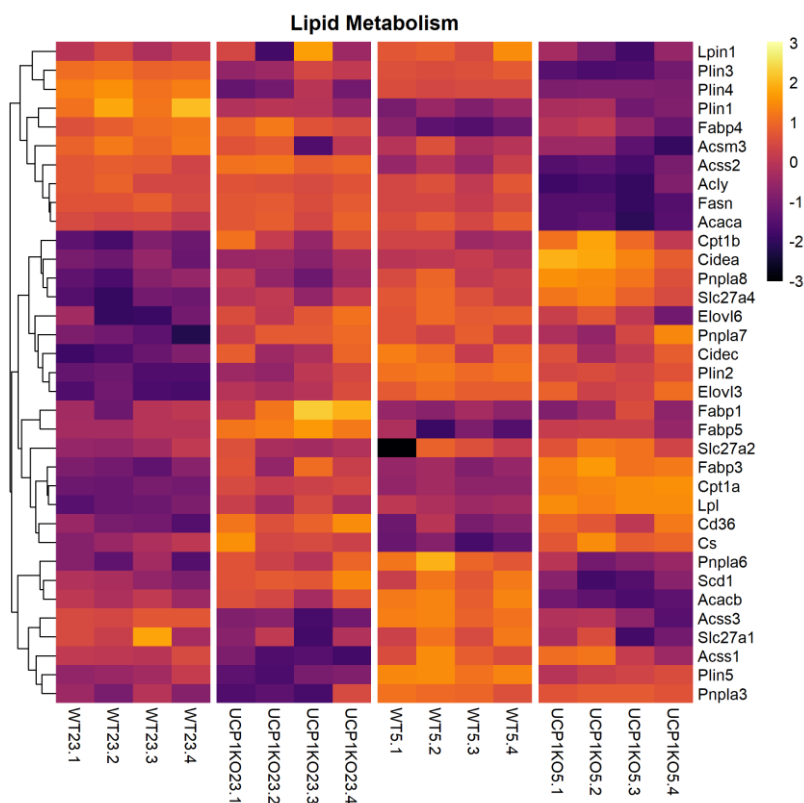
Figure 21: Regulation of proteins related to lipid metabolism in iBAT of wild type and UCP1-knockout mice housed at room temperature and cold. *Regulation of proteins associated with lipid metabolism in iBAT of C57BL/6N WT and UCP1KO mice acclimated to 23 °C or 5 °C. The complete set of analyzed data can be found online as supplementary data to this article[69]. n = 4 animals. Column labels represent individual mice: WT (WT23) and UCP1KO (UCP1KO23) mice acclimated to 23 °C, WT (WT5) and UCP1KO (UCP1KO5) mice acclimated to 5°C. Row labels represent gene symbols of proteins. Normalized protein intensities were scaled by calculating z-scores for each protein. Cell color indicates z-score. Proteins are designated by their gene name in parentheses: Acetyl-CoA carboxylase alpha (Acaca), acetyl-CoA carboxylase beta (Acacb), ATP citrate lyase (Acly), acyl-CoA synthetase medium chain family member (Acsm), acyl-CoA synthetase short chain family member (Acss), CD36 molecule (Cd36), cell death inducing DFFA like effector a (Cidea), cell death inducing DFFA like effector c (Cidec), carnitine palmitoyltransferase 1A (Cpt1a), carnitine palmitoyltransferase 1B (Cpt1b), citrate synthase (Cs), ELOVL fatty acid elongase (Elovl), fatty acid binding protein (Fabp), fatty acid synthase (Fasn), lipin 1 (Lpin1), lipoprotein lipase (Lpl), perilipin (Plin), patatin like phospholipase domain containing (Pnpla), stearoyl-CoA desaturase 1 (Scd1), Fatp (Slc27a).*

On the contrary, FA-binding protein (FABP) expression levels were consistently higher in UCP1KO animals independent of the housing temperature. Enzymes participating in *de novo* FA synthesis, namely acetyl-CoA carboxylase (ACAC) and FA synthase (FASN), were massively downregulated in the cold-acclimated UCP1KO group, while citrate synthase levels were significantly increased. However, CD36, a protein facilitating the uptake of FAs into cells, and lipoprotein lipase (LPL), an enzyme catalyzing lipolytic degradation of TGs from TG-rich lipoproteins, were upregulated in UCP1-ablated mice and the trend was further enhanced with cold-acclimation. Moreover, UCP1KO mice acclimated to 23 °C had higher CPT1 protein levels, which controls mitochondrial β-oxidation, compared to WT controls, and recruited even significantly more CPT1 when housed at 5°C. Overall, it appears that adaptations of the proteome create a pro-lipolytic environment in iBAT of UCP1KO mice to provide more FAs from both intracellular stores and extracellular sources. However, in this scenario, *de novo* FA biogenesis does not appear to be of greater importance, whereas the enzymatic capacity to degrade FA and utilize acetyl-CoA in the TCA cycle drastically is expanded.

Changes indicating the recruitment of other UCP1-independent thermogenic mechanisms could also be detected. SERCA2b (Atp2a2) was significantly higher in UCP1KO mice acclimated to 23 °C compared to WT animals (Figure 22). WT mice still increased expression after cold acclimation, which UCP1KO mice did not, therefore no difference between genotypes was observed at 5°C. SERCA1 (Atp2a1) was also upregulated by lowering the ambient temperature in both groups, although protein expression tended to be greater in WT mice but not significantly different. Surprisingly, at 23 °C, there were no differences between genotypes with respect to inositol 1,4,5-trisphosphate receptor type 1 (ITPR1) and ITPR2, whereas both ER-localized Ca^{2+} channels were massively reduced in cold-acclimated UCP1KO mice and rather increased in cold-acclimated WT controls. Genotype and housing temperature had no significant effect on RYR1, with UCP1KO mice generally tending to have slightly higher expression levels. With regard to proteins associated with creatine cycling, CK M-type (CKM) and mitochondrial CK S-type (CKMT2) tended to be expressed at a higher level in iBAT of UCP1KO mice (Figure 22). Nevertheless, CK B-type (CKB) and TNAP (Alpl) were significantly induced by lowering the housing temperature from 23 °C to 5 °C, and were almost twice as abundant in UCP1KO animals as in WT controls.
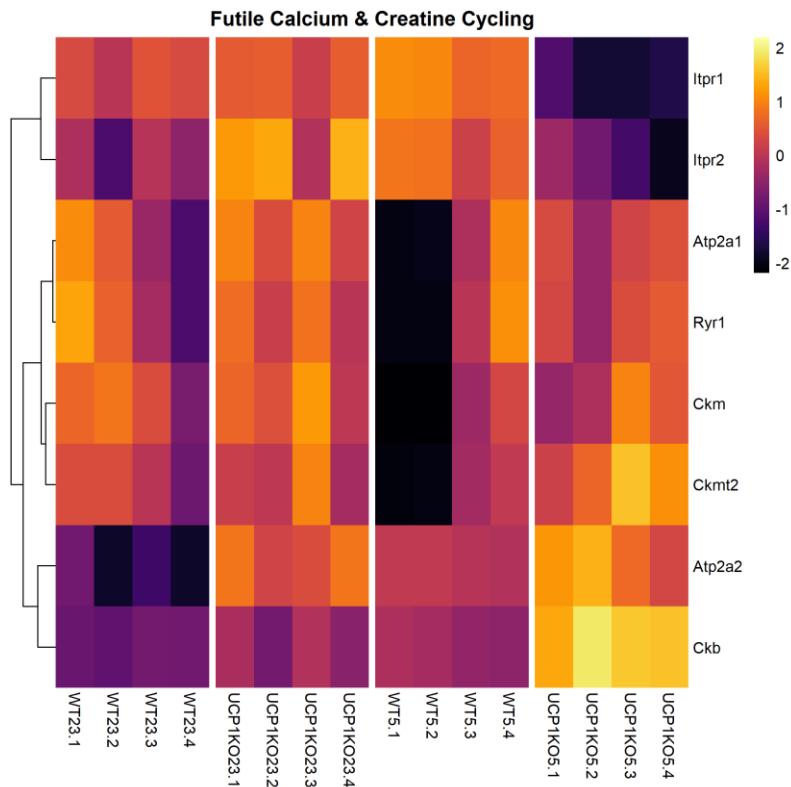
Figure 22: Regulation of proteins related to Ca²⁺and creatine metabolism in iBAT of wild type and UCP1-knockout mice housed at room temperature and cold. *Regulation of proteins associated with futile Ca²⁺ and creatine cycling in iBAT of C57BL/6N WT and UCP1KO mice acclimated to 23 °C or 5 °C. The complete set of analyzed data can be found online as supplementary data to this article[69]. n = 4 animals. Column labels represent individual mice: WT (WT23) and UCP1KO (UCP1KO23) mice acclimated to 23 °C, WT (WT5) and UCP1KO (UCP1KO5) mice acclimated to 5°C. Row labels represent gene symbols of proteins. Normalized protein intensities were scaled by calculating z-scores for each protein. Cell color indicates z-score. Proteins are designated by their gene name in parentheses: ATPase sarcoplasmic/endoplasmic reticulum Ca²⁺ transporting (Atp2a), creatine kinase B (Ckb), creatine kinase, M-type (Ckm), creatine kinase, mitochondrial 2 (Ckmt2), inositol 1,4,5-trisphosphate receptor type (Itpr), ryanodine receptor 1 (Ryr1).*

Taken together, these findings clearly show that UCP1KO mice already exhibit a very characteristic proteome signature indicative of a futile substrate FA/TG cycle in brown adipocytes when exposed to mild cold (23 °C). Moreover, stepwise cold-acclimation led to a further induction of the majority of involved key enzymes but only in UCP1-ablated animals, again highlighting the theoretical thermogenic importance of this mechanism. Although the functional *in vitro* data at least argue against an involvement of futile Ca²⁺ and creatine cycling in UCP1-independent NST, a considerable upregulation of proteins associated with futile Ca²⁺ and creatine cycles was found. However, since it cannot be assessed how much each of these mechanisms contributes to heat production *in vivo* and whether flux rates are in fact increased, it definitely cannot be excluded that all three mechanisms and perhaps as yet unknown thermogenic processes may mediate NST in iBAT of UCP1KO mice.

At this point, it is essential to briefly mention an important methodological consideration that will be addressed in more detail later in the discussion. Analogous to immunoblotting, proteome analysis determines relative "protein concentrations". The same absolute amount of total protein is analyzed

across all samples and experimental conditions, and the abundance of a particular protein within the entire proteome is quantified. This allows a quick overview of changes under different conditions, but does not necessarily allow conclusions to be drawn about an entire organ or tissue, especially when capacity is recruited and tissues of transgenic mice differ greatly from those of WT animals in weight and size. However, it has been shown, although these findings are largely ignored, that UCP1KO mice acclimated to mild cold or cold have a significantly larger iBAT and a considerably higher total protein content per whole iBAT depot compared to WT controls. Since in relation to whole body thermogenesis, not a relative rate but particularly a depot's total thermogenic capacity is of interest, it is extremely important to consider differences in depot mass. In this case, this explicitly means that the observed differences between WT and UCP1KO mice may be even more pronounced for proteins that were more abundant in UCP1-ablated animals, or in fact smaller than initially thought for proteins that were less abundant in UCP1-ablated animals. This conceptual consideration is directly related to the next and also last point that will be presented below.

3.7 Brown adipose tissue of UCP1KO mice has sufficient oxidative capacity to sustain heat production during mild cold exposure

A serious and fundamental criticism of UCP1KO iBAT being able to substantially contribute to maintaining normothermia at all is that a few publications reported mitochondrial defects and a depletion of the mitochondrial ETC in iBAT from UCP1KO mice[116,117]. These detrimental changes occurred even after mild cold exposure (usually room temperature) and were exacerbated at lower temperatures. If oxidative capacity and the ability to maintain a mitochondrial membrane potential were indeed impaired to such a degree, mitochondrial supply of ATP would consequently also cease. Anaerobic glycolysis might be able to partially compensate to an unknown degree, but undeniably, the overall cellular capacity to generate ATP would be severely limited. This poses a major problem because, although other organs can provide substrates, energy in the form of ATP can only be generated locally within each cell, and each tissue must therefore supply itself. Accordingly, it would be physiologically irrelevant that enzymes, which are part of futile substrate cycles, are enriched, since heat can only be generated by an increased substrate flux, which in turn is sustained by elevated synthesis and turnover of ATP. However, the aforementioned publications did not take the higher tissue weight and protein content of UCP1KO iBAT into account, and thus only included "relative expression levels" of mitochondrial ETC complexes without providing an arbitrary "absolute expression per whole depot". To make up for this limitation and to generate initial preliminary data from different UCP1KO models (on different genetic backgrounds), mice from regular breeding colonies were studied. Although this approach was not ideal, as the animals were group housed and fed a regular breeding diet, it should be sufficient to detect general tendencies, because all animals nevertheless experienced

mild cold stress (23 °C housing temperature) and were continuously exposed to this environment since birth.
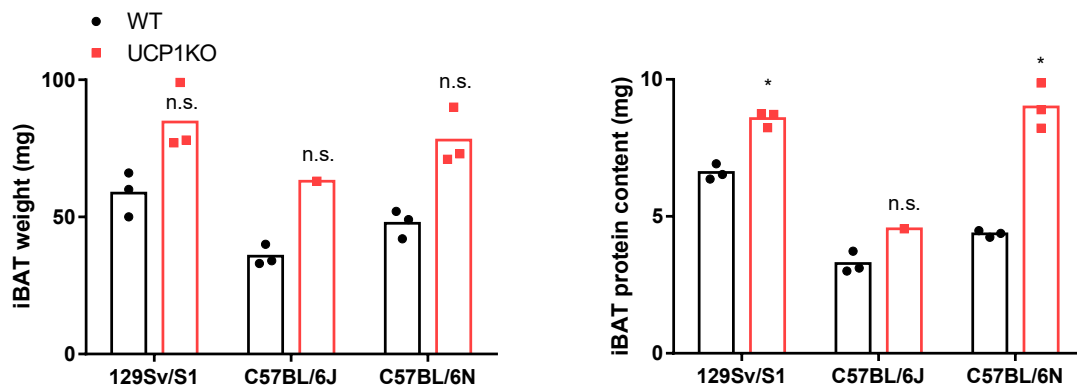
Figure 23: UCP1-knockout mice recruit iBAT mass. *Weight and protein content of iBAT from adult 129Sv/S1, C57BL/6J, and C57BL/6N wild type (WT) and UCP1-knockout (UCP1KO) mice from regular breeding colonies, i.e. group-housed at 23 °C. n = 1 – 3 animals. A two-tailed Welch-test was applied. (*) indicates a significant difference between the WT and UCP1KO group within each genetic background. Not statistically significant (n.s.).*

Nevertheless, in line with previous publications[69,124,125], iBAT of UCP1KO mice was in terms of gross appearance very different from iBAT of WT mice. UCP1KO iBAT depots were larger and less intensely red and brown in color. This was also reflected in a higher tissue weight and protein content per depot (Figure 23). Depending on the mouse strain, iBAT of UCP1KO animals was between 1.4-fold and 1.7-fold heavier than iBAT of WT controls and contained between 1.2-fold and up to twofold more protein in total.
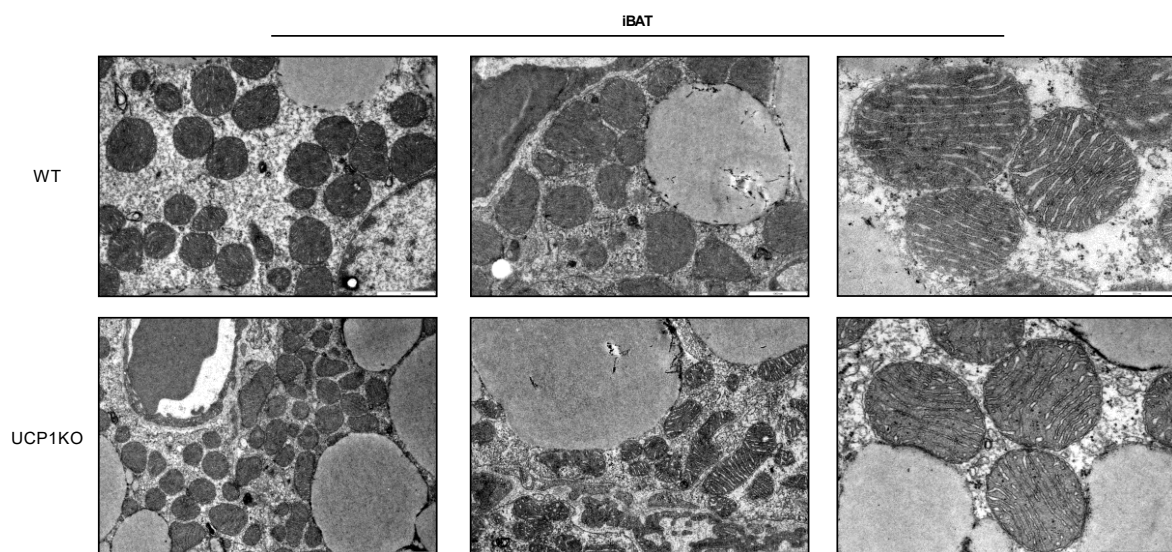
Figure 24: Brown fat mitochondria of UCP1-knockout mice exposed to mild cold have a normal cristae architecture and structure. *Representative electron micrographs of iBAT from adult 129Sv/S1 wild type (WT) and UCP1-knockout (UCP1KO) mice from regular breeding colonies, i.e. group-housed at 23 °C. n = 1 WT mouse and 2 UCP1KO mice.*

Of note, electron micrographs clearly showed that iBAT mitochondria of these UCP1KO mice have a normal morphology and cristae architecture (Figure 24), and that very few, if any, mitochondria appear structurally aberrant. Moreover and very surprisingly, depletion of the respiratory chain in iBAT of UCP1KO mice was by far not as severe as previously described. Only complex I (NDUFB8) and complex IV (MTCO1) were affected, while complex II (SDHB) and III (UQCRC2) protein levels were not largely different between WT and UCP1KO iBAT (Figure 25).
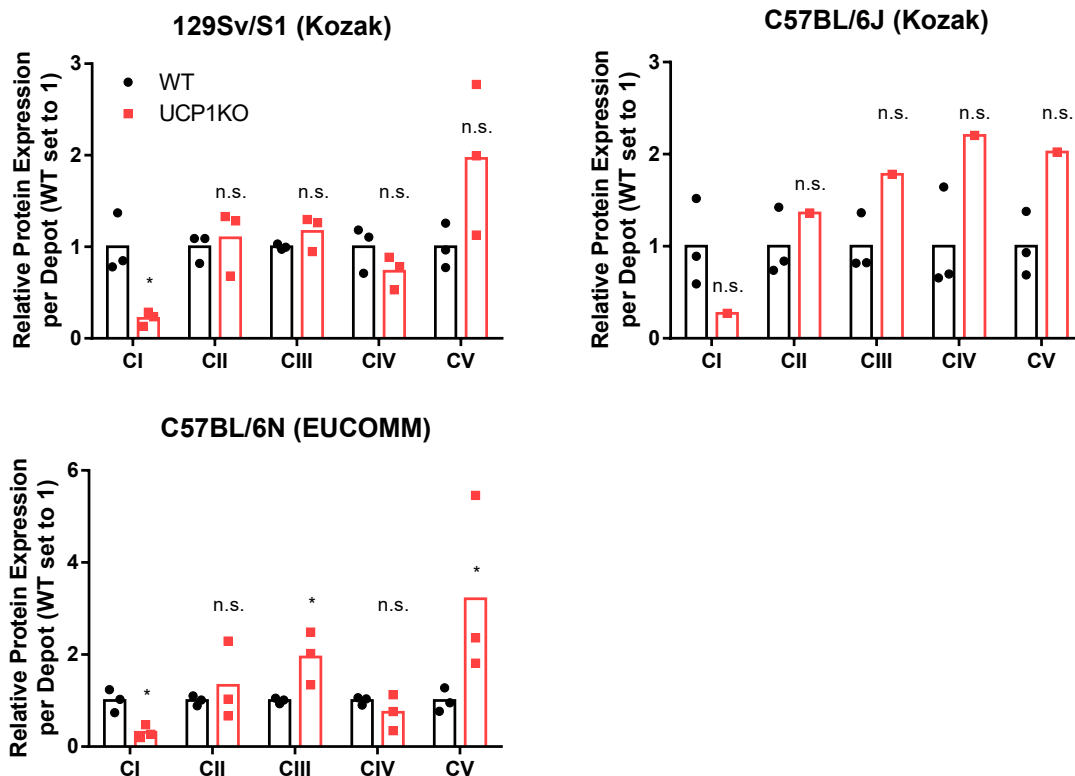
Figure 25: Brown adipose tissue of UCP1-knockout mice has sufficient oxidative capacity to sustain heat production during mild cold exposure. Protein expression of electron transport chain complexes in iBAT of adult 129Sv/S1, C57BL/6J, and C57BL/6N wild type (WT) and UCP1-knockout (UCP1KO) mice from regular breeding colonies, i.e. group-housed at 23 °C. n = 1 – 3 animals. A two-tailed Welch-test was applied. (*) indicates a significant difference between the WT and UCP1KO group. Not statistically significant (n.s.).

On the contrary, protein expression of ATP5A1, a subunit of the catalytic domain of the mitochondrial ATP synthase (complex V), was even 2-fold higher in UCP1-ablated mice. Complex II and III tended to be more abundant in iBAT of UCP1KO mice, whereas complex IV was only minimally decreased. Due to the small sample size, however, the results should be interpreted qualitatively rather than necessarily quantitatively, and differences between the three mouse strains will not be discussed further. Taken together, these data suggest that in this scenario depletion of the mitochondrial respiratory chain is, if at all, only very mild in UCP1KO mice housed at 23 °C and that not all complexes are negatively affected, while complex V is consistently and significantly upregulated. Moreover,

increased protein mass per iBAT depot may compensate for and eventually even outweigh the impairment of the oxidative phosphorylation machinery in UCP1-ablated animals. Since the futile FA/TG substrate cycle only depends on ATP synthesis and turnover, a decreased amount of complex I to IV would not preclude UCP1-independent thermogenesis as long as their capacity is high enough to cover the dissipation of protonmotive force by a fully active ATP synthase. Therefore, it is concluded that iBAT of UCP1KO mice has the electron transport chain machinery required to substantially contribute to NST.

4 Summary

While multiple hypothesis for UCP1-independent NST in adipose tissues surrounding futile substrate cycles have been put forward, no definitive conclusion has been offered yet. UCP1-independent NST has been puzzling scientists for decades, as on the one hand it was extremely surprising that explants from otherwise considered metabolically inert WAT greatly increased their oxygen consumption after addition of a direct-acting sympathomimetic, and as on the other hand UCP1KO mice can be acclimated to cold – which was long unthinkable – when ambient temperature is lowered gradually. The only logical conclusion from this is that there definitely must exist UCP1-independent thermogenic mechanisms in rodents but also very likely in humans. The appealing part of this thought is that these mechanisms can per definition occur not only in BAT, which is the sole tissue in mammals that has such a high UCP1 expression, but also in WAT, which is known to express very low levels of UCP1 or even none at all. This fact in particular is very important, since in the meantime the initial euphoria after the "rediscovery" of metabolically active brown fat in humans has subsided, because the prevalence, the amount and the resulting theoretical maximum contribution to human whole body thermogenesis and energy expenditure seem to be much lower than scientists had privately hoped for. Based on the premise of potential future therapeutic exploitation, whether to modulate energy expenditure or substrate partitioning, a strategy, which does not exclusively depend on UCP1, appears to be far more promising.

The present work sought to comprehensively characterize futile substrate cycles in brown UCP1KO adipocytes and to finally delineate the nature of UCP1-independent NST. In good agreement with previous publications, proteome analysis of brown WT and UCP1KO adipocytes confirmed Ca^{2+} and FA/TG cycling as putative futile thermogenic substrate cycles. Primary cultures of brown UCP1KO adipocytes were used to study UCP1-independent NST *in vitro*. Microplate-based respirometry demonstrated that brown UCP1KO cells, almost comparable to WT adipocytes, drastically increase their oxygen consumption in response to adrenergic stimulation. While stimulated respiration in WT cells does not depend on aerobic ATP synthesis and is fully explained by UCP1 activity, respiration rates in UCP1KO cells strictly depend on the actions of mitochondrial ATP synthase, and therefore could be

largely mediated by futile ATP-consuming substrate cycles. In a series of experiments, using chemical and pharmacological inhibitors and RNA interference technology, the previously objectively selected metabolic pathways and additionally creatine cycling, despite the fact that associated enzymes were not significantly enriched in the proteome analysis, were investigated more closely.

Although evidence in the literature indicating that a futile creatine cycle may mediate UCP1-independent NST was compelling, at that time the enzymes involved had not been identified beyond doubt. Thus, the experimental approach applied in the present study was not very sophisticated and targeted rather large areas of creatine metabolism. Nevertheless, neither blocking TNAP-mediated dephosphorylation of phosphocreatine – and TNAP has now been proven unequivocally to be one of two key enzymes – nor lowering intracellular creatine availability had any effect on adrenergically stimulated futile turnover of ATP in brown UCP1KO adipocytes. Therefore, it was concluded that a futile creatine substrate cycle does not contribute to cellular NST in brown UCP1KO adipocytes.

Futile Ca^{2+} cycling was investigated next and, in contrast to thermogenesis based on creatine metabolism, the involved enzymes and channels had already been established. Consequently, SERCA2b was knocked down with siRNA in a targeted manner, but also thapsigargin was used to inhibit all SERCA isoforms in parallel. No impact on respiration rates was detected and not even broad complexation of free cytosolic Ca^{2+} affected ATP-dependent oxygen consumption after treatment with an adrenergic agonist. Thus, UCP1-independent NST in this model cannot be accounted for by a futile Ca^{2+} substrate cycle either.

The last mechanism studied, and at the same time the only mechanism that has been intertwined with UCP1-independent NST for decades, was futile lipid cycling. Blocking lipolysis completely prevented any increase in oxygen consumption over basal rates in response to adrenergic stimulation, whereas, individually, pharmacological inhibition of ATGL had the greatest impact and HSL inhibition only caused a modest reduction. Reducing ATP-dependent activation of long chain FAs drastically attenuated stimulated oxygen consumption rates. Activated FAs may undergo either re-esterification mediated by acyltransferases or degradation during mitochondrial β-oxidation. Nevertheless, since etomoxir, a substance that blocks the import of long chain FAs into mitochondria, had no effect at all on cellular oxygen consumption, this finding factually precludes the possibility that newly released FAs are predominantly broken down into acetyl-CoA, which is then again used for *de novo* FA synthesis. In contrast, inhibiting DGAT1-mediated re-esterification had a significant impact on isoproterenol-stimulated oxygen consumption, while targeting DGAT2 did not have any effect. These findings clearly indicate that a substantial portion of FAs released from lipid droplets during active lipolysis in brown UCP1KO adipocytes is immediately re-esterified onto acylglycerols in a futile substrate cycle, and thereby constitute a major contributor to cellular energy expenditure. Moreover, the addition of FAs

to the culture medium alone without adrenergic stimulation was sufficient to trigger ATP-dependent oxygen consumption, which proves that not only intracellularly stored but also exogenously derived FAs can sustain futile FA/TG cycling. Lastly, all these mechanistic insights could be largely confirmed using a completely independent method, i.e. quantification of glycerol and FAs in the medium, which emphasizes the experimental robustness of this observation.

In the last stage of the *in vitro*-based part, light was shed on the interplay between glucose and lipid metabolism, and the multifaceted relationship between PDM, futile lipid cycling, and ER stress was uncovered. It was assumed that glycolysis might provide G3P backbones onto which activated FAs are attached. Blocking glycolysis in brown UCP1KO adipocytes or removing glucose from the assay medium caused respiration rates to stay on the basal level despite treatment with isoproterenol. As the simultaneous addition of pyruvate was not able to restore cellular respiration, glucose is most likely converted to dihydroxyacetonephosphate, which is consecutively metabolized to G3P by GPD1. Knocking down GPD1 confirmed its role in this process, because reduced Gpd1 expression translated into a lower stimulated oxygen consumption. Thus, glucose and lipid metabolism are even more closely connected in the absence of UCP1, and this intricate connection may be of even greater importance by flexibly providing pyruvate, reducing equivalents, and glycerol backbones especially during high rates of futile FA/TG cycling. Since active ATP-dependent re-esterification of FAs locally creates a substantial energy demand, specifically mitochondria in the immediate proximity of nascent and growing lipid droplets need to directly supply ATP. This subtype is relatively distinct from regular cytoplasmic mitochondria and is thought to harbor specific adaptions to support its functional requirements. Interestingly, PDM occur more frequently in the absence of UCP1 and it is suggested that this association may be related to futile FA/TG cycling. However, this interaction and the spatial proximity of organelles may be crucial not only to fuel UCP1-independent NST, but also to maintain lipid homeostasis and preserve the extremely fragile lipid composition of ER and mitochondrial membranes. While WT adipocytes were in principle less susceptible to ER stress, it was shown that inhibiting DGAT1-mediated re-esterification or limiting overall re-esterification capacity during active lipolysis leads to an induction of UPR genes predominantly in UCP1KO adipocytes. These data suggest that FA/TG cycling may help to avert the detrimental accumulation of lipids and alleviate ER stress in brown UCP1-ablated cells.

Furthermore, we aimed to provide a first overview of cold-induced adaptations *in vivo* by analyzing the iBAT proteome of WT and UCP1KO mice at different housing temperatures. UCP1KO mice already when acclimated to room temperature showed a strong recruitment of proteins related to futile substrate cycles and this genotype-dependent divergence seemed to be further increasing when ambient temperature was lowered. In descending order of their enrichment, the signature was

clearest for futile FA/TG cycling, as the enzymes involved were always higher in UCP1KO-ablated animals and upregulated proportionally to the reduction in ambient temperature. With respect to creatine cycling, the association was slightly weaker, whereas individual proteins related to the Ca^{2+} cycle were still higher in UCP1KO mice, but did not follow the expected pattern as a function of ambient temperature. Based on these findings, it seems at least plausible that all three of the previously described UCP1-independent mechanisms, namely Ca^{2+}, creatine, and FA/TG cycling, mediate NST in iBAT of UCP1KO mice. Finally yet importantly, the common misconception that brown UCP1KO mitochondria would exhibit a dramatic reduction in ETC abundance, and thus rendering UCP1KO iBAT incapable of contributing to whole body thermogenesis, was dispelled. Western blot analysis clearly revealed that only complex I and IV of the ETC were reduced in UCP1KO iBAT, whereas complex V was strongly upregulated. Because these reductions were even partly compensated by an increase in total depot mass, it was concluded that oxidative capacity in iBAT of UCP1KO mice housed at 23 °C is not severely impaired in comparison to WT iBAT. Therefore, it is evident that, at least during mild cold stress, iBAT of UCP1-ablated mice can be a major source of NST.

Taken together, murine brown UCP1KO adipocytes recruit futile FA/TG cycling for adaptive thermogenesis. Adrenergic signaling activates FA/TG cycling that strictly depends on the continuous release of FAs catalyzed by ATGL and HSL. At the same time, DGAT1 mediates ATP-dependent re-esterification of FAs onto glycerol backbones derived in part from glycolysis, thereby connecting glucose and lipid metabolism. Moreover, so far largely unrecognized implications beyond the proposed thermogenic properties especially in terms of the dynamic interaction between mitochondria and lipid droplets, and a potential role in protecting against lipotoxicity were explored. Finally, it was demonstrated that iBAT of UCP1KO mice kept at room temperature or below shows changes at the protein level indicating the adaptive recruitment of futile substrate cycles for NST. Therefore, the present study identified and characterized a UCP1-independent mechanism, which contributes to NST and energy expenditure.

5 Discussion

5.1 Only UCP1 can mediate adaptive non-shivering thermogenesis in the cold?

UCP1 is widely considered to have provided a key thermoregulatory and evolutionary advantage to the eutherian lineage, particularly for small-bodied and hibernating species[126]. While BAT in larger-bodied species (e.g., humans) is drastically reduced with the onset of adulthood, it has been generally understood to still play a vital role in their neonates[127]. Most of our understanding of UCP1's functionality comes from a single constitutive KO mouse model generated in Leslie Kozak's laboratory already 25 years ago[38]. UCP1KO mice develop hypothermia after only a few hours of acute cold exposure underlining the critical importance of UCP1 in maintaining body temperature in extreme environments. This finding and the fact that UCP1KO mice did not significantly increase heat production following an injection with NE led to the conclusion that "[…] no other mechanism is present in any organ that can take over from UCP1 as a mediator of any form of non-shivering thermogenesis, even after prolonged time in the cold. UCP1 is therefore the only protein capable of mediating any form of cold acclimation-recruited non-shivering thermogenesis"[128]. Nevertheless, UCP1KO mice can be acclimated to cold[40,117,125,129-131], when the ambient temperature is lowered gradually, but this observation is difficult to reconcile with the previous statement. To invalidate this argument, which could suggest the presence of adaptive UCP1-independent NST, it is typically cited that muscle shivering does not cease in cold-acclimated UCP1KO mice[129]. Consequently, no alternative thermogenic mechanism that is powerful enough to compensate the absence of UCP1 would be recruited, if shivering-based thermogenesis had to persist on a constantly high level. While this explanation relies on the assumption that shivering thermogenesis is the only source of heat production in cold-acclimated UCP1KO mice allowing them to maintain their body temperature, it is in turn strongly contradicted by the following three points.

Firstly, recruitment of UCP1-independent NST in UCP1KO animals has never been experimentally disproven, and the evidence provided is almost exclusively based on the reasoning outlined before.

Secondly, it was found that muscle shivering activity is significantly higher in UCP1KO mice compared to WT mice during acute cold exposure[129]. Nevertheless, electromyogram recordings taken at 4 °C were qualitatively and quantitatively not different between UCP1KO animals acclimated to 30 ° C or 4 °C. Since warm-acclimated UCP1KO mice developed hypothermia after only a few hours and cold-acclimated animals survived for weeks, whereas shivering intensity was equally high in both groups, these results rather suggest that shivering thermogenesis is not the critical factor mediating cold tolerance. Moreover, long-term skeletal muscle shivering activity should result in a recruitment of

additional capacity, but the apparent training effect in cold-acclimated WT and UCP1KO mice was not different[130].

Thirdly, it has been demonstrated that the acute severe cold sensitivity is unique to UCP1KO mice on a congenic background[40,125]. The individual genetic background even determines the penetrance of this phenotype, since two third of the UCP1KO mice on a BL/6J background were resistant to cold, while almost 9 out of 10 animals on a 129S background were not able to defend their body temperature during acute cold exposure[40]. Moreover, when these two congenic UCP1KO lines were crossed, the entire resulting F1 hybrid generation was able to defend its body temperature during acute and chronic cold challenge virtually like the WT counterparts. Taken together, these results, which are largely disregarded, strongly indicate that UCP1 is dispensable for cold-induced thermogenesis, and thus very likely not "the only protein capable of mediating any form of cold acclimation-recruited non-shivering thermogenesis".

Consequently, we hypothesized that the loss of UCP1 would be compensated by the recruitment of additional thermogenic mechanisms. These alternative pathways were studied by leveraging UCP1KO mice, which, by definition, solely rely on UCP1-independent sources of heat generation. Of course, the choice of model organism may be challenged. In other words, why should we characterize a physiological process that is predominantly found in mice lacking one of the most abundant mitochondrial proteins in BAT? As mentioned before, average BAT mass in adult humans is quite low, the contribution of BAT to total energy expenditure is negligible without stimulation, and the amount of active BAT is inversely correlated with age, BMI, and unfavorable metabolic outcomes, such as type 2 diabetes and dyslipidemia[54,132-134]. Therefore, to exploit thermogenic fat, i.e. UCP1-positive adipose tissue, as a therapeutic target, significant amounts of UCP1 would first need to be recruited and then safely activated, which still presents a major challenge to date[135]. Considering recent developments, the uncertainties associated with UCP1-mediated thermogenesis in humans, and the sheer mass of adipose tissue not expressing UCP1, it seems much more likely that UCP1-independent NST impacts our energy expenditure and glucose as well as lipid metabolism[136]. This served as an incentive to shed more light on alternative thermogenic mechanisms, which are recruited when UCP1 is absent or expression levels are very low, and to quantify their relative contribution to cellular NST.

5.2 A (un)biased pre-selection of thermogenic processes

The results of the initial screening coincided well with the most extensively described mechanisms previously associated with UCP1-independent thermogenesis. Changes in individual protein levels were rather small upon stimulation with isoproterenol, but this is not very surprising given the short incubation time of only 30 minutes (this regime was deliberately chosen as it was intended to best

mimic the standardized conditions of follow-up functional bioenergetics analyses). Since protein synthesis is a process that takes rather hours than minutes, the observed changes were most likely caused by an altered rate of protein degradation and/or export. Nevertheless, these small differences, as they were consistent, resulted in an enrichment of proteins associated with specific pathways eventually forming larger distinguishable patterns. A major drawback of this type of bioinformatics analysis is that the result is highly dependent on how complete the annotation of a given gene ontology or KEGG term is and how carefully it has been curated. To give an example: CKB is associated with the GO terms "phosphorylation" and "cellular chloride ion homeostasis". These terms are very generic, and thus would not necessarily point towards the induction of an alternative thermogenic mechanism. Moreover, 3642 proteins besides CKB fall into the category "phosphorylation", which is why it is less likely – in purely numerical terms – that this GO term is significantly enriched due to a different expression of proteins related to futile creatine cycling[137]. Accordingly, not only FA and Ca^{2+} cycling, which were identified objectively, but also creatine cycling was further investigated.

5.3   Lack of reproducibility due to different mouse models?

The mechanisms behind Ca^{2+} and creatine recycling shall not be further discussed here, because at least in the cell system used in the present work these two futile substrate cycles are of practically no significance with regard to UCP1-independent NST. The underlying reason remains elusive and is a matter of speculation at this point. A crucial difference is that in the majority of publications only WT mice were studied[53,77,78], which in addition also had a different genetic background. Moreover, when UCP1KO mice were employed, they had previously been crossed with another transgenic mouse line overexpressing PRDM16[70], making a valid comparison difficult. Since these animals were maintained on an C57BL/6N, C57BL/6J, or an unspecified C57BL/6 background, whereas the present study used cells derived from mice on a 129S1 background, it stands to reason that this may account for the different phenotypes observed. Given that UCP1KO mice on a C57BL/6J background are less cold sensitive[40], it is tempting to speculate that these animals recruit multiple UCP1-independent thermogenic mechanisms. In contrast, 129S1 UCP1KO mice were reported to be more susceptible to hypothermia, which might be explained by the fact that these animals only (can) recruit fewer alternative mechanisms, such as lipid cycling but just not Ca^{2+} and creatine cycling. This would be in good agreement with the *in vitro* data presented here, which clearly prove that a futile cycle of lipolysis and re-esterification of FAs is the single and major contributor to UCP1-independent thermogenesis in cultured brown 129S1 UCP1KO adipocytes. However, future studies investigating how the genetic background of commonly employed UCP1KO mouse models predetermines the recruitment of certain thermogenic processes in the absence of UCP1 will finally settle the debate about which mechanisms confer UCP1-independent NST.

5.4   Futile lipid cycling: a historical perspective

The general theoretical basis of futile substrate cycles has already been explained and accordingly the focus will now be on particular enzymes and reactions that have been demonstrated to be, or that could be, part of futile lipid cycling. Adipocytes harbor the enzymes to simultaneously break down stored fat and immediately recycle the reaction products to effectively replenish their lipid stores[98,138]. When both reactions are operating at the same time, many additional FAs have to be activated. This series of reactions generates heat, because the activation of one FA molecule consumes two ATP equivalents, and this process is already known to represent a major ATP sink in adipose tissues[139]. FAs can be released from intracellular TG stores, or they could have an extracellular origin and are supplied by the blood stream as TG-rich lipoproteins or directly as FAs derived from food. Since the addition of palmitate to the assay medium led to an acute increase in oligomycin-sensitive respiration, it is evident that adipocytes can rapidly take up extracellular FAs, which consequently triggers re-esterification and turnover of ATP. Hence, activation of intracellular lipolysis may be sufficient, although it is most likely dispensable to initiate futile lipid cycling. This clear advantage of futile lipid cycling distinguishes it from the other futile substrate cycles, since lipolysis/the provision of FAs and re-esterification can occur in different cell types of a tissue or even spatially separated in different organs. It has long been suspected that a futile FA/TG cycle could exist, since adrenergic stimulation enhances both lipolysis and TG synthesis, and over the years, more and more evidence has been added[97,98]. Interestingly, not only cold exposure[82,140] but also treatment with PPARγ agonists[48] causes an induction of genes related to anabolic and catabolic processes involved in lipid metabolism. Early studies in the 1980s tried to quantify rates of lipid cycling in rodent adipose tissues. Glyceroneogenesis and FA synthesis were approximated by measuring the incorporation of ^{3}H into glycerol and FA moieties, which can be used to calculate a cycling rate. Fasting and refeeding caused a significant induction of FA/TG cycling in WAT, whereas short-term cold exposure doubled cycling rates only in murine BAT but not WAT[44,47]. More recent studies, in which ^{3}H was replaced by ^{2}H, and nuclear magnetic resonance (NMR) or mass spectrometry (MS) was used for detection, reported very similar findings[81,82,141]. Consistent with previous results, adrenergic stimulation led to an increase in futile lipid cycling activity in adipose tissues with the strongest effect detected in iBAT. Due to the largely improved sensitivity, it could be shown that even eWAT ramps up re-esterification of FAs during chronic cold exposure. These findings collectively suggest that futile FA/TG cycling, which is regulated by various hormones and stimuli, occurs in murine BAT and WAT. Nevertheless, only adipose tissues from WT mice were examined in these studies (although the very limited amount of UCP1 in eWAT is probably not relevant and this depot could be considered UCP1-negative in functional terms). In the present study, potential mechanisms of UCP1-independent heat generation in murine brown adipocytes were investigated. A futile substrate cycle of lipolysis and FA re-esterification was identified as the major source of NST in

brown adipocytes of UCP1KO mice. The underlying theoretical framework that futile substrate cycles and in particular futile lipid cycling could contribute to NST was proposed already 60 years ago[46]. Since then, the topic has been picked up from time to time but meanwhile sank into obscurity again, aside from a few exceptions. Only recently futile cycles experience a renaissance. For decades, it has been known that adipocytes with low UCP1 levels, i.e. white adipocytes, and since more recently, brown and white UCP1KO adipocytes increase their oxygen consumption in response to adrenergic stimulation[46,59,72,142,143].

5.5 Lipolysis and re-esterification vs. breakdown and synthesis of fatty acids

Scientists hypothesized that FAs released during lipolysis may either undergo ATP dependent re-esterification or degradation through β-oxidation, or may cause beneficial mild mitochondrial uncoupling. However, the exact mechanism of this phenomenon has never been fully resolved, as the molecular evidence provided was rather anecdotal. Since β-adrenergically stimulated respiration rates of brown UCP1-knockout adipocytes were fully sensitive to inhibition of the mitochondrial ATP synthase, potential mild non-specific uncoupling due to excess FAs[90,91] could be excluded. Moreover, it was ruled out that active lipolysis and the resulting increase in FA levels caused opening of the mitochondrial permeability transition pore[92,93], and thus leak respiration, because cyclosporin A did not reduce stimulated respiration rates. Unlike previously assumed, blocking the import of FAs into mitochondria has proven that mitochondrial β-oxidation is not in any way part of futile FA/TG cycling, other than as a source of reducing equivalents. However, etomoxir blocks CPT1 and the uptake of long chain FAs, but short chain FAs released from TGs do not require CPT1 for uptake into mitochondria[144]. Although short chain FAs are a small minority of FAs released, they could be significant at high levels of lipolysis as studied here. However, as outlined before, the ATP-dependent activation of FAs either prior re-esterification or before import into mitochondria is the main ATP consuming step. Therefore, if large quantities of short chain FAs entered mitochondria, they would per definition not contribute to the large increase in ATP-dependent oxygen consumption following the addition of isoproterenol, because they do not require activation. Accordingly, short chain FAs passing the inner mitochondrial membrane on a larger scale may even cause unspecific uncoupling and would thereby lead to a higher proton leak-linked (oligomycin-insensitive) respiration. Since proton leak-linked respiration (oxygen consumption after the addition of isoproterenol and oligomycin) was always nearly identical to respiration rates in the basal states and it was not affected by treatment with etomoxir, it is completely implausible that breakdown of short chain FAs could explain the FA/TG cycling phenotype described here.

5.6 Potential pitfalls associated with pharmacological inhibitors

After these imponderables were ruled out, FA/TG cycling key enzymes were pinpointed on a cellular level and the role of glucose for UCP1-independent NST was elucidated. Furthermore, brown adipocyte organelle crosstalk and potential implications for energy metabolism and lipid homeostasis were described. Yet, a few open questions demand a critical appraisal of the key findings.

Pharmacological inhibition of long-chain acyl-CoA synthetase activity (triacsin C), i.e. ATP-dependent activation of FAs, did not fully abolish oxygen consumption linked to futile TG cycling. This suggests that either the enzyme was not completely inhibited, since a high cellular lipid content[145,146] and bovine serum albumin-buffered assay medium are strongly affecting substance partitioning and availability[147], or different isoforms[148] or even short and medium-chain acyl-CoA synthetases also contribute to the activation of FAs prior to re-esterification during active lipolysis. Interestingly, triacsin C was ultimately even slightly more potent than oligomycin in decreasing free FA re-esterification rates. Although oligomycin can fully reverse the isoproterenol-induced increase in oxygen consumption, a certain amount of FAs may still be activated and re-esterified as long as glycolytic ATP production can compensate for the inhibition of the mitochondrial ATP synthase. However, triacsin C may be a problematic compound, because it is not a highly selective inhibitor and off-target effects on mitochondrial respiration were reported. Nevertheless, triacsin C was demonstrated to reduce the amount of intracellular long chain acyl-CoAs, which is the intended effect, without negatively affecting lipolytic capacity[149,150]. Moreover, oxygen consumption data in the present work prove that cells treated with triacsin C still have enough spare respiratory capacity to increase respiration upon FCCP-mediated uncoupling over preceding rates following the addition of isoproterenol. This clearly indicates that impairment of oxidative capacity by triacsin C cannot explain the observed phenotype. In conclusion, these findings are very compelling and the available data definitely outweigh hypothetical off-target effects, because triacsin C does not interfere with two of the main parameters determining TG/FA cycling, such as lipolysis and oxidative capacity. Thus, triacsin C supposedly limits the ATP-dependent activation of long chain FAs eventually resulting in less DGAT1-mediated re-esterification and a lower futile lipid cycling activity.

Similarly, combining both DGAT inhibitors did not fully prevent increased respiration rates following adrenergic stimulation. This may be explained by the activity of different acyltransferases, such as GPATs and AGPATs, which may also catalyze re-esterification of FAs during active lipolysis. However, specific and well characterized inhibitors targeting these enzymes are not available at the moment. Thus, it still has to be resolved if this futile substrate cycle involves the whole TG synthesis pathway from G3P to TGs or if it is predominantly restricted to di- and triglycerides. Since futile lipid cycling activity apparently depends on glycolytic provision of G3P *in vitro*, the first steps of lipid synthesis

might also have a greater importance than initially assumed. One additional concern is that blocking the action of DGAT, which is the last step in the TG synthesis pathway, may increase the concentration of upstream substrates and precursor molecules, such as MGs and DGs, which are known to be potent signaling molecules[151]. It is therefore not entirely clear how the effects of DGAT inhibition are in fact sensed, and whether they are mediated by the accumulation of other lipid species or by the reduction of total FA re-esterification capacity. Indeed, inhibiting DGAT1-mediated FA re-esterification during active lipolysis causes an accumulation of DGs and MGs. However, DGAT1 inhibition does not have an effect on ATGL or HSL protein expression, and it does not impair isoproterenol-stimulated lipolysis, judging by the release of FAs into the medium[105]. Moreover, it was shown that DGAT1 inhibitors specifically reduce TG synthesis. Apart from this, respirometry data presented here clearly prove that inhibition of DGAT1 and the consequent accumulation of DGs does not impair oxidative capacity to a degree such that it would interfere with ATP provision, because FCCP-stimulated rates markedly exceed prior rates following isoproterenol treatment. Lastly, albeit DGs are potent signal molecules, a causal relationship between an accumulation of DGs and the activation/inhibition of lipolysis has not been established. Thus, as the accumulation of DGs does not impair lipolysis and does not compromise oxidative capacity, while the available inhibitors specifically block DGAT1-mediated re-esterification of FAs during active lipolysis, it is evident that the strongly impaired FA/TG cycling rates cannot be explained by an increase in DG levels.

The present work also highlights the interdependence of glucose and lipid metabolism, and clearly suggest that brown UCP1KO adipocytes do not exclusively convert glucose to pyruvate, but rather metabolize glucose to G3P via dihydroxyacetonephosphate. Thus, besides transporting reducing equivalents, G3P can serve as a backbone for re-esterification of FAs and TG synthesis sustaining futile lipid cycling upon adrenergic stimulation. This dual role could partially explain the impressive glucose uptake rates of activated BAT in UCP1KO mice. However, the use of 2DG to block glycolysis may be criticized, since it obviously reduces the total cellular capacity to form ATP, besides halting glycolytic flux. Thus, especially when lipolysis is active and the ATP demand is high, artificially decreasing cellular ATP levels may cause multiple systemic effects independent of reduced G3P provision. However, three points strongly contradict this hypothesis.

Firstly, the observed phenotype could be replicated without 2DG by just acutely removing glucose from the medium, which argues against any 2DG off-target effects.

Secondly, the increase in oxygen consumption following the treatment of brown UCP1KO adipocytes with isoproterenol is fully dependent on the activity of the mitochondrial ATP synthase, i.e. sensitive to oligomycin. Consequently, only and exclusively aerobic mitochondrial ATP synthesis, and not glycolytic ATP production, is reflected in respiration rates. Thus, even if treatment with 2DG or the

removal of glucose from the medium reduces total cellular ATP production, the mitochondrial ETC is still fully operational, because isoproterenol is injected prior to oligomycin. Nevertheless, it would still be conceivable that both treatments could impair oxidative capacity resulting in lower mitochondrial ATP production. This is not the case, as in both conditions FCCP-stimulated respiration rates exceed prior values during adrenergic stimulation, which clearly indicates that sufficient protonmotive force could be generated, if the ATP demand were higher. Moreover, if oxidative capacity were the limiting factor, excess supplementation with pyruvate should have rescued the phenotype, but it did not. Thirdly, this work demonstrates that the effect of 2DG and glucose removal on isoproterenol-stimulated respiration rates of cultured adipocytes is genotype-dependent and by far not as pronounced in WT cells as in UCP1KO cells. Thus, if off-target effects were responsible for the observed phenotype, we would expect the same off-target effects independent of the genotype.

5.7 *In vitro* to *in vivo* translation

5.7.1 The importance of ATGL for thermogenesis

However, several points need to be highlighted here, which suggest that mechanistic cell culture data may not be directly transferable to the *in vivo* situation. It has been convincingly demonstrated that ATGL-mediated lipolysis in BAT is dispensable for NST as long as exogenously FAs released from WAT or taken up from the diet are available. This does not conflict with the futile FA/TG cycle proposed here, as extracellular FAs can trigger futile lipid cycling as well. Nevertheless, neither study, dictated by the available conditional knockout models, examined whether ATGL-mediated lipolysis in brown fat can be sufficient/is indispensable when exogenous fatty acids are not supplied to BAT. The results published by Shin et al.[152] confirm earlier observations[72] and are in good agreement with the results of this work proving that lipolytic release of FAs catalyzed by ATGL is key in fueling brown adipocyte oxygen consumption following adrenergic stimulation *in vitro*. However, cell culture medium contains high amounts of glucose and cultured adipocytes have considerable intracellular glycogen and lipid stores[59,115], while there is no extracellular source of FAs, TGs, and glycerol as in the *in vivo* situation. This also explains why intracellular lipolysis strictly controls UCP1-dependent and –independent thermogenesis in cultured adipocytes. FAs can only originate from lipid droplets or membrane lipids, since there is no other source in this setting. Furthermore, it is also immediately clear why oxygen consumption rates depend primarily on ATGL rather than HSL, MGL, or LPL activity. TGs account for more than 90 % of total neutral lipids[153], and thus ATGL with the highest maximum conversion rate among lipases has also by far the most substrate available to convert.

5.7.2 Substrate availability

In contrast, in mice, a considerable amount of substrates and metabolites is transported to iBAT via the blood[106,154], whereas intracellular nutrient stores, such as lipid droplets and in particular glycogen,

may be substantially depleted during prolonged cold exposure[115,155-158]. Consequently, not only the type of substrates available, but also most likely the quantity is very different in these two scenarios. Since cells are cultured in an abundance of nutrients and in the virtual absence of any pro-lipolytic stimulus during differentiation, they do not need to significantly tap into their own stores. Consequently, the almost unlimited abundance of glucose, FAs, and even amino acids allows cultured adipocytes to use energetically unfavorable pathways and reactions (less ATP/reducing equivalents/e⁻ yielded per molecule of substrate).

5.7.3   The glycerol-3-phosphote shuttle and its function in lipid metabolism

This, in turn, also affects the interpretation of data regarding the role of glucose and GPD1, because the conversion of glucose to G3P and subsequent oxidation is bioenergetically highly inefficient compared to the complete oxidation of glucose via pyruvate and the TCA cycle[159,160]. GPD1-mediated generation of G3P for FA re-esterification is even more inefficient, since G3P is converted to an acylglycerol and cannot be oxidized in this case. Therefore, this reaction would presumably no longer occur, if the overall substrate supply was severely limited or if the available energy had to be carefully managed. On the other hand, GPD1 has the function of transferring e⁻ from cytosolic reducing equivalents to the ETC, while glucose is still completely oxidized to CO_2. Thereby, NAD^+ can be regenerated in the cytosol from NADH through the conversion of DHAP to G3P. This mechanism ensures that glycolysis can proceed and still provide cytosolic ATP, while NST is active. Additionally, the G3P shuttle controls G3P levels that are available for TG synthesis. GPD1 has a significantly lower K_m than GPD2, but both isoforms have a considerable maximal capacity, which enables stimulated brown adipocytes to maintain high G3P levels. This serves a dual purpose, since G3P can function as an e⁻ donor but also as a source of glycerol backbones for lipid synthesis[109]. Notably, FAs and acyl-CoAs negatively regulate GPD2 activity[161,162], which effectively suppresses oxidation of G3P. Adrenergic stimulation and the concomitant activation of lipolysis therefore support conditions enabling G3P to be used for TG synthesis. Taken together, the G3P shuttle in BAT is a metabolic regulator and the major site of cytosolic regeneration of NAD^+. GPD1 and GPD2 may contribute to metabolic inefficiency in brown adipocytes, but their main function is probably to facilitate rapid switches between anabolic metabolism and thermogenesis by keeping cytosolic NADH levels low and precisely orchestrating the fate of G3P. This could also explain why NST mediated by FA/TG cycling strictly depends on functional glucose metabolism, whereas glycolysis is party dispensable for UCP1-dependent thermogenesis. As lipid cycling constantly requires a readily accessible pool of FAs for re-esterification, newly released FAs must not be oxidized, otherwise FA flux and futile substrate cycling capacity would be limited. In contrast, UCP1 is already activated by small amounts of FAs[163], and thus the majority of FAs released during active lipolysis can be supplied to β-oxidation, which is probably why WT cells are more flexible

with regard to the choice of substrate. In line with this hypothesis, it was demonstrated that stimulated brown UCP1KO cells oxidize less FAs than WT controls despite having almost identical respiration rates[59]. Moreover, a few studies indeed attribute a lower metabolic flexibility and a numerically slightly higher respiratory quotient to cold-acclimated UCP1KO mice[130,131]. These findings may indicate that mice lacking UCP1 have temporarily higher glucose oxidation rates and that a switch in the fuel source needs to be controlled even more tightly and carefully balanced during cold exposure *in vivo*.

5.7.4   The unknown contribution of glycerol kinase

In this context, also the role of GK-mediated G3P recycling needs to be discussed, as there is a growing body of evidence suggesting considerable GK activity in iBAT and beige adipose tissues[164-167]. Cold exposure induces GK expression specifically in thermogenic adipose tissues and previous studies found a more pronounced cold-stimulated induction in iBAT of UCP1-ablated mice[69,165,167]. Additionally, it has been demonstrated that GPD1 transcript and protein levels are lower, and GK levels are significantly higher in iBAT of UCP1KO mice at lower temperatures and expression of these two proteins follows a completely different pattern compared to their WT counterparts[69]. This could indicate that mild cold stress still allows UCP1KO mice to use G3P as substrate for oxidation and backbone for re-esterification. However, severe cold stress and the concomitant elevated energetic demand may *de facto* exclude the metabolic inefficiency connected to the conversion of glucose to G3P. Consequently, UCP1KO mice may provide as little as possible but as much as required G3P via glycolysis under cold stress, while the importance of regenerating G3P through GK activity drastically grows. In this scenario, the majority of glucose is probably metabolized to pyruvate and fully oxidized supporting ATP synthesis via oxidative phosphorylation, and only a minor fraction is converted to G3P. Another crucial difference is that we are only capturing a short period (minutes or hours) after acute activation of FA/TG cycling in the cell model. In publications employing animal models, however, a longer acclimation period (weeks) is obligatory, and therefore rather chronic processes were studied that may have been preceded by other acute changes. At least the process of cold adaptation could be simulated by chronically treating brown adipocytes with moderate doses of isoproterenol or better norepinephrine over the course of differentiation. Taken together, the *in vitro* data presented here were essentially generated in an environment in which substrate is virtually inexhaustible, and are more likely to represent the situation in which a UCP1KO mouse, previously maintained in a thermoneutral environment, is exposed to subthermoneutral temperatures for the first time. These seemingly small differences could nevertheless be crucial and explain why glucose might have a slightly different intracellular fate in cultured adipocytes and why ATGL-mediated lipolysis and glycerol recycling by GK might have a different importance in cultured brown adipocytes than in iBAT of mice.

The unknown contribution of GK is a limitation possibly also affecting the measured *in vitro* re-esterification rates. The equation used to calculate these rates relies on the assumption that for one molecule of TG that is completely hydrolyzed three FA molecules are expected to be released into the medium. Just like microplate-based respirometry, this approach has its own limitations. Since GK activity in cultured adipocytes was not measured, a putative genotype-dependent difference in recycling of glycerol to G3P mediated by GK cannot be included in the calculation. If the importance of GK in providing glycerol backbones was indeed higher in UCP1KO cells, the actual rate of re-esterification would be even greater than the calculated one. Nevertheless, published literature consistently demonstrated higher GK expression in UCP1KO BAT suggesting a higher GK activity, but this remains to be tested. Moreover, small amounts of FAs can be used in other processes than re-esterification, such as β-oxidation and phospholipid synthesis. Although calculated cycling rates based on the release of glycerol and FAs might be skewed, this method still provides an adequate approximation and complements well with respiration measurements. As there is currently no method to precisely quantify flux of FAs and corresponding FA/TG cycling rates, it cannot be assessed whether flux rates based on respirometry or on glycerol and FA release are more accurate. However, it is extremely reassuring that the inhibitors used for respirometry also caused similar qualitative changes when calculating a re-esterification rate based on glycerol an FA release.

5.8   Peridroplet mitochondria: cause or consequence

Apart from this, the loss of UCP1 may have an even more far-reaching impact, since striking differences between WT and UCP1KO cells pertaining the interaction between mitochondria and lipid droplets were found. Therefore, it is enticing to speculate that this shift in mitochondrial subpopulations at least partly supports the observed functional phenotypic differences. Brown WT adipocytes carry out UCP1-mediated thermogenesis, and thus would require less PDM and more CM, as CM are specialized on β-oxidation that fuels thermogenesis. In stark contrast, UCP1KO adipocytes have an increased ATP demand due to higher rates of FA re-esterification that would favor the occurrence of PDM supporting NST mediated by FA/TG cycling. However, an important question that has not been answered yet is, whether the overall closer inter-action between mitochondria and lipid droplets in UCP1-ablated cells is a causative factor or if it is rather a consequence of intensified FA/TG cycling. A very simple first experiment would be to acclimate WT and UCP1KO mice to different temperatures, i.e. 30 °C, 20 °C, and 5 °C, and then determine the percentage of CM and PDM in adipose tissues using electron microscopy. According to the hypothesis above, the association of mitochondria and lipid droplets should be stronger in adipose tissues of UCP1KO mice compared to WT mice, and the number of PDM should increase along with FA/TG cycling activity, when the ambient temperature falls below thermoneutrality. Vice versa, in cultured adipocytes the association of mitochondria with lipid droplets

can be artificially promoted by overexpressing PLIN5[113]. This enables characterizing the causal link between PDM and FA/TG cycling-dependent respiration rates. A tighter association of mitochondria with lipid droplets and an increased abundance of PDM could aid in expanding FA/TG cycling capacity eventually resulting in enhanced stimulated respiration rates. Taken together, monitoring the dynamic interaction between mitochondria and lipid droplets upon adrenergic stimulation, or during states of impaired lipid cycling will clearly show, whether the emergence of certain mitochondrial populations correlates with futile cycling activity, lipid turnover and ATP consumption.

5.9 Lipid cycling as a valve for ROS or detoxification of fatty acids

Up to this point, the data regarding the mechanism at the cellular level including the enzymes involved are clear. From an evolutionary point of view, however, it is still largely unknown whether this compensatory mechanism arose primarily to protect cells from lipotoxicity and whether the associated heat production, which is always emphasized especially in the context of UCP1, is only a welcome side effect due to an acceleration of energy metabolism. Notably, BAT of cold-acclimated UCP1KO mice exhibits a pronounced upregulation of inflammatory and ER stress markers[116,117]. These alterations, which are associated with depletion of the ETC and mitochondrial dysfunction, are strictly dependent on housing temperature and only occur, when UCP1KO mice are maintained at room temperature or below. Thus, this phenomenon is not a direct consequence of the loss of UCP1, but is only induced when a cold stimulus is additionally present, which increases sympathetic output and ultimately activates lipolysis. Similarly, these aberrations are not present in mouse pups and *in vitro* differentiated cells, which also supports the notion that this is a secondarily acquired defect. Nevertheless, it is still completely unknown what causes these changes and how the causative factors are integrated. There are some theories that try to explain this observation, but the available data supporting these claims are sparse. One possible explanation is that UCP1KO BAT mitochondria have a lower mitochondrial Ca^{2+} buffering capacity and are more prone to ROS-induced opening of the PTP. Interestingly, in addition to mediating NST, UCP1 may control ROS levels in BAT by reducing protonmotive force[168]. Once UCP1 is active and protonmotive force is dissipated, which is equivalent to a significantly higher mitochondrial proton leak, the ETC redox state is altered, thereby potentially diminishing ROS production[169]. Since ETC complex levels (I – IV) and oxidative capacity in BAT largely exceed ATP synthase levels and the capacity to form ATP, the ablation of UCP1 could pose a major problem, because the higher protonmotive force due to adrenergic stimulation, for the most part, cannot be released anymore. This, in turn, can promote ROS production, because a high proton gradient in conjunction with many e^- entering the ETC favors the generation of superoxide or hydrogen peroxide. However, proton leak kinetics have not been systematically assessed in WT and UCP1KO mitochondria under different conditions (phosphorylating respiration, uncoupled respiration, etc.), and measuring

oxygen consumption alone can serve only as a qualitative readout of mitochondrial proton leak due to its non-ohmic behavior[170]. Quantifying true proton conductance across the inner mitochondrial membrane requires determination of membrane potential in combination with mitochondrial oxygen consumption. However, it is almost impossible to isolate the effect of elevated ROS production and impaired FA re-esterification, because the treatment with oligomycin, which was highly effective in reducing FA/TG cycling activity, also completely blocks the single most potent means of dissipating protonmotive force in UCP1KO adipocytes. Oligomycin inhibits the mitochondrial ATP synthase causing a hyperpolarization of the inner mitochondrial membrane, because one large consumer of the H^+ gradient is not operational, while adrenergically stimulated substrate oxidation is still high. Thus, protonmotive force temporarily increases, which may lead to a higher mitochondrial ROS production. However, drastically reducing ATP levels due to complex V inhibition will inevitably limit re-esterification capacity at the same time, because activation of FAs requires ATP. This will directly cause intracellular FA levels to surge, since sequestration of FAs by lipid synthesis and TG storage is severely impaired. As already outlined before, detoxification of harmful FA species is another possible explanation of how FA/TG cycling may protect brown UCP1KO adipocytes from ER stress and prevent UPR. The uncontrolled accumulation of FAs can compromise the integrity of the ER and mitochondrial membranes, and lead to non-specific uncoupling[105,171,172]. Similarly, as oligomycin is not the perfect choice in this context, any compound that impairs FA re-esterification, such as the DGAT1 and DGAT2 inhibitors employed in the present work, will cause a buildup of potentially toxic lipids but also significantly reduce the potential to dissipate protonmotive force. Inhibiting DGAT1 clearly lowered stimulated respiration rates and consequently ATP turnover, which most likely also results in a hyperpolarization of the mitochondrial membrane. This again clearly illustrates how ATP turnover, FA/TG cycling, and lipotoxicity/ROS production mutually influence each other. Notably, treatment with isoproterenol and oligomycin leads to an upregulation of ER stress markers in brown UCP1KO cells after only a few hours. When oxygen consumption was measured under similar conditions, it was observed that respiration rates began to increase after just one hour, despite the addition of oligomycin. Approximately four hours after the start of the experiment, oxygen consumption rates of the two groups treated with either isoproterenol alone or oligomycin in addition were nearly identical. This demonstrates that once lipolysis exceeds re-esterification, and the FA-buffering capacity of BSA is exhausted, the uncontrolled accumulation of FAs will unavoidably result in mitochondrial uncoupling. Since UCP1-mediated uncoupling, mitochondrial ATP synthesis, and FA-induced uncoupling presumably equally dissipate protonmotive force (all three processes facilitate/mediate the entry of H^+ into the matrix), the magnitude of ROS production should also be at least comparable in the experiment just described. Consequently, this then argues against the ROS hypothesis and is more in favor of the lipotoxicity hypothesis, since signs of ER stress accompany only the condition in which

exceedingly high intracellular FA levels prevail (even though this is of course only a simplification of a very complex multidimensional process). Nevertheless, these findings cannot account for the genotype-dependent differences in susceptibility to ER stress during adrenergic stimulation. Based on the *in vitro* data, maximum respiration rates of WT and UCP1KO cells during adrenergic stimulation are almost identical, and thus ETC capacity would not be greater than that of ATP synthase. However, there is strong evidence indicating that the measured respiration values do not correspond to and underestimate true values, since oxygen consumption after the addition of isoproterenol or FCCP is so high that a hypoxic environment is temporarily created in the transient microchamber[173,174]. Therefore, it cannot be excluded after all that even in cultures of brown UCP1KO adipocytes maximal mitochondrial ATP synthesis rate is far below the maximal oxidative capacity as previous publications using freshly isolated mature adipocytes or mitochondria reported[175]. Furthermore, there is a major difference in the role of FAs for UCP1-mediated or UCP1-independent thermogenesis. UCP1-independent NST mediated by FA/TG cycling requires continuous handling of FAs, because once either provision or re-esterification of FAs stalls, futile lipid cycling will halt. In WT cells, by contrast, only a certain amount of FAs is required to activate UCP1, and these then probably stay bound to UCP1. FAs released beyond this can be directed towards β-oxidation to generate reducing equivalents. This represents a significant advantage, because brown WT cells can simply "burn" toxic lipid species (observed as counterregulatory response in lipotoxicity models), while UCP1KO adipocytes do not have this option, since oxidizing significant amounts of FAs would drastically limit their thermogenic potential. Although a few candidates have been identified, it remains elusive which lipid classes have a toxic potential, how these compounds damage cells and organelles, and we are only beginning to understand how free FA levels are sensed by adipocytes. Taken together, it is certain that regardless of the original or primary function of lipid cycling in UCP1KO adipocytes, FA flux, intracellular FA levels, and turnover of ATP are inextricably linked.

5.10 AMPK and adrenergic signaling control lipid cycling rates

Nevertheless, AMPK represents, among many others, an additional important regulatory layer, which has to be considered in this context. AMPK is a central hub of metabolic control that integrates the cellular energy status by directly interacting with AMP, ADP, and ATP[110]. Declining energy levels reflected by an elevated AMP/ATP ratio lead to the activation of AMPK. Once active, AMPK regulates an array of downstream enzymes, signaling pathways, and transcription factors to induce acute and chronic adjustments to enhance substrate oxidation, OXPHOS capacity, and consequently energy supply. Interestingly, AMPK has been shown to regulate lipolysis presumably by directly phosphorylating regulatory sites on HSL and possibly ATGL, and indirectly by phosphorylation of PLIN[176,177]. Activation of AMPK impairs lipolysis in response to adrenergic stimulation, while AMPK

inhibition leads to a higher release of FAs. However, the role of AMPK in lipolysis and FA metabolism in adipose tissues is still controversial[178-183], and thus these findings should be interpreted cautiously. In good agreement with data previously published[180], pharmacological inhibition of AMPK and its catalytic activity led to significantly higher basal respiration rates most likely due to an activation of lipolysis and ultimately FA/TG cycling. Stimulated oxygen consumption was apparently not affected, but this may be an artefact attributable to the limited dynamic range of the respirometer and the outstandingly high oxidative capacity of brown adipocytes. On the contrary, treating UCP1KO adipocytes with an AMP analogue to stimulate AMPK activity had no effect on baseline oxygen consumption rates, despite some studies reporting a weak induction of lipolysis by AICAR treatment. Given that AICAR alone decreases HSL activity and supposedly activates ATGL under normal conditions[181,183], the two effects might balance out and thus only a minimal or no change at all in lipolytic activity occurs. Nevertheless, oxygen consumption in response to isoproterenol was drastically blunted by AICAR treatment, since a higher AMPK activity significantly impairs adrenergically stimulated release of FAs, which consequently lowers FA re-esterification rates. Taken together, catalytic activity of AMPK modulates lipolysis, but also the release of FAs itself can act as a feedback signal that in turn regulates AMPK activation state[184]. Moreover, adrenergic signaling has been demonstrated to negatively regulate AMPK. In the active state, PKA associates with AMPK and phosphorylates a specific serine, thereby precluding phosphorylation of known sites in the immediate proximity[185]. These particular adjacent sites are associated with increased AMPK activity and are known to be phosphorylated as a consequence of increased FA levels (independent of cAMP-PKA-signaling). One link between lipolysis and AMPK activation is the fact that a considerable fraction of newly released FAs is re-esterified. This process is energetically very costly and shifts the AMP:ATP ratio towards AMP, which is directly sensed by AMPK. Moreover, long chain FA-CoAs represent a negative feedback loop on AMPK signaling[184], as they can allosterically activate AMPK to effectively match substrate use and availability. Thus, phosphorylation of AMPK by PKA counteracts the action of upstream kinases, ATP consumption due to FA/TG cycling, and generation of high-energy FA-CoAs that activate AMPK, which first enables efficient release of FAs in response to adrenergic stimulation. In summary, lipolysis need to be tightly regulated and above all adjusted to cellular energy levels. Therefore, the actions of PKA and AMPK need to be carefully balanced in a coordinated manner. It seems plausible that AMPK protects against needless depletion of ATP due to lipolysis rates largely exceeding the factual demand. This may be of particular importance during exercise or starvation, i.e. situations in which energy is locally or systemically strongly limited. Therefore, substrates and specifically FAs could be released where it can be afforded, and the breakdown of TGs may be reduced where energy needs to be conserved and the demand is high. Otherwise, an adrenergic stimulus would always entail more thermogenesis, even if ATP rather than heat should be generated.

5.11 Mitochondria in brown fat of UCP1-knockout mice are functional

After a very clear picture had emerged at the cellular level, it was assessed whether the amount of heat generated (or energy expended by these processes) could be biologically relevant at the level of an organism. The final step was to gather initial evidence for UCP1-independent NST and particularly FA/TG cycling *in vivo*. A few publications raised serious concerns about the structural integrity of mitochondria in UCP1KO BAT and the intactness of their OXPHOS machinery[116,117]. When UCP1KO mice were housed at temperatures below their thermoneutral zone, it was found that their brown fat mitochondria exhibited substantial morphological defects and a significantly reduced ETC protein abundance. These findings have spurred serious criticism of the classic UCP1KO mouse model per se and the concept of UCP1-independent NST in BAT. This has led to the retrospectively premature conclusion that even if futile substrate cycles existed and even if they were significantly upregulated in the absence of UCP1, the severely impaired oxidative capacity compared to WT BAT in combination with the inherently negligible ATP synthase levels in brown fat, would preclude any alternative UCP1-independent thermogenic mechanism.

In cultured cells, these defects were not observed and it has already been extensively discussed what the reason could be. Nevertheless, structural integrity of mitochondria and a normal cristae architecture are obvious key factors for proper mitochondrial function in BAT. Electron micrographs of iBAT from WT and UCP1KO mice housed at 23 °C clearly demonstrate that there are indeed small morphological changes and a few mitochondria with aberrant cristae morphology in UCP1KO iBAT. However, these defects appear to be minor at room temperature and only a small subset of mitochondria were affected. The severity of this defect largely depends on the housing temperature, and thus the depletion of the electron transport chain complexes was most likely not a direct consequence of the absence of UCP1 and subsequent failure to develop BAT, but rather acquired and caused by secondary changes in response to a cold environment. Taken together, the two factors, housing temperature and duration of the exposure, determine the extent to which electron transport chain proteins are affected in a dose-dependent manner, and therefore it is conclusive that the severity of reduction at room temperature is intermediate between the phenotype observed at thermoneutrality and during cold exposure.

Nevertheless, in line with the results of the present work researchers measured lower complex I and IV levels in iBAT of UCP1KO mice[69,116,117]. As oxygen, the terminal electron acceptor, is reduced to water by cytochrome c oxidase (COX, complex IV), which represents the rate-limiting reaction of oxidative phosphorylation, significantly impaired COX activity would reduce a tissue's capacity to consume oxygen and consequently to expend energy. Hofmann et al. reported that COX activity was around 1.3 times higher in brown WT compared to UCP1KO mitochondria[125]. However, these metrics were again

expressed as relative activities per mg of protein, and also in this study, BAT depot weights were significantly different between genotypes. Therefore, the apparent reduction in relative COX activity may be compensated for or ultimately exceeded in total by the higher tissue mass resulting in comparable or higher overall capacity to consume oxygen when an entire depot is considered as a functional unit. It has to be emphasized that this is based on the assumption that complex I to III activity is not rate-limiting. Lastly, COX activity is subject to regulation on multiple layers, and therefore protein or expression levels might be sometimes misleading[186]. Hofmann et al. additionally measured mitochondrial GPD activity, which was 50 % higher in BAT mitochondria from UCP1KO mice[125]. This finding may indicate an altered preference towards substrates feeding electrons into the respiratory chain via complex II, thereby potentially compensating for reduced complex I levels. However, a surprisingly large number of studies using isolated brown WT and UCP1KO mitochondria[125,187-190] and one study using freshly isolated floating adipocytes[191] could not detect significantly different FCCP-stimulated maximal respiration rates between genotypes in the presence of single substrates or combination of substrates, i.e. pyruvate, G3P, succinate, or FAs. Therefore, substrate transport, oxidation, and electron transport chain capacity in brown mitochondria are most likely not impaired by the ablation of UCP1, because maximal uncoupled respiration in response to FCCP is a function of these three parameters. Additionally, as pyruvate, a complex I substrate, was offered alone and still no difference between genotypes was detected, these findings strongly indicate that complex I activity is in fact not reduced in brown UCP1KO mitochondria. An altered H^+/O ratio (rather than P/O, because in all but one study ADP was not added, and thus aerobic ATP synthesis should be negligible) between WT and UCP1KO mitochondria can be excluded as well, since complex I and II substrates were each considered separately. Only one study quantified the response to ADP in isolated brown fat mitochondria respiring on G3P, but no difference between WT and UCP1KO mitochondria could be detected[190]. In the same study, ADP-stimulated respiration of liver mitochondria was assessed. Respiration in BAT mitochondria was about 50 % lower compared to mitochondria from liver. Consequently, assuming a P/O ratio of 2.654 for liver mitochondria[160] (respiring on pyruvate) and a ratio of 1.63 for BAT mitochondria[160] (respiring on G3P), brown fat mitochondria would have around one-third the ATP synthesis capacity of liver mitochondria, which would still be quite substantial.

Taking the results of this work and published functional data together, it can be concluded that at least at room temperature, i.e. mild cold exposure, BAT mitochondria of UCP1KO mice are functional and do not have severe defects that would effectively preclude them from establishing and maintaining a membrane potential as well as generating ATP to sustain futile FA/TG cycling. Moreover, protonmotive force should be more than sufficient to power the ATP synthase, especially since UCP1, one of the main consumers of membrane potential in activated BAT, is absent. Nevertheless, it is of course true that in an *in vivo* situation the P/O ratio might be altered, although it seems highly unlikely that either only

complex I or II substrates are oxidized, as BAT can utilize virtually any source of energy, be it amino acids, FAs, or glucose.

5.12 Futile lipid cycling *in vivo*: the supposed lessons from mouse models

Most encouragingly, only recently, it was convincingly demonstrated for the first time that futile lipid cycling in iBAT is part of adaptive thermogenesis in mice[69]. Cycling rates were consistently higher in UCP1KO animals, and FA/TG cycling activity increased inversely related to ambient temperature. This publication clearly proved that UCP1KO mice, and also WT mice but to a lesser extent, partly rely on UCP1-independent sources of heat, i.e. a futile cycle of lipolysis and re-esterification, to maintain normothermia at room temperature and below. As already mentioned, previous publications reported that UCP1KO mice had higher respiratory quotient values than WT animals during chronic cold exposure and an acute cold limit test, suggesting that fewer FAs are oxidized to ensure adequate flux on the re-esterification side. In summary, it is now evident that futile FA/TG cycling occurs in an *in vivo* setting and that it has a greater biological significance in the absence of UCP1. However, unlike the cell culture data presented in this work, the reactions and enzymes potentially involved have not yet been experimentally validated in mice. We can only speculate by assessing the phenotypes of mouse models with global or targeted deletions of key enzymes mediating FA esterification along the TG synthesis pathway.

5.12.1 GPATs, AGPATs, and LIPINs

The Kennedy glycerol phosphate pathway is the predominant mechanism of TG synthesis in adipose tissues. GPAT4, one of the enzymes that catalyze the formation of MGs, associates to the ER and is highly expressed in BAT[192]. Mice with a global GPAT4KO weighed significantly less than WT controls and had a reduced fat mass[193]. Food intake and physical activity was not different, but energy expenditure was higher in GPAT4KO animals. Mice deficient in GPAT4 were resistant to diet- and genetically-induced obesity. However, this phenotype is hard to interpret, since the loss of GPAT4 caused impaired lipid storage in adipose and non-adipose tissues and a large reduction in circulating leptin levels, although cold-induced NST was apparently intact. Partial or specifically subdermal lipodystrophy may lead to increased heat loss due to attenuated insulation (or excessive loss of water due to an impaired skin barrier), and thus explain the higher heat production. Because of the far-reaching phenotypic consequences, it cannot be conclusively assessed whether lipid cycling activity may have been altered, or whether adipose tissue dysfunction or reduced thermal insulation caused the increased energy expenditure. Among AGPATs, which mediate the generation of PA that is the immediate precursor of DGS, AGPAT2 is the most highly expressed isoform[194]. Mutations in the *Agpat2* gene cause congenital generalized lipodystrophy in humans. Similarly, whole body AGPAT2KO mice exhibit a severe lipodystrophic phenotype and all the associated metabolic derangements including

extreme hyperphagia[195]. Only 20 % of the homozygous AGPAT2KO offspring are viable and these mice fail to develop adipose tissues, while they still have an increased energy expenditure. However, since the phenotype is again rather complex, the underlying reason for this observation is still unknown. Further along the TG synthesis pathway, the LIPIN family is responsible for the conversion of PA to DGs. LIPIN1 is the predominant isoform in adipose tissues[196], and accordingly it is not entirely surprising that LIPIN1-ablated mice suffer from lipodystrophy. On the contrary, adipose tissue-specific overexpression of LIPIN1 under the control of the *Fabp4* promoter improved insulin sensitivity and protected mice against high fat diet-induced insulin resistance and disturbances of glucose metabolism without affecting body weight or energy expenditure[197]. The authors of this publication speculate that LIPIN overexpression prevents ectopic lipid accumulation, thereby preventing pancreatic β-cell dysfunction and reduced nutrient uptake into skeletal muscle. While this may explain the protective effect in mice fed a high-fat diet, it cannot explain that circulating glucose levels are lower even in transgenic mice on a regular chow diet (there was even a trend towards improved insulin sensitivity). It is enticing to speculate that higher LIPIN1 levels per se enhance re-esterification capacity, which entails a higher demand of glycerol backbones possibly deriving from glycolysis. Thus, glucose from the blood stream may be channeled into adipose tissues where it supports FA/TG cycling. Moreover, this might indicate that DG synthesis capacity was enhanced, and thus more DGs are available as glycerol backbones for re-esterification ultimately increasing total flux through the FA/TG cycle. However, the authors did not measure DGAT expression and because available data on this genetic model are scarce, no definitive cause can be found that fully explains the observed phenotype. Taken together, deleting enzymes that synthesize precursor molecules of phospholipids does not appear to be a suitable option to modulate FA/TG cycling activity. Nevertheless, it has to be mentioned that most of these mouse lines are global and not tissue-specific knockout models, which additionally favors the occurrence of unwanted systemic effects outside adipose tissues. On the contrary, it is highly questionable whether an adipose tissue-specific KO of the aforementioned enzymes would abolish some of the unwanted "side-effects", such as reduced viability, failure to develop adipose tissues, and defective adipokine secretion. The loss of every single of these enzymes would still most likely impair local phospholipid synthesis and consequently also the formation of biological membranes and cell organelles in adipocytes. Thus, GPATs, AGPATs, and LIPINs are probably not viable targets to specifically decrease lipid cycling capacity.

5.12.2 DGAT1 and DGAT2

DGAT1 and DGAT2 catalyze the last step of TG synthesis using DGs and fatty acyl-CoA as substrates[198-200]. Mice with a global KO for either of the two enzymes have astonishingly different phenotypes highlighting their individual roles in metabolism. DGAT2KO mice are not viable and die within hours

after birth[201]. Defective lipid synthesis in the skin probably impairs its barrier function leading to fatal dehydration due to loss of water across the epidermis. On the contrary, DGAT1KO mice are viable, have an increased energy expenditure, lower tissue levels of TGs, an improved insulin sensitivity, and they are even partially protected from diet-induced obesity[202-205]. However, a combination of secondary effects that manifest predominantly in fat depots, liver, and the small intestine most likely cause these complex phenotypes[104,202]. The resulting metabolic derangements and disturbed inter-organ crosstalk overshadow the isolated effect of impaired adipose tissue TG synthesis. Conditional gene manipulation confirmed that mice lacking DGAT1 specifically in adipose tissue are less prone to diet-induced obesity[105]. Nevertheless, protection from excessive fat storage on a high-fat diet (HFD) is accompanied by signs of lipotoxicity, such as ER stress and upregulation of inflammatory markers, and concomitant insulin resistance. As more evidence comes to light, it seems clear that TG synthesis mediated by DGAT1 protects against lipotoxicity due to excess FAs. Accordingly, overexpression of DGAT1 in various tissues has been shown to have a protective effect[206-210], while targeted deletion outside of fat depots exacerbates lipotoxicity[211,212]. On the contrary, mice lacking DGAT2 in adipose tissues had no apparent metabolic phenotype with normal lipid storage and glucose metabolism[101]. When fed a HFD, key enzymes for *de novo* FA synthesis were slightly downregulated, but apart from this, no other effects were observed. These findings demonstrate that DGAT1 and DGAT2 are functionally redundant and in principle can compensate for each other under basal conditions, because the deletion of either enzyme in adipocytes resulted in no major detectable phenotype and normal development of adipose tissues[101]. This fact is in good agreement with previous publications showing that inhibition of either DGAT enzyme does not affect TG synthesis and lipid accumulation in cultured adipocytes[105,213]. However, DGAT2 is not able to compensate for DGAT1 as soon as intracellular FA levels exceed a certain threshold due to lipolytic release from lipid droplets (adrenergic stimulation) or delivery with the blood stream from exogenous sources (HFD feeding)[101,105]. Taken together, DGAT1-mediated TG synthesis not only helps to store energy but also to protect adipocytes from lipotoxicity during active lipolysis. DGAT2 catalyzes the esterification of FAs when low and steady FA levels prevail, and recent publications established a causal link between DGAT2 activity and DNL[101,206,214]. As similar as the basic function of these enzymes is, their sequence is different, which is because they belong to two distinct families. DGAT2 is an evolutionarily conserved major player in eukaryotic TG synthesis[104,215], whereas DGAT1 belongs to the MBOAT (membrane bound O-acyl transferase) gene family[216,217], whose members mediating FA esterification are known to sequester deleterious lipid species and thereby avert ER stress. Accordingly, it is currently assumed that DGAT2 has a more ancient function in mediating TG synthesis utilizing *de novo* synthesized FAs, and DGAT1 with its lower substrate specificity has a very defined function in re-esterification of FAs during active lipolysis, and consequently ER protection. Unfortunately, the contribution of DGAT1 and DGAT2 to UCP1-

independent thermogenesis and cold resistance has not been rigorously tested. However, very little or no effect would be expected in WT animals, because UCP1, which mediates the vast majority of adaptive NST, is abundantly expressed. The key experiment will be to delete DGAT1 and/or DGAT2 specifically in BAT of UCP1KO mice. Since these animals completely rely on UCP1-independent sources of thermogenesis, impairing futile lipid cycling should dramatically increase cold sensitivity. Coupling this approach with *in vivo* labeling methods will allow us to correlate FA/TG cycling activity with oxygen consumption measurements and cold tolerance. Notably, DGAT activity and lipid droplets in BAT are dispensable for cold-induced NST in WT mice[115]. Brown adipocytes develop normally in the absence of TG storage and retain their metabolic functions including substrate partitioning, thermogenesis, and adipokine secretion. However, loss of TG synthesis in Ucp1-positive tissues does not promote ER stress and lipotoxicity, which emphasizes the complex relationship between oxidative capacity, UCP1 expression, DGAT-mediated re-esterification, and controlled lipid handling. Nevertheless, especially due to the aforementioned findings, the effects of whole body but also tissue-specific deletion of enzymes related to acylglycerol synthesis on metabolic efficiency and total energy expenditure have to be interpreted very cautiously. In fact, these models argue against a contribution of futile lipid cycling to energy turnover, because most of them have elevated energy expenditure rates and are protected from diet-induced obesity[202-205]. However, as already briefly outlined, the resulting phenotypes may be caused by reduced overall physical insulation secondary to defective cutaneous and subcutaneous lipid storage. Moreover, intestinal lipid uptake and further distribution is impaired in the majority of these KO mouse lines resulting in heavily altered circulating lipid profiles. On the surface, these intrinsically unfavorable changes result in a favorable phenotype towards energy dissipation that is in turn associated with severe metabolic defects. It is clear that the (re-)generation of glycerol backbones and FA activation are sufficiently energy intensive and represent the largest ATP sink within adipose tissues[46,218-220], but it remains to be determined whether flux rates are large enough to ramp up whole body energy expenditure in a biologically relevant way. Taken together, targeting DGAT1 in *Ucp1*-positive cells appears to be a very promising approach to manipulate FA/TG cycling capacity, because adipose tissues should develop normally, the secretory function of adipocytes should be retained, and ER lipid as well as protein handling is expected to be unaffected. However, these assumptions are based on data obtained from WT mice. Thus, it is still unclear whether the impairment of lipid cycling in BAT of UCP1KO mice will cause far-reaching and potentially unintended changes, besides reduced NST, especially with regard to ROS production, ER stress/UPR, and lipotoxicity.

5.13 Perspective

As an outlook and to move away from the entirely BAT-centric view, it is very likely that, in addition to BAT, white and beige adipocytes are actively involved in FA/TG cycling-dependent thermogenesis[40,54,69,81,82,131]. These cells were long thought to solely represent an energy store that can be rapidly emptied or filled as needed. Nevertheless, it is known that white adipocytes increase the lipolytic breakdown of TGs and, at the same time, the incorporation of glycerol and FAs into TGs following cold exposure, while UCP1-dependent uncoupling remains unchanged[221,222]. Moreover, as ATP turnover but not UCP1 activity largely determines FA oxidation in beige adipocytes[222], one of the main functions of cold-activated WAT may be to export and take up FAs for futile FA/TG cycling[152,223]. This seems particularly interesting in light of a futile inter-organ cycle, as most recent quantitative lipid cycling and gene expression data from cold-acclimated WT and UCP1KO mice support this notion[69]. Interestingly, these results even suggest depot-specific specializations within WAT. eWAT is most likely the classic lipid store that is sacrificed upon cold exposure, whereas iWAT of UCP1KO mice seems to represent and intermediate phenotype between BAT and WAT, unifying lipid storage and thermogenic properties. Whether this is simply due to a higher number of beige adipocytes and a higher browning capacity, or has other causes, such as the specific recruitment of UCP1-negative adipocytes equipped with the enzymatic machinery required for alternative UCP1-independent thermogenic pathways, remains unclear and will be the subject of future investigations. Finally, the results presented here and the latest publications corroborate beyond doubt that futile lipid cycling in iBAT is part of adaptive thermogenesis in mice. Furthermore, it is evident that FA/TG cycling and probably other alternative thermogenic mechanisms are specifically recruited in the absence of UCP1. UCP1-independent NST in brown fat is fueled by a variety of substrates derived from intracellular stores or extracellular sources. Other adipose tissue depots and organs may provide energy substrates, such as glucose and lipids, which are then delivered to iBAT via the blood stream. Past work has already pointed towards an important role for FA/TG cycling as an ATP-sink in adipose tissues, which might be powerful enough to drive enhanced energy expenditure[48,54,71,81,82,138,224]. Current efforts concentrate on the question whether this process involves even more enzymes and reactions than already anticipated, and whether it has more unexpected implications in addition to the suggested thermogenic function, primarily regarding the dynamic interplay between lipid droplets and mitochondria, and its putative lipid detoxifying ability. Moreover, further studies focusing on the inter-organ aspect of futile lipid cycling and the importance of UCP1-independent thermogenesis are urgently required[83]. Over the coming years, the generation of novel mouse models with (brown) adipose tissue-specific deletions of enzymes mediating FA re-esterification and TG synthesis, i.e. DGAT1, will finally shed light on the absolute contribution of futile FA/TG cycling to NST, whole body energy expenditure, and the susceptibility to develop diet-induced obesity.

References

1   Grigg, G. C., Beard, L. A. & Augee, M. L. The evolution of endothermy and its diversity in mammals and birds. *Physiological and biochemical zoology : PBZ* **77**, 982-997, doi:10.1086/425188 (2004).

2   Girardier, L. & Stock, M. J. in *Mammalian Thermogenesis* (eds Lucien Girardier & Michael J. Stock) 1-7 (Springer Netherlands, 1983).

3   Crompton, A. W., Taylor, C. R. & Jagger, J. A. Evolution of homeothermy in mammals. *Nature* **272**, 333-336, doi:10.1038/272333a0 (1978).

4   Foster, D. O. & Frydman, M. L. Tissue distribution of cold-induced thermogenesis in conscious warm- or cold-acclimated rats reevaluated from changes in tissue blood flow: The dominant role of brown adipose tissue in the replacement of shivering by nonshivering thermogenesis. *Canadian Journal of Physiology and Pharmacology* **57**, 257-270, doi:10.1139/y79-039 %M 445227 (1979).

5   Gessner, C. *Conradi Gesneri medici Tigurini Historiae animalium liber primus de quadrupedibus viuiparis : opus philosophis, medicis, grammaticis, philologis, poëtis, & omnibus rerum linguarumꝗue variarum studiosis, vtilissimum simul iucundissimumꝗue futurum*. Editio secunda nouis iconibus nec non obseruationibus non paucis auctior atque etiam multis in locis emendatior. edn, Vol. Lib.1 (1551);Lib.2 (1586) (In Bibliopolio Cambieriano, 1551).

6   Smith, R. Thermogenic activity of the hibernating gland in the cold-acclimated rat. *Physiologist* **4**, 113 (1961).

7   Heaton, G. M., Wagenvoord, R. J., Kemp, A., Jr. & Nicholls, D. G. Brown-adipose-tissue mitochondria: photoaffinity labelling of the regulatory site of energy dissipation. *European journal of biochemistry* **82**, 515-521, doi:10.1111/j.1432-1033.1978.tb12045.x (1978).

8   Cinti, S. in *Adipose Tissue and Adipokines in Health and Disease* (eds Giamila Fantuzzi & Theodore Mazzone) 3-19 (Humana Press, 2007).

9   De Matteis, R., Ricquier, D. & Cinti, S. TH-, NPY-, SP-, and CGRP-immunoreactive nerves in interscapular brown adipose tissue of adult rats acclimated at different temperatures: an immunohistochemical study. *Journal of neurocytology* **27**, 877-886, doi:10.1023/a:1006996922657 (1998).

10   Honek, J. *et al.* Brown adipose tissue, thermogenesis, angiogenesis: pathophysiological aspects. *Hormone Molecular Biology and Clinical Investigation* **19**, 5-11, doi:doi:10.1515/hmbci-2014-0014 (2014).

11   Matthias, A. *et al.* Thermogenic Responses in Brown Fat Cells Are Fully UCP1-dependent: UCP2 or UCP3 do not substitute for UCP1 in adrenergically or fatty acid-induced thermogenesis. *Journal of Biological Chemistry* **275**, 25073-25081, doi:10.1074/jbc.M000547200 (2000).

12   Heldmaier, G. & Neuweiler, G. *Vergleichende Tierphysiologie*. (Springer-Verlag, 2013).

13   Ricquier, D. & Kader, J. C. Mitochondrial protein alteration in active brown fat: a soidum dodecyl sulfate-polyacrylamide gel electrophoretic study. *Biochemical and biophysical research communications* **73**, 577-583, doi:10.1016/0006-291x(76)90849-4 (1976).

14   Aquila, H., Link, T. A. & Klingenberg, M. The uncoupling protein from brown fat mitochondria is related to the mitochondrial ADP/ATP carrier. Analysis of sequence homologies and of folding of the protein in the membrane. *The EMBO Journal* **4**, 2369-2376, doi:https://doi.org/10.1002/j.1460-2075.1985.tb03941.x (1985).

15   Lin, C. S. & Klingenberg, M. Isolation of the uncoupling protein from brown adipose tissue mitochondria. *FEBS letters* **113**, 299-303, doi:10.1016/0014-5793(80)80613-2 (1980).

16   Shabalina, I. G. *et al.* Uncoupling protein-1 is not leaky. *Biochimica et Biophysica Acta (BBA)-Bioenergetics* **1797**, 773-784 (2010).

17   Hittelman, K., Lindberg, O. & Cannon, B. Oxidative phosphorylation and compartmentation of fatty acid metabolism in brown fat mitochondria. *European journal of biochemistry* **11**, 183-192 (1969).

18   Rafael, J., Ludolph, H. & Hohorst, H. Mitochondria from brown adipose tissue: uncoupling of respiratory chain phosphorylation by long fatty acids and recoupling by guanosine triphosphate. *Hoppe-Seyler's Zeitschrift fur physiologische Chemie* **350**, 1121-1131 (1969).

19   Bertholet, A. M. & Kirichok, Y. Mitochondrial H$^+$ Leak and Thermogenesis. *Annual Review of Physiology* **84**, 381-407 (2022).

20   Rial, E., Poustie, A. & NICHOLLS, D. G. Brown-adipose-tissue mitochondria: the regulation of the 32 000-Mr uncoupling protein by fatty acids and purine nucleotides. *European journal of biochemistry* **137**, 197-203 (1983).

21   Nicholls, D. G. The physiological regulation of uncoupling proteins. *Biochimica et Biophysica Acta (BBA) - Bioenergetics* **1757**, 459-466, doi:https://doi.org/10.1016/j.bbabio.2006.02.005 (2006).

22   Klingenberg, M. & Huang, S.-G. Structure and function of the uncoupling protein from brown adipose tissue. *Biochimica et Biophysica Acta (BBA)-Biomembranes* **1415**, 271-296 (1999).

23   Garlid, K. D., Jabůrek, M. & Ježek, P. The mechanism of proton transport mediated by mitochondrial uncoupling proteins. *FEBS letters* **438**, 10-14 (1998).

24   Fedorenko, A., Lishko, P. V. & Kirichok, Y. Mechanism of fatty-acid-dependent UCP1 uncoupling in brown fat mitochondria. *Cell* **151**, 400-413 (2012).

25   Klingenspor, M. *et al.* in *Adipose Tissue Biology* (ed Michael E. Symonds) 91-147 (Springer International Publishing, 2017).

26   Braun, K., Oeckl, J., Westermeier, J., Li, Y. & Klingenspor, M. Non-adrenergic control of lipolysis and thermogenesis in adipose tissues. *Journal of Experimental Biology* **221**, jeb165381 (2018).

27   Zimmermann, R. *et al.* Fat mobilization in adipose tissue is promoted by adipose triglyceride lipase. *Science* **306**, 1383-1386 (2004).

28   Vaughan, M., Berger, J. E. & Steinberg, D. Hormone-sensitive lipase and monoglyceride lipase activities in adipose tissue. *Journal of Biological Chemistry* **239**, 401-409 (1964).

29   Grabner, G. F., Xie, H., Schweiger, M. & Zechner, R. Lipolysis: cellular mechanisms for lipid mobilization from fat stores. *Nature metabolism* **3**, 1445-1465, doi:10.1038/s42255-021-00493-6 (2021).

30   Scholander, P., Hock, R., Walters, V., Johnson, F. & Irving, L. Heat regulation in some arctic and tropical mammals and birds. *The Biological Bulletin* **99**, 237-258 (1950).

31   Scholander, P., Walters, V., Hock, R. & Irving, L. Body insulation of some arctic and tropical mammals and birds. *The Biological Bulletin* **99**, 225-236 (1950).

32   Heldmaier, G., Klaus, S. & Wiesinger, H. in *Thermoreception and temperature regulation*   235-243 (Springer, 1990).

33   Nedergaard, J. & Cannon, B. UCP1 mRNA does not produce heat. *Biochimica et Biophysica Acta (BBA)-Molecular and Cell Biology of Lipids* **1831**, 943-949 (2013).

34   Bukowiecki, L. J., Géloën, A. & Collet, A. J. Proliferation and differentiation of brown adipocytes from interstitial cells during cold acclimation. *The American journal of physiology* **250**, C880-887, doi:10.1152/ajpcell.1986.250.6.C880 (1986).

35   Wu, J., Cohen, P. & Spiegelman, B. M. Adaptive thermogenesis in adipocytes: is beige the new brown? *Genes & development* **27**, 234-250 (2013).

36   Lončar, D., Afzelius, B. A. & Cannon, B. Epididymal white adipose tissue after cold stress in rats I. Nonmitochondrial changes. *Journal of Ultrastructure and Molecular Structure Research* **101**, 109-122, doi:https://doi.org/10.1016/0889-1605(88)90001-8 (1988).

37   Shabalina, Irina G. *et al.* UCP1 in Brite/Beige Adipose Tissue Mitochondria Is Functionally Thermogenic. *Cell reports* **5**, 1196-1203, doi:https://doi.org/10.1016/j.celrep.2013.10.044 (2013).

38   Enerbäck, S. *et al.* Mice lacking mitochondrial uncoupling protein are cold-sensitive but not obese. *Nature* **387**, 90-94, doi:10.1038/387090a0 (1997).

39   Golozoubova, V. *et al.* Only UCP1 can mediate adaptive nonshivering thermogenesis in the cold. *The FASEB Journal* **15**, 2048-2050, doi:https://doi.org/10.1096/fj.00-0536fje (2001).

40   Ukropec, J., Anunciado, R. P., Ravussin, Y., Hulver, M. W. & Kozak, L. P. UCP1-independent Thermogenesis in White Adipose Tissue of Cold-acclimated Ucp1-/- Mice. *Journal of Biological Chemistry* **281**, 31894-31908, doi:10.1016/S0021-9258(19)84104-2 (2006).

41   Newsholme, E. A. & Crabtree, B. Substrate cycles in metabolic regulation and in heat generation. *Biochemical Society symposium*, 61-109 (1976).

42   Newsholme, E. A. Substrate cycles: their metabolic, energetic and thermic consequences in man. *Biochemical Society symposium*, 183-205 (1978).

43   Newsholme, E. A. Sounding Board. A possible metabolic basis for the control of body weight. *The New England journal of medicine* **302**, 400-405, doi:10.1056/nejm198002143020711 (1980).

44   Newsholme, E. A., Arch, J. R., Brooks, B. & Surholt, B. The role of substrate cycles in metabolic regulation. *Biochemical Society transactions* **11**, 52-56, doi:10.1042/bst0110052 (1983).

45   Newsholme, E. A., Challiss, R. A. J. & Crabtree, B. Substrate cycles: their role in improving sensitivity in metabolic control. *Trends in Biochemical Sciences* **9**, 277-280, doi:10.1016/0968-0004(84)90165-8 (1984).

46   Ball, E. G. & Jungas, R. L. On the action of hormones which accelerate the rate of oxygen consumption and fatty acid release in rat adipose tissue in vitro. *Proceedings of the National Academy of Sciences of the United States of America* **47**, 932-941, doi:10.1073/pnas.47.7.932 (1961).

47   Brooks, B., Arch, J. R. & Newsholme, E. A. Effects of hormones on the rate of the triacylglycerol/fatty acid substrate cycle in adipocytes and epididymal fat pads. *FEBS letters* **146**, 327-330, doi:10.1016/0014-5793(82)80945-9 (1982).

48   Guan, H. P. *et al.* A futile metabolic cycle activated in adipocytes by antidiabetic agents. *Nature medicine* **8**, 1122-1128, doi:10.1038/nm780 (2002).

49   Elia, M., Zed, C., Neale, G. & Livesey, G. The energy cost of triglyceride-fatty acid recycling in nonobese subjects after an overnight fast and four days of starvation. *Metabolism: clinical and experimental* **36**, 251-255, doi:10.1016/0026-0495(87)90184-3 (1987).

50   Surholt, B. & Newsholme, E. A. The rate of substrate cycling between glucose and glucose 6-phosphate in muscle and fat-body of the hawk moth (Acherontia atropos) at rest and during flight. *The Biochemical journal* **210**, 49-54, doi:10.1042/bj2100049 (1983).

51   Morrissette, J. M., Franck, J. P. G. & Block, B. A. Characterization of ryanodine receptor and Ca^{2+}-ATPase isoforms in the thermogenic heater organ of blue marlin (Makaira nigricans). *Journal of Experimental Biology* **206**, 805-812, doi:10.1242/jeb.00158 (2003).

52   Ikeda, K., Maretich, P. & Kajimura, S. The common and distinct features of brown and beige adipocytes. *Trends in Endocrinology & Metabolism* **29**, 191-200 (2018).

53   Kazak, L. *et al.* A creatine-driven substrate cycle enhances energy expenditure and thermogenesis in beige fat. *Cell* **163**, 643-655, doi:10.1016/j.cell.2015.09.035 (2015).

54   Blondin, D. P. *et al.* Human Brown Adipocyte Thermogenesis Is Driven by β2-AR Stimulation. *Cell metabolism* **32**, 287-300.e287, doi:10.1016/j.cmet.2020.07.005 (2020).

55   Chondronikola, M. *et al.* Brown Adipose Tissue Activation Is Linked to Distinct Systemic Effects on Lipid Metabolism in Humans. *Cell metabolism* **23**, 1200-1206, doi:10.1016/j.cmet.2016.04.029 (2016).

56   Dieckmann, S. *et al.* Susceptibility to diet-induced obesity at thermoneutral conditions is independent of UCP1. *American journal of physiology. Endocrinology and metabolism* **322**, E85-e100, doi:10.1152/ajpendo.00278.2021 (2022).

57   Oeckl, J., Bast-Habersbrunner, A., Fromme, T., Klingenspor, M. & Li, Y. Isolation, Culture, and Functional Analysis of Murine Thermogenic Adipocytes. *STAR Protocols* **1**, 100118, doi:https://doi.org/10.1016/j.xpro.2020.100118 (2020).

58   Schweiger, M. *et al.* Adipose triglyceride lipase and hormone-sensitive lipase are the major enzymes in adipose tissue triacylglycerol catabolism. *The Journal of biological chemistry* **281**, 40236-40241, doi:10.1074/jbc.M608048200 (2006).

59   Schweizer, S., Oeckl, J., Klingenspor, M. & Fromme, T. Substrate fluxes in brown adipocytes upon adrenergic stimulation and uncoupling protein 1 ablation. *Life science alliance* **1**, e201800136, doi:10.26508/lsa.201800136 (2018).

60   Ruprecht, B. *et al.* Hydrophilic Strong Anion Exchange (hSAX) Chromatography Enables Deep Fractionation of Tissue Proteomes. *Methods in molecular biology (Clifton, N.J.)* **1550**, 69-82, doi:10.1007/978-1-4939-6747-6_7 (2017).

61   Yu, P. *et al.* Trimodal Mixed Mode Chromatography That Enables Efficient Offline Two-Dimensional Peptide Fractionation for Proteome Analysis. *Analytical Chemistry* **89**, 8884-8891, doi:10.1021/acs.analchem.7b01356 (2017).

62   Cox, J. & Mann, M. MaxQuant enables high peptide identification rates, individualized p.p.b.-range mass accuracies and proteome-wide protein quantification. *Nature Biotechnology* **26**, 1367-1372, doi:10.1038/nbt.1511 (2008).

63   Käll, L., Canterbury, J. D., Weston, J., Noble, W. S. & MacCoss, M. J. Semi-supervised learning for peptide identification from shotgun proteomics datasets. *Nature methods* **4**, 923-925 (2007).

64   Vizcaíno, J. A. *et al.* The PRoteomics IDEntifications (PRIDE) database and associated tools: status in 2013. *Nucleic acids research* **41**, D1063-D1069 (2012).

65   Tyanova, S. *et al.* The Perseus computational platform for comprehensive analysis of (prote)omics data. *Nature Methods* **13**, 731-740, doi:10.1038/nmeth.3901 (2016).

66   Team, R. C. R: A language and environment for statistical computing. (2013).

67   Cox, J. & Mann, M. 1D and 2D annotation enrichment: a statistical method integrating quantitative proteomics with complementary high-throughput data. *BMC bioinformatics* **13**, 1-11 (2012).

68   Schindelin, J. *et al.* Fiji: an open-source platform for biological-image analysis. *Nature methods* **9**, 676-682 (2012).

69   Oeckl, J. *et al.* Loss of UCP1 function augments recruitment of futile lipid cycling for thermogenesis in murine brown fat. *Molecular metabolism* **61**, 101499 (2022).

70   Ikeda, K. *et al.* UCP1-independent signaling involving SERCA2b-mediated calcium cycling regulates beige fat thermogenesis and systemic glucose homeostasis. *Nature medicine* **23**, 1454-1465, doi:10.1038/nm.4429 (2017).

71   Veliova, M. *et al.* Blocking mitochondrial pyruvate import in brown adipocytes induces energy wasting via lipid cycling. *EMBO reports* **21**, e49634, doi:10.15252/embr.201949634 (2020).

72   Li, Y., Fromme, T., Schweizer, S., Schöttl, T. & Klingenspor, M. Taking control over intracellular fatty acid levels is essential for the analysis of thermogenic function in cultured primary brown and brite/beige adipocytes. *EMBO reports* **15**, 1069-1076, doi:10.15252/embr.201438775 (2014).

73   Nicholls, D. G. Mitochondrial proton leaks and uncoupling proteins. *Biochimica et Biophysica Acta (BBA) - Bioenergetics* **1862**, 148428, doi:https://doi.org/10.1016/j.bbabio.2021.148428 (2021).

74   Lytton, J., Westlin, M. & Hanley, M. R. Thapsigargin inhibits the sarcoplasmic or endoplasmic reticulum Ca-ATPase family of calcium pumps. *Journal of Biological Chemistry* **266**, 17067-17071 (1991).

75   Deng, J. *et al.* Lipolysis response to endoplasmic reticulum stress in adipose cells. *The Journal of biological chemistry* **287**, 6240-6249, doi:10.1074/jbc.M111.299115 (2012).

76   Collatz, M. B., Rüdel, R. & Brinkmeier, H. Intracellular calcium chelator BAPTA protects cells against toxic calcium overload but also alters physiological calcium responses. *Cell calcium* **21**, 453-459, doi:10.1016/s0143-4160(97)90056-7 (1997).

77   Rahbani, J. F. *et al.* Creatine kinase B controls futile creatine cycling in thermogenic fat. *Nature* **590**, 480-485, doi:10.1038/s41586-021-03221-y (2021).

78   Sun, Y. *et al.* Mitochondrial TNAP controls thermogenesis by hydrolysis of phosphocreatine. *Nature* **593**, 580-585, doi:10.1038/s41586-021-03533-z (2021).

79   Fitch, C. D. & Chevli, R. Inhibition of creatine and phosphocreatine accumulation in skeletal muscle and heart. *Metabolism: clinical and experimental* **29**, 686-690 (1980).

80   Dahl, R. *et al.* Discovery and validation of a series of aryl sulfonamides as selective inhibitors of tissue-nonspecific alkaline phosphatase (TNAP). *Journal of medicinal chemistry* **52**, 6919-6925, doi:10.1021/jm900383s (2009).

81   Bardova, K. *et al.* Additive Effects of Omega-3 Fatty Acids and Thiazolidinediones in Mice Fed a High-Fat Diet: Triacylglycerol/Fatty Acid Cycling in Adipose Tissue. *Nutrients* **12**, doi:10.3390/nu12123737 (2020).

82   Flachs, P. *et al.* Induction of lipogenesis in white fat during cold exposure in mice: link to lean phenotype. *International journal of obesity (2005)* **41**, 372-380, doi:10.1038/ijo.2016.228 (2017).

83   Hui, S. *et al.* Quantitative Fluxomics of Circulating Metabolites. *Cell metabolism* **32**, 676-688.e674, doi:10.1016/j.cmet.2020.07.013 (2020).

84   Kalderon, B., Mayorek, N., Berry, E., Zevit, N. & Bar-Tana, J. Fatty acid cycling in the fasting rat. *American journal of physiology. Endocrinology and metabolism* **279**, E221-227, doi:10.1152/ajpendo.2000.279.1.E221 (2000).

85   Patel, D. & Kalhan, S. Glycerol Metabolism and Triglyceride-Fatty Acid Cycling in the Human Newborn: Effect of Maternal Diabetes and Intrauterine Growth Retardation. *Pediatric Research* **31**, 52-58, doi:10.1203/00006450-199201000-00010 (1992).

86   Wolfe, R. R., Herndon, D. N., Jahoor, F., Miyoshi, H. & Wolfe, M. Effect of severe burn injury on substrate cycling by glucose and fatty acids. *The New England journal of medicine* **317**, 403-408, doi:10.1056/nejm198708133170702 (1987).

87   Reidy, S. P. & Weber, J.-M. Accelerated substrate cycling: a new energy-wasting role for leptin in vivo. *American Journal of Physiology-Endocrinology and Metabolism* **282**, E312-E317, doi:10.1152/ajpendo.00037.2001 (2002).

88   Solinas, G. *et al.* The direct effect of leptin on skeletal muscle thermogenesis is mediated by substrate cycling between de novo lipogenesis and lipid oxidation. *FEBS letters* **577**, 539-544, doi:https://doi.org/10.1016/j.febslet.2004.10.066 (2004).

89   Mayer, N. *et al.* Development of small-molecule inhibitors targeting adipose triglyceride lipase. *Nat Chem Biol* **9**, 785-787, doi:10.1038/nchembio.1359 (2013).

90   Wojtczak, L. & Lehninger, A. L. Formation and disappearance of an endogenous uncoupling factor during swelling and contraction of mitochondria. *Biochimica et biophysica acta* **51**, 442-456, doi:10.1016/0006-3002(61)90600-x (1961).

91   Wojtczak, L. & Schönfeld, P. Effect of fatty acids on energy coupling processes in mitochondria. *Biochimica et biophysica acta* **1183**, 41-57, doi:10.1016/0005-2728(93)90004-y (1993).

92   Penzo, D., Tagliapietra, C., Colonna, R., Petronilli, V. & Bernardi, P. Effects of fatty acids on mitochondria: implications for cell death. *Biochimica et Biophysica Acta (BBA) - Bioenergetics* **1555**, 160-165, doi:https://doi.org/10.1016/S0005-2728(02)00272-4 (2002).

93   Di Paola, M. & Lorusso, M. Interaction of free fatty acids with mitochondria: coupling, uncoupling and permeability transition. *Biochimica et biophysica acta* **1757**, 1330-1337, doi:10.1016/j.bbabio.2006.03.024 (2006).

94   Yehuda-Shnaidman, E., Buehrer, B., Pi, J., Kumar, N. & Collins, S. Acute stimulation of white adipocyte respiration by PKA-induced lipolysis. *Diabetes* **59**, 2474-2483, doi:10.2337/db10-0245 (2010).

95   Montero, M., Lobatón, C. D., Gutierrez-Fernández, S., Moreno, A. & Alvarez, J. Calcineurin-independent inhibition of mitochondrial Ca2+ uptake by cyclosporin A. *British journal of pharmacology* **141**, 263-268, doi:10.1038/sj.bjp.0705609 (2004).

96   Kiorpes, T. C. *et al.* Identification of 2-tetradecylglycidyl coenzyme A as the active form of methyl 2-tetradecylglycidate (methyl palmoxirate) and its characterization as an irreversible, active site-directed inhibitor of carnitine palmitoyltransferase A in isolated rat liver mitochondria. *The Journal of biological chemistry* **259**, 9750-9755 (1984).

97   Edens, N. K., Leibel, R. L. & Hirsch, J. Mechanism of free fatty acid re-esterification in human adipocytes in vitro. *Journal of lipid research* **31**, 1423-1431 (1990).

98   Yu, X. X., Lewin, D. A., Forrest, W. & Adams, S. H. Cold elicits the simultaneous induction of fatty acid synthesis and β-oxidation in murine brown adipose tissue: prediction from differential gene expression and confirmation in vivo. *The FASEB Journal* **16**, 155-168, doi:https://doi.org/10.1096/fj.01-0568com (2002).

99   Igal, R. A., Wang, P. & Coleman, R. A. Triacsin C blocks de novo synthesis of glycerolipids and cholesterol esters but not recycling of fatty acid into phospholipid: evidence for functionally separate pools of acyl-CoA. *The Biochemical journal* **324 (Pt 2)**, 529-534, doi:10.1042/bj3240529 (1997).

100   Vessey, D. A., Kelley, M. & Warren, R. S. Characterization of triacsin C inhibition of short-, medium-, and long-chain fatty acid: CoA ligases of human liver. *Journal of biochemical and molecular toxicology* **18**, 100-106, doi:10.1002/jbt.20009 (2004).

101   Chitraju, C., Walther, T. C. & Farese, R. V., Jr. The triglyceride synthesis enzymes DGAT1 and DGAT2 have distinct and overlapping functions in adipocytes. *Journal of lipid research* **60**, 1112-1120, doi:10.1194/jlr.M093112 (2019).

102   Qian, Y. *et al.* Discovery of orally active carboxylic acid derivatives of 2-phenyl-5-trifluoromethyloxazole-4-carboxamide as potent diacylglycerol acyltransferase-1 inhibitors for the potential treatment of obesity and diabetes. *Journal of medicinal chemistry* **54**, 2433-2446, doi:10.1021/jm101580m (2011).

103   Futatsugi, K. *et al.* Discovery and optimization of imidazopyridine-based inhibitors of diacylglycerol acyltransferase 2 (DGAT2). *Journal of medicinal chemistry* **58**, 7173-7185 (2015).

104   Yen, C.-L. E., Stone, S. J., Koliwad, S., Harris, C. & Farese, R. V. Thematic review series: glycerolipids. DGAT enzymes and triacylglycerol biosynthesis. *Journal of lipid research* **49**, 2283-2301 (2008).

105   Chitraju, C. *et al.* Triglyceride Synthesis by DGAT1 Protects Adipocytes from Lipid-Induced ER Stress during Lipolysis. *Cell metabolism* **26**, 407-418.e403, doi:10.1016/j.cmet.2017.07.012 (2017).

106   Maurer, S. F., Fromme, T., Mocek, S., Zimmermann, A. & Klingenspor, M. Uncoupling protein 1 and the capacity for nonshivering thermogenesis are components of the glucose homeostatic system. *American Journal of Physiology-Endocrinology and Metabolism* **318**, E198-E215, doi:10.1152/ajpendo.00121.2019 (2020).

107   Olsen, J. M. *et al.* β(3)-Adrenergically induced glucose uptake in brown adipose tissue is independent of UCP1 presence or activity: Mediation through the mTOR pathway. *Mol Metab* **6**, 611-619, doi:10.1016/j.molmet.2017.02.006 (2017).

108   Wick, A. N., Drury, D. R., Nakada, H. I. & Wolfe, J. B. Localization of the primary metabolic block produced by 2-deoxyglucose. *The Journal of biological chemistry* **224**, 963-969 (1957).

109   Houstěk, J., Cannon, B. & Lindberg, O. Gylcerol-3-phosphate shuttle and its function in intermediary metabolism of hamster brown-adipose tissue. *European journal of biochemistry* **54**, 11-18, doi:10.1111/j.1432-1033.1975.tb04107.x (1975).

110   Herzig, S. & Shaw, R. J. AMPK: guardian of metabolism and mitochondrial homeostasis. *Nature Reviews Molecular Cell Biology* **19**, 121-135, doi:10.1038/nrm.2017.95 (2018).

111   Corton, J. M., Gillespie, J. G., Hawley, S. A. & Hardie, D. G. 5-Aminoimidazole-4-carboxamide ribonucleoside: a specific method for activating AMP-activated protein kinase in intact cells? *European journal of biochemistry* **229**, 558-565 (1995).

112   Zhou, G. *et al.* Role of AMP-activated protein kinase in mechanism of metformin action. *The Journal of clinical investigation* **108**, 1167-1174, doi:10.1172/jci13505 (2001).

113   Benador, I. Y. *et al.* Mitochondria Bound to Lipid Droplets Have Unique Bioenergetics, Composition, and Dynamics that Support Lipid Droplet Expansion. *Cell metabolism* **27**, 869-885.e866, doi:10.1016/j.cmet.2018.03.003 (2018).

114   Hetz, C. The unfolded protein response: controlling cell fate decisions under ER stress and beyond. *Nature Reviews Molecular Cell Biology* **13**, 89-102, doi:10.1038/nrm3270 (2012).

115   Chitraju, C., Fischer, A. W., Farese, R. V., Jr. & Walther, T. C. Lipid Droplets in Brown Adipose Tissue Are Dispensable for Cold-Induced Thermogenesis. *Cell reports* **33**, 108348, doi:10.1016/j.celrep.2020.108348 (2020).

116   Bond, L. M., Burhans, M. S. & Ntambi, J. M. Uncoupling protein-1 deficiency promotes brown adipose tissue inflammation and ER stress. *PloS one* **13**, e0205726, doi:10.1371/journal.pone.0205726 (2018).

117   Kazak, L. *et al.* UCP1 deficiency causes brown fat respiratory chain depletion and sensitizes mitochondria to calcium overload-induced dysfunction. *Proceedings of the National Academy of Sciences of the United States of America* **114**, 7981-7986, doi:10.1073/pnas.1705406114 (2017).

118   Ku, H.-C. & Cheng, C.-F. Master Regulator Activating Transcription Factor 3 (ATF3) in Metabolic Homeostasis and Cancer. *Frontiers in Endocrinology* **11**, doi:10.3389/fendo.2020.00556 (2020).

119   Kopp, M. C., Larburu, N., Durairaj, V., Adams, C. J. & Ali, M. M. U. UPR proteins IRE1 and PERK switch BiP from chaperone to ER stress sensor. *Nature Structural & Molecular Biology* **26**, 1053-1062, doi:10.1038/s41594-019-0324-9 (2019).

120   Tabas, I. & Ron, D. Integrating the mechanisms of apoptosis induced by endoplasmic reticulum stress. *Nature cell biology* **13**, 184-190 (2011).

121   Hu, H., Tian, M., Ding, C. & Yu, S. The C/EBP Homologous Protein (CHOP) Transcription Factor Functions in Endoplasmic Reticulum Stress-Induced Apoptosis and Microbial Infection. *Frontiers in Immunology* **9**, doi:10.3389/fimmu.2018.03083 (2019).

122   Yoshida, H., Matsui, T., Yamamoto, A., Okada, T. & Mori, K. XBP1 mRNA is induced by ATF6 and spliced by IRE1 in response to ER stress to produce a highly active transcription factor. *Cell* **107**, 881-891 (2001).

123   Zha, B. S. & Zhou, H. ER Stress and Lipid Metabolism in Adipocytes. *Biochemistry Research International* **2012**, 312943, doi:10.1155/2012/312943 (2012).

124   Feldmann, H. M., Golozoubova, V., Cannon, B. & Nedergaard, J. UCP1 ablation induces obesity and abolishes diet-induced thermogenesis in mice exempt from thermal stress by living at thermoneutrality. *Cell metabolism* **9**, 203-209, doi:10.1016/j.cmet.2008.12.014 (2009).

125   Hofmann, W. E., Liu, X., Bearden, C. M., Harper, M. E. & Kozak, L. P. Effects of genetic background on thermoregulation and fatty acid-induced uncoupling of mitochondria in UCP1-deficient mice. *The Journal of biological chemistry* **276**, 12460-12465, doi:10.1074/jbc.M100466200 (2001).

126   Gaudry, M. J., Campbell, K. L. & Jastroch, M. Evolution of UCP1. *Handbook of experimental pharmacology* **251**, 127-141, doi:10.1007/164_2018_116 (2019).

127   Leitner, B. P. *et al.* Mapping of human brown adipose tissue in lean and obese young men. *Proceedings of the National Academy of Sciences* **114**, 8649-8654, doi:doi:10.1073/pnas.1705287114 (2017).

128   Nedergaard, J. *et al.* UCP1: the only protein able to mediate adaptive non-shivering thermogenesis and metabolic inefficiency. *Biochimica et Biophysica Acta (BBA) - Bioenergetics* **1504**, 82-106, doi:https://doi.org/10.1016/S0005-2728(00)00247-4 (2001).

129   Golozoubova, V., Cannon, B. & Nedergaard, J. UCP1 is essential for adaptive adrenergic nonshivering thermogenesis. *American Journal of Physiology-Endocrinology and Metabolism* **291**, E350-E357, doi:10.1152/ajpendo.00387.2005 (2006).

130   Meyer, C. W. *et al.* Adaptive thermogenesis and thermal conductance in wild-type and UCP1-KO mice. *American journal of physiology. Regulatory, integrative and comparative physiology* **299**, R1396-1406, doi:10.1152/ajpregu.00021.2009 (2010).

131   Keipert, S. *et al.* Long-Term Cold Adaptation Does Not Require FGF21 or UCP1. *Cell metabolism* **26**, 437-446.e435, doi:10.1016/j.cmet.2017.07.016 (2017).

132   Blondin, D. P. *et al.* Contributions of white and brown adipose tissues and skeletal muscles to acute cold-induced metabolic responses in healthy men. *The Journal of physiology* **593**, 701-714, doi:10.1113/jphysiol.2014.283598 (2015).

133   Carpentier, A. C., Blondin, D. P., Haman, F. & Richard, D. Brown adipose tissue - a translational perspective. *Endocrine reviews*, doi:10.1210/endrev/bnac015 (2022).

134   Laurila, S. *et al.* Secretin activates brown fat and induces satiation. *Nature metabolism* **3**, 798-809, doi:10.1038/s42255-021-00409-4 (2021).

135   Herz, C. T. & Kiefer, F. W. Adipose tissue browning in mice and humans. *Journal of Endocrinology* **241**, R97-R109, doi:10.1530/JOE-18-0598 (2019).

136   Brownstein, A. J., Veliova, M., Acin-Perez, R., Liesa, M. & Shirihai, O. S. ATP-consuming futile cycles as energy dissipating mechanisms to counteract obesity. *Reviews in endocrine & metabolic disorders* **23**, 121-131, doi:10.1007/s11154-021-09690-w (2022).

137   Kanehisa, M. & Goto, S. KEGG: kyoto encyclopedia of genes and genomes. *Nucleic Acids Res* **28**, 27-30, doi:10.1093/nar/28.1.27 (2000).

138   Granneman, J. G., Burnazi, M., Zhu, Z. & Schwamb, L. A. White adipose tissue contributes to UCP1-independent thermogenesis. *American Journal of Physiology-Endocrinology and Metabolism* **285**, E1230-E1236, doi:10.1152/ajpendo.00197.2003 (2003).

139   Steinberg, D. Fatty acid mobilization--mechanisms of regulation and metabolic consequences. *Biochemical Society symposium* **24**, 111-143 (1963).

140   Mottillo, E. P. *et al.* Coupling of lipolysis and de novo lipogenesis in brown, beige, and white adipose tissues during chronic $β_3$-adrenergic receptor activation. *Journal of lipid research* **55**, 2276-2286, doi:10.1194/jlr.M050005 (2014).

141   Flachs, P., Rossmeisl, M., Kuda, O. & Kopecky, J. Stimulation of mitochondrial oxidative capacity in white fat independent of UCP1: a key to lean phenotype. *Biochimica et biophysica acta* **1831**, 986-1003, doi:10.1016/j.bbalip.2013.02.003 (2013).

142   Keipert, S. & Jastroch, M. Brite/beige fat and UCP1 - is it thermogenesis? *Biochimica et biophysica acta* **1837**, 1075-1082, doi:10.1016/j.bbabio.2014.02.008 (2014).

143   Yehuda-Shnaidman, E., Buehrer, B., Pi, J., Kumar, N. & Collins, S. Acute Stimulation of White Adipocyte Respiration by PKA-Induced Lipolysis. *Diabetes* **59**, 2474-2483, doi:10.2337/db10-0245 (2010).

144   Schönfeld, P. & Wojtczak, L. Short- and medium-chain fatty acids in energy metabolism: the cellular perspective. *Journal of lipid research* **57**, 943-954, doi:10.1194/jlr.R067629 (2016).

145   Dubey, R. *et al.* Lipid droplets can promote drug accumulation and activation. *Nature Chemical Biology* **16**, 206-213, doi:10.1038/s41589-019-0447-7 (2020).

146   Sorger, D., Athenstaedt, K., Hrastnik, C. & Daum, G. A Yeast Strain Lacking Lipid Particles Bears a Defect in Ergosterol Formation*. *Journal of Biological Chemistry* **279**, 31190-31196, doi:https://doi.org/10.1074/jbc.M403251200 (2004).

147   Gülden, M., Mörchel, S., Tahan, S. & Seibert, H. Impact of protein binding on the availability and cytotoxic potency of organochlorine pesticides and chlorophenols in vitro. *Toxicology* **175**, 201-213, doi:10.1016/s0300-483x(02)00085-9 (2002).

148   Lewin, T. M., Kim, J.-H., Granger, D. A., Vance, J. E. & Coleman, R. A. Acyl-CoA Synthetase Isoforms 1, 4, and 5 Are Present in Different Subcellular Membranes in Rat Liver and Can Be Inhibited Independently*. *Journal of Biological Chemistry* **276**, 24674-24679, doi:https://doi.org/10.1074/jbc.M102036200 (2001).

149   Gauthier, M. S. *et al.* AMP-activated protein kinase is activated as a consequence of lipolysis in the adipocyte: potential mechanism and physiological relevance. *The Journal of biological chemistry* **283**, 16514-16524, doi:10.1074/jbc.M708177200 (2008).

150   Paar, M. *et al.* Remodeling of lipid droplets during lipolysis and growth in adipocytes. *The Journal of biological chemistry* **287**, 11164-11173, doi:10.1074/jbc.M111.316794 (2012).

151   Eichmann, T. O. & Lass, A. DAG tales: the multiple faces of diacylglycerol—stereochemistry, metabolism, and signaling. *Cellular and Molecular Life Sciences* **72**, 3931-3952, doi:10.1007/s00018-015-1982-3 (2015).

152   Shin, H. *et al.* Lipolysis in Brown Adipocytes Is Not Essential for Cold-Induced Thermogenesis in Mice. *Cell metabolism* **26**, 764-777.e765, doi:10.1016/j.cmet.2017.09.002 (2017).

153   Schweizer, S. *et al.* The lipidome of primary murine white, brite, and brown adipocytes—Impact of beta-adrenergic stimulation. *PLOS Biology* **17**, e3000412, doi:10.1371/journal.pbio.3000412 (2019).

154   Khedoe, P. P. S. J. *et al.* Brown adipose tissue takes up plasma triglycerides mostly after lipolysis. *Journal of lipid research* **56**, 51-59, doi:https://doi.org/10.1194/jlr.M052746 (2015).

155   Carmean, C. M., Bobe, A. M., Yu, J. C., Volden, P. A. & Brady, M. J. Refeeding-induced brown adipose tissue glycogen hyper-accumulation in mice is mediated by insulin and catecholamines. *PloS one* **8**, e67807, doi:10.1371/journal.pone.0067807 (2013).

156   Farkas, V., Kelenyi, G. & Sandor, A. A dramatic accumulation of glycogen in the brown adipose tissue of rats following recovery from cold exposure. *Archives of biochemistry and biophysics* **365**, 54-61, doi:10.1006/abbi.1999.1157 (1999).

157   Jakus, P. B., Sandor, A., Janaky, T. & Farkas, V. Cooperation between BAT and WAT of rats in thermogenesis in response to cold, and the mechanism of glycogen accumulation in BAT during reacclimation. *Journal of lipid research* **49**, 332-339, doi:10.1194/jlr.M700316-JLR200 (2008).

158   Steiner, G. & G. F. Cahill, J. Brown and white adipose tissue metabolism in cold-exposed rats. *American Journal of Physiology-Legacy Content* **207**, 840-844, doi:10.1152/ajplegacy.1964.207.4.840 (1964).

159   Mráček, T., Drahota, Z. & Houštěk, J. The function and the role of the mitochondrial glycerol-3-phosphate dehydrogenase in mammalian tissues. *Biochimica et Biophysica Acta (BBA) - Bioenergetics* **1827**, 401-410, doi:https://doi.org/10.1016/j.bbabio.2012.11.014 (2013).

160   Mookerjee, S. A., Gerencser, A. A., Nicholls, D. G. & Brand, M. D. Quantifying intracellular rates of glycolytic and oxidative ATP production and consumption using extracellular flux measurements. *The Journal of biological chemistry* **292**, 7189-7207, doi:10.1074/jbc.M116.774471 (2017).

161   Houštěk, J. & Drahota, Z. The regulation of glycerol 3-phosphate oxidase of rat brownadipose tissue mitochondria by long-chain free fatty acids. *Molecular and cellular biochemistry* **7**, 45-50 (1975).

162   Bukowiecki, L. & Lindberg, O. Control of sn-glycerql 3-phosphate oxidation in brown adipose tissue mitochondria by calcium and ACYL-CoA. *Biochimica et Biophysica Acta (BBA)-Lipids and Lipid Metabolism* **348**, 115-125 (1974).

163   Shabalina, I. G., Jacobsson, A., Cannon, B. & Nedergaard, J. Native UCP1 displays simple competitive kinetics between the regulators purine nucleotides and fatty acids. *The Journal of biological chemistry* **279**, 38236-38248, doi:10.1074/jbc.M402375200 (2004).

164   Festuccia, W. T. *et al.* The PPARgamma agonist rosiglitazone enhances rat brown adipose tissue lipogenesis from glucose without altering glucose uptake. *American journal of physiology. Regulatory, integrative and comparative physiology* **296**, R1327-1335, doi:10.1152/ajpregu.91012.2008 (2009).

165   Keipert, S. *et al.* Genetic disruption of uncoupling protein 1 in mice renders brown adipose tissue a significant source of FGF21 secretion. *Molecular Metabolism* **4**, 537-542, doi:https://doi.org/10.1016/j.molmet.2015.04.006 (2015).

166   Lasar, D. *et al.* Peroxisome Proliferator Activated Receptor Gamma Controls Mature Brown Adipocyte Inducibility through Glycerol Kinase. *Cell reports* **22**, 760-773, doi:10.1016/j.celrep.2017.12.067 (2018).

167   Rosell, M. *et al.* Brown and white adipose tissues: intrinsic differences in gene expression and response to cold exposure in mice. *American Journal of Physiology-Endocrinology and Metabolism* **306**, E945-E964, doi:10.1152/ajpendo.00473.2013 (2014).

168   Jastroch, M. Uncoupling protein 1 controls reactive oxygen species in brown adipose tissue. *Proceedings of the National Academy of Sciences of the United States of America* **114**, 7744-7746, doi:10.1073/pnas.1709064114 (2017).

169   Zhao, R. Z., Jiang, S., Zhang, L. & Yu, Z. B. Mitochondrial electron transport chain, ROS generation and uncoupling (Review). *International journal of molecular medicine* **44**, 3-15, doi:10.3892/ijmm.2019.4188 (2019).

170   Jastroch, M., Divakaruni, A. S., Mookerjee, S., Treberg, J. R. & Brand, M. D. Mitochondrial proton and electron leaks. *Essays in biochemistry* **47**, 53-67, doi:10.1042/bse0470053 (2010).

171   Engin, A. B. What Is Lipotoxicity? *Advances in experimental medicine and biology* **960**, 197-220, doi:10.1007/978-3-319-48382-5_8 (2017).

172   Piccolis, M. *et al.* Probing the Global Cellular Responses to Lipotoxicity Caused by Saturated Fatty Acids. *Molecular cell* **74**, 32-44.e38, doi:10.1016/j.molcel.2019.01.036 (2019).

173   Divakaruni, A. S. & Jastroch, M. A practical guide for the analysis, standardization and interpretation of oxygen consumption measurements. *Nature metabolism* **4**, 978-994, doi:10.1038/s42255-022-00619-4 (2022).

174   Gerencser, A. A. *et al.* Quantitative Microplate-Based Respirometry with Correction for Oxygen Diffusion. *Analytical Chemistry* **81**, 6868-6878, doi:10.1021/ac900881z (2009).

175   Kramarova, T. V. *et al.* Mitochondrial ATP synthase levels in brown adipose tissue are governed by the c-Fo subunit P1 isoform. *FASEB journal : official publication of the Federation of American Societies for Experimental Biology* **22**, 55-63, doi:10.1096/fj.07-8581com (2008).

176   Zhu, J. *et al.* Phosphorylation of PLIN3 by AMPK promotes dispersion of lipid droplets during starvation. *Protein & Cell* **10**, 382-387, doi:10.1007/s13238-018-0593-9 (2019).

177   Kim, S.-J. *et al.* AMPK Phosphorylates Desnutrin/ATGL and Hormone-Sensitive Lipase To Regulate Lipolysis and Fatty Acid Oxidation within Adipose Tissue. *Molecular and Cellular Biology* **36**, 1961-1976, doi:doi:10.1128/MCB.00244-16 (2016).

178   Wang, Q., Liu, S., Zhai, A., Zhang, B. & Tian, G. AMPK-Mediated Regulation of Lipid Metabolism by Phosphorylation. *Biological and Pharmaceutical Bulletin* **41**, 985-993, doi:10.1248/bpb.b17-00724 (2018).

179   Wu, L. *et al.* AMP-Activated Protein Kinase (AMPK) Regulates Energy Metabolism through Modulating Thermogenesis in Adipose Tissue. *Frontiers in Physiology* **9**, doi:10.3389/fphys.2018.00122 (2018).

180   Gauthier, M.-S. *et al.* AMP-activated Protein Kinase Is Activated as a Consequence of Lipolysis in the Adipocyte: Potential mechanism and physiological relevance *. *Journal of Biological Chemistry* **283**, 16514-16524, doi:10.1074/jbc.M708177200 (2008).

181   Gaidhu, M. P. *et al.* Prolonged AICAR-induced AMP-kinase activation promotes energy dissipation in white adipocytes: novel mechanisms integrating HSL and ATGL. *Journal of lipid research* **50**, 704-715, doi:10.1194/jlr.M800480-JLR200 (2009).

182   Anthony, N. M., Gaidhu, M. P. & Ceddia, R. B. Regulation of Visceral and Subcutaneous Adipocyte Lipolysis by Acute AICAR-induced AMPK Activation. *Obesity* **17**, 1312-1317, doi:https://doi.org/10.1038/oby.2008.645 (2009).

183   Gaidhu, M. P., Bikopoulos, G. & Ceddia, R. B. Chronic AICAR-induced AMP-kinase activation regulates adipocyte lipolysis in a time-dependent and fat depot-specific manner in rats. *American Journal of Physiology-Cell Physiology* **303**, C1192-C1197, doi:10.1152/ajpcell.00159.2012 (2012).

184   Pinkosky, S. L. *et al.* Long-chain fatty acyl-CoA esters regulate metabolism via allosteric control of AMPK β1 isoforms. *Nature metabolism* **2**, 873-881, doi:10.1038/s42255-020-0245-2 (2020).

185   Djouder, N. *et al.* PKA phosphorylates and inactivates AMPKα to promote efficient lipolysis. *The EMBO Journal* **29**, 469-481, doi:https://doi.org/10.1038/emboj.2009.339 (2010).

186   Kadenbach, B. Complex IV - The regulatory center of mitochondrial oxidative phosphorylation. *Mitochondrion* **58**, 296-302, doi:10.1016/j.mito.2020.10.004 (2021).

187   Monemdjou, S., Kozak, L. P. & Harper, M. E. Mitochondrial proton leak in brown adipose tissue mitochondria of Ucp1-deficient mice is GDP insensitive. *The American journal of physiology* **276**, E1073-1082, doi:10.1152/ajpendo.1999.276.6.E1073 (1999).

188   Shabalina, I. G. *et al.* Uncoupling protein-1 is not leaky. *Biochimica et biophysica acta* **1797**, 773-784, doi:10.1016/j.bbabio.2010.04.007 (2010).

189   Shabalina, I. G., Kramarova, T. V., Nedergaard, J. & Cannon, B. Carboxyatractyloside effects on brown-fat mitochondria imply that the adenine nucleotide translocator isoforms ANT1 and ANT2 may be responsible for basal and fatty-acid-induced uncoupling respectively. *The Biochemical journal* **399**, 405-414, doi:10.1042/BJ20060706 (2006).

190   Matthias, A., Jacobsson, A., Cannon, B. & Nedergaard, J. The bioenergetics of brown fat mitochondria from UCP1-ablated mice. Ucp1 is not involved in fatty acid-induced de-energization ("uncoupling"). *The Journal of biological chemistry* **274**, 28150-28160, doi:10.1074/jbc.274.40.28150 (1999).

191   Matthias, A. *et al.* Thermogenic responses in brown fat cells are fully UCP1-dependent. UCP2 or UCP3 do not substitute for UCP1 in adrenergically or fatty scid-induced thermogenesis. *The Journal of biological chemistry* **275**, 25073-25081, doi:10.1074/jbc.M000547200 (2000).

192   Nagle, C. A. *et al.* Identification of a novel sn-glycerol-3-phosphate acyltransferase isoform, GPAT4, as the enzyme deficient in Agpat6$^{-/-}$ mice. *Journal of lipid research* **49**, 823-831, doi:10.1194/jlr.M700592-JLR200 (2008).

193   Vergnes, L. *et al.* Agpat6 deficiency causes subdermal lipodystrophy and resistance to obesity. *Journal of lipid research* **47**, 745-754, doi:10.1194/jlr.M500553-JLR200 (2006).

194   Agarwal, A. K. *et al.* AGPAT2 is mutated in congenital generalized lipodystrophy linked to chromosome 9q34. *Nature Genetics* **31**, 21-23, doi:10.1038/ng880 (2002).

195   Cortés, V. A. *et al.* Molecular Mechanisms of Hepatic Steatosis and Insulin Resistance in the AGPAT2-Deficient Mouse Model of Congenital Generalized Lipodystrophy. *Cell metabolism* **9**, 165-176, doi:10.1016/j.cmet.2009.01.002 (2009).

196   Péterfy, M., Phan, J., Xu, P. & Reue, K. Lipodystrophy in the fld mouse results from mutation of a new gene encoding a nuclear protein, lipin. *Nature Genetics* **27**, 121-124, doi:10.1038/83685 (2001).

197   Phan, J. & Reue, K. Lipin, a lipodystrophy and obesity gene. *Cell metabolism* **1**, 73-83, doi:10.1016/j.cmet.2004.12.002 (2005).

198   Cases, S. *et al.* Identification of a gene encoding an acyl CoA: diacylglycerol acyltransferase, a key enzyme in triacylglycerol synthesis. *Proceedings of the National Academy of Sciences* **95**, 13018-13023 (1998).

199   Cases, S. *et al.* Cloning of DGAT2, a second mammalian diacylglycerol acyltransferase, and related family members. *Journal of Biological Chemistry* **276**, 38870-38876 (2001).

200   Lardizabal, K. D. *et al.* DGAT2 is a new diacylglycerol acyltransferase gene family: purification, cloning, and expression in insect cells of two polypeptides from Mortierella ramanniana with diacylglycerol acyltransferase activity. *Journal of Biological Chemistry* **276**, 38862-38869 (2001).

201   Stone, S. J. *et al.* Lipopenia and skin barrier abnormalities in DGAT2-deficient mice. *Journal of Biological Chemistry* **279**, 11767-11776 (2004).

202   Smith, S. J. *et al.* Obesity resistance and multiple mechanisms of triglyceride synthesis in mice lacking Dgat. *Nature genetics* **25**, 87-90 (2000).

203   Chen, H. C. *et al.* Increased insulin and leptin sensitivity in mice lacking acyl CoA: diacylglycerol acyltransferase 1. *The Journal of clinical investigation* **109**, 1049-1055 (2002).

204   Chen, H. C., Stone, S. J., Zhou, P., Buhman, K. K. & Farese Jr, R. V. Dissociation of obesity and impaired glucose disposal in mice overexpressing acyl coenzyme a: diacylglycerol acyltransferase 1 in white adipose tissue. *Diabetes* **51**, 3189-3195 (2002).

205   Streeper, R. S. *et al.* Deficiency of the lipid synthesis enzyme, DGAT1, extends longevity in mice. *Aging (Albany NY)* **4**, 13 (2012).

206   Monetti, M. *et al.* Dissociation of hepatic steatosis and insulin resistance in mice overexpressing DGAT in the liver. *Cell metabolism* **6**, 69-78 (2007).

207   Villanueva, C. J. *et al.* Specific role for acyl CoA: Diacylglycerol acyltransferase 1 (Dgat1) in hepatic steatosis due to exogenous fatty acids. *Hepatology* **50**, 434-442 (2009).

208   Listenberger, L. L. *et al.* Triglyceride accumulation protects against fatty acid-induced lipotoxicity. *Proceedings of the National Academy of Sciences* **100**, 3077-3082 (2003).

209   Koliwad, S. K. *et al.* DGAT1-dependent triacylglycerol storage by macrophages protects mice from diet-induced insulin resistance and inflammation. *The Journal of clinical investigation* **120**, 756-767 (2010).

210   Liu, L. *et al.* Upregulation of myocellular DGAT1 augments triglyceride synthesis in skeletal muscle and protects against fat-induced insulin resistance. *The Journal of clinical investigation* **117**, 1679-1689 (2007).

211   Vujic, N. *et al.* Acyl-CoA: diacylglycerol acyltransferase 1 expression level in the hematopoietic compartment impacts inflammation in the vascular plaques of atherosclerotic mice. *PloS one* **11**, e0156364 (2016).

212   Liu, L. *et al.* Cardiomyocyte-specific loss of diacylglycerol acyltransferase 1 (DGAT1) reproduces the abnormalities in lipids found in severe heart failure. *Journal of Biological Chemistry* **289**, 29881-29891 (2014).

213   Harris, C. A. *et al.* DGAT enzymes are required for triacylglycerol synthesis and lipid droplets in adipocytes [S]. *Journal of lipid research* **52**, 657-667 (2011).

214   Choi, C. S. *et al.* Suppression of diacylglycerol acyltransferase-2 (DGAT2), but not DGAT1, with antisense oligonucleotides reverses diet-induced hepatic steatosis and insulin resistance. *Journal of Biological Chemistry* **282**, 22678-22688 (2007).

215   Liu, Q., Siloto, R. M., Lehner, R., Stone, S. J. & Weselake, R. J. Acyl-CoA: diacylglycerol acyltransferase: molecular biology, biochemistry and biotechnology. *Progress in lipid research* **51**, 350-377 (2012).

216   DeVries-Seimon, T. *et al.* Cholesterol-induced macrophage apoptosis requires ER stress pathways and engagement of the type A scavenger receptor. *The Journal of cell biology* **171**, 61-73 (2005).

217   Chang, C. C. Y., Sun, J. & Chang, T.-Y. Membrane-bound O-acyltransferases (MBOATs). *Frontiers in Biology* **6**, 177-182, doi:10.1007/s11515-011-1149-z (2011).

218   Lehninger, A. L. On the activation of fatty acid oxidation. *Journal of Biological Chemistry* **161**, 437-451, doi:https://doi.org/10.1016/S0021-9258(17)41479-7 (1945).

219   Vaughan, M. The production and release of glycerol by adipose tissue incubated in vitro. *The Journal of biological chemistry* **237**, 3354-3358 (1962).

220   Jensen, M. D., Ekberg, K. & Landau, B. R. Lipid metabolism during fasting. *American Journal of Physiology-Endocrinology and Metabolism* **281**, E789-E793, doi:10.1152/ajpendo.2001.281.4.E789 (2001).

221   Ellis, J. M. *et al.* Adipose Acyl-CoA Synthetase-1 Directs Fatty Acids toward β-Oxidation and Is Required for Cold Thermogenesis. *Cell metabolism* **12**, 53-64, doi:10.1016/j.cmet.2010.05.012 (2010).

222   Sepa-Kishi, D. M., Jani, S., Eira, D. D. & Ceddia, R. B. Cold acclimation enhances UCP1 content, lipolysis, and triacylglycerol resynthesis, but not mitochondrial uncoupling and fat oxidation, in rat white adipocytes. *American Journal of Physiology-Cell Physiology* **316**, C365-C376, doi:10.1152/ajpcell.00122.2018 (2019).

223   Schreiber, R. *et al.* Cold-Induced Thermogenesis Depends on ATGL-Mediated Lipolysis in Cardiac Muscle, but Not Brown Adipose Tissue. *Cell metabolism* **26**, 753-763.e757, doi:10.1016/j.cmet.2017.09.004 (2017).

224   Rohm, M. *et al.* An AMP-activated protein kinase-stabilizing peptide ameliorates adipose tissue wasting in cancer cachexia in mice. *Nature medicine* **22**, 1120-1130, doi:10.1038/nm.4171 (2016).

Publications

- Wang, J., Onogi, Y., Krueger, M., **Oeckl, J.**, Karlina, R., Singh, I., Hauck, S. M., Feederle, R., Li, Y. & Ussar, S. **PAT2 regulates vATPase assembly and lysosomal acidification in brown adipocytes. Mol Metab** 61, 101508, doi:10.1016/j.molmet.2022.101508 (2022).

- **Oeckl, J.**, Janovska, P., Adamcova, K., Bardova, K., Brunner, S., Dieckmann, S., Ecker, J., Fromme, T., Funda, J., Gantert, T, Giansanti, P., Hidrobo, M. S., Kuda, O., Kuster, B., Li, Y., Pohl, R., Schmitt, S., Schweizer, S., Zischka, H., Zouhar, P., Kopecky, J. & Klingenspor, M. **Loss of UCP1 function augments recruitment of futile lipid cycling for thermogenesis in murine brown fat. Mol Metab** 61, 101499 (2022).

- Boerboom, G., Ganslmaier, E., **Oeckl, J.**, Busink, R., Martín-Tereso, J., Windisch, W. & Brugger, D. **Dietary l-glutamic acid N, N-diacetic acid improves short-term maintenance of zinc homoeostasis in a model of subclinical zinc deficiency in weaned piglets. British Journal of Nutrition**, 1-10 (2022).

- Gantert, T., Henkel, F., Wurmser, C., **Oeckl, J.**, Fischer, L., Haid, M., Adamski, J., Esser-von Bieren, J., Klingenspor, M. & Fromme, T. **Fibroblast growth factor induced Ucp1 expression in preadipocytes requires PGE2 biosynthesis and glycolytic flux. FASEB journal** 35, e21572, doi:10.1096/fj.202002795R (2021).

- **Oeckl, J.**, Bast-Habersbrunner, A., Fromme, T., Klingenspor, M. & Li, Y. **Isolation, Culture, and Functional Analysis of Murine Thermogenic Adipocytes. STAR Protocols** 1, 100118, doi:https://doi.org/10.1016/j.xpro.2020.100118 (2020).

- Schweizer, S., Liebisch, G., **Oeckl, J.**, Hoering, M., Seeliger, C., Schiebel, C., Klingenspor, M. & Ecker, J. **The lipidome of primary murine white, brite, and brown adipocytes—Impact of beta-adrenergic stimulation. PLOS Biology** 17, e3000412, doi:10.1371/journal.pbio.3000412 (2019).

- Schweizer, S., **Oeckl, J.**, Klingenspor, M. & Fromme, T. **Substrate fluxes in brown adipocytes upon adrenergic stimulation and uncoupling protein 1 ablation. Life science alliance** 1, e201800136, doi:10.26508/lsa.201800136 (2018).

- Braun, K., **Oeckl, J.**, Westermeier, J., Li, Y. & Klingenspor, M. **Non-adrenergic control of lipolysis and thermogenesis in adipose tissues. Journal of Experimental Biology** 221, jeb165381 (2018).